The Dissertation Committee for Robbyn K. Perdue certifies that this is the approved version of the following dissertation:

Electrokinetic Focusing of Charged Species at a Bipolar Electrode in a Microfluidic Device

Committee:

Richard M. Crooks, Supervisor

Allen J. Bard

Keith J. Stevenson

C. Buddie Mullins

John F. Stanton

Electrokinetic Focusing of Charged Species at a Bipolar Electrode in a Microfluidic Device

by

Robbyn K. Perdue, B.A.

Dissertation

Presented to the Faculty of the Graduate School of

The University of Texas at Austin

in Partial Fulfillment

of the Requirements

for the Degree of

Doctor of Philosophy

The University of Texas at Austin

December, 2010

Dedication

To my husband,

Anand for his endless

patience and support,

and my parents,

R. Kim and Mary Anne

for their love and guidance

Acknowledgments

I would like to sincerely thank my research advisor, Dr. Richard M. Crooks for believing in me even when I did not and for helping me to find the light switch.

I would also like to thank Dr. Allen J. Bard, Dr. Keith J. Stevenson, Dr. C. Buddie Mullins, and Dr. John F. Stanton for being my committee members. Special thanks go to Dr. Bard for being a perennial teacher, always taking time to answer my questions.

My gratitude goes to Dr. Li Sun for being a friend and mentor during my first year of graduate school. His presence in the Crooks group has been sorely missed. I would like to thank my fellow Crooks group members for embodying Proverbs 27:17, “As iron sharpens iron, so one man sharpens another.”

I want to acknowledge my husband for bringing joy and calm to my life and my parents for reminding me to pray.

Finally, I would like to thank my Lord and Savior Jesus Christ for being my anchor and for teaching me to pursue truth. Without Him I am nothing.

Electrokinetic Focusing of Charged Species at a Bipolar Electrode in a Microfluidic Device

Publication No._____

Robbyn K. Perdue, Ph. D.

The University of Texas at Austin, 2010

Supervisor: Richard M. Crooks

The development and characterization of bipolar electrode (BPE) focusing is described. BPE focusing is an electrokinetic equilibrium technique in which charged analytes are focused and locally enriched on an electric field gradient in the presence of a counter-flow. This electric field gradient is formed at the boundary of an ion depletion zone – the direct result of faradaic reactions occurring at the BPE in the presence of an externally applied electric field.

Direct measurement of the electric field strength in the ion depletion region shows that the electric field is enhanced in this region and takes on a gradient shape, confirming the results of numerical simulations. Transient

electric field measurements with simultaneous monitoring of a focused fluorescent tracer reveal that the field gradient forms rapidly upon application of the external field and remains stable over time with the tracer focused at a local field strength predicted by simple electrokinetic equations.

These transient electric field measurements probe the effect of individual experimental parameters on the electric field gradient and the focused band. The results of these studies indicate that a steeper field gradient leads to enhanced concentration enrichment of the analyte. The slope of the gradient is increased with higher concentration of the running buffer and higher applied field strength. The addition of pressure driven flow across the microchannel moves the location of the field gradient and the position of the focused band. Further enhancement of enrichment is achieved through the suppression of Taylor dispersion after coating the microchannel with a non-ionic surfactant.

The findings of these studies have motivated the transition of BPE focusing to smaller microchannels. A decrease in microchannel size not only decreases Taylor dispersion, but also provides access to higher buffer

concentration and higher applied field strength, both of which enhance enrichment. The result is a three-order-of-magnitude increase in total analyte enrichment at a much higher enrichment rate. Furthermore, a dual channel configuration for BPE focusing is introduced which provides greater control over focusing conditions.

Finally, the formation of ion depletion and enrichment zones at a BPE in a microchannel is shown to mimic ion concentration polarization (ICP) at micro-/nano-channel junctions. This is significant because this faradaic ICP provides a model to which traditional ICP can be compared and is achieved in a more easily fabricated device.

In summary, the fundamental principles of BPE focusing are described. A greater understanding of the effect of experimental parameters on the focusing process leads to an unprecedented magnitude and rate of enrichment in a simple device architecture.

Table of Contents

Chapter 1: Introduction

1.1 Bipolar Electrochemistry

A bipolar electrode (BPE) is an electronic conductor in contact with an ionically conductive phase. When a sufficiently high electric field is applied across the ionic phase, faradaic reactions occur at the ends of the BPE even though there is no direct electrical connection between it and the external power supply. This lack of a requirement for external connections is one of the greatest advantages of BPEs making them ideal for both miniaturization and array format sensing. A further advantage of BPEs is that they can be used to carry out faradaic electrochemistry in the presence of a strong electric field – a goal that is very difficult to accomplish with a traditional 3-electrode electrochemical cell. An example of a BPE is illustrated in Scheme 1.1a by a strip of Au in the bottom of a microchannel filled with an electrolyte solution. A potential (E_{tot}) is applied across the microchannel by driving electrodes located in the reservoirs, and the applied potential is dropped approximately linearly along its length (Scheme 1.1b). The potential of the BPE (E_{elec}) floats to a value intermediate

Scheme 1.1

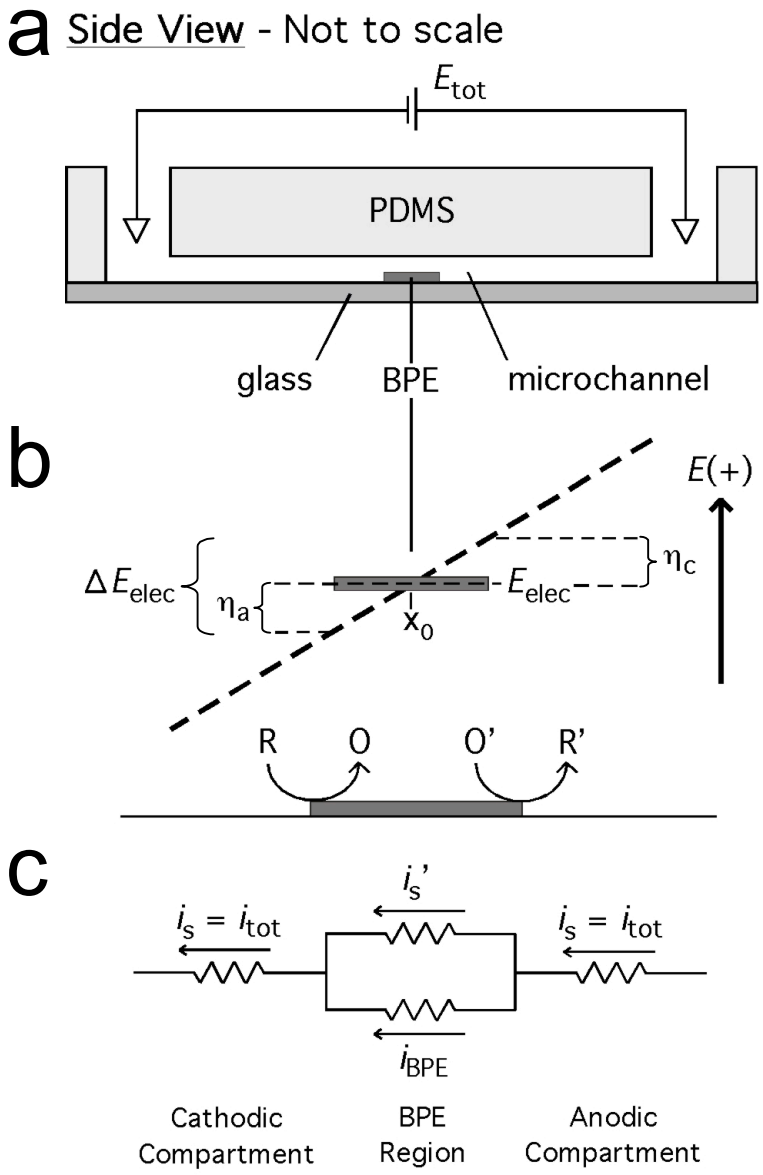
a Side View - Not to scale
E_{tot}
PDMS
glass
BPE
microchannel
b
$E(+)$
ΔE_{elec}
η_a
E_{elec}
η_c
x_0
R
O
O'
R'
c
i_s'
$i_s = i_{tot}$
$i_s = i_{tot}$
i_{BPE}
Cathodic Compartment
BPE Region
Anodic Compartment

to the solution potential at its ends such that the solution potential at one end is more positive than E_{elec}, driving the reduction of species in solution and at the other end more negative, driving oxidations. If the difference in potential experienced by the ends of the BPE (ΔE_{elec}) is sufficiently large, oxidation and reduction reactions can occur simultaneously – albeit at opposite ends.

The difference in potential between E_{elec} and the solution contacting the BPE at the BPE cathode is the cathodic overpotential (η_c) and at the BPE anode, the anodic overpotential (η_a) (Scheme 1.1b). The magnitude of η_c and η_a decrease from the BPE ends to a point at which the solution potential is equal to E_{elec} ($\eta_c = \eta_a = 0$) labeled in Scheme 1.1c as x_0, which may or may not be at the center of the BPE. If η_c and η_a are sufficiently large, they drive cathodic (i_c) and anodic (i_a) currents, respectively, the magnitude of which varies at each point along the BPE depending on the local value of η_c and η_a, mass transport limitations, and the electron transfer kinetics of the faradaic reactions.

While either η_c or η_a may be large enough to drive faradaic electrochemistry, the condition of

electroneutrality of the BPE dictates that at all times $i_c = i_a$. This condition can be satisfied by the BPE because its potential, E_{elec}, is allowed to float. Therefore, if for example the driving force (η_c) for reduction is too large, E_{elec} will become more positive, decreasing η_c and increasing η_a until $i_c = i_a$. This increase in E_{elec} will also cause x_0 to shift towards the BPE cathode.

Importantly, the oxidation and reduction reactions at the opposite ends of the BPE are linked such that one cannot occur without the other. Therefore, the magnitude of ΔE_{elec} required to drive the two reactions simultaneously must be close to the difference in the formal reduction potentials of the two half-reactions. Additional overpotential may be required to drive kinetically slow reactions at the desired rate.

The magnitude of ΔE_{elec} is a function of the length of the BPE and the applied driving potential (E_{tot}) and is approximated by the following equation.

$$\Delta E_{elec} = ((E_{tot} - E_{dr})/l_{channel})(l_{elec}) \qquad (1.1)$$

Here, E_{dr} is the potential dropped at the driving electrodes, $l_{channel}$ is the length of the microchannel, and l_{elec} the length of the BPE. Note that $(E_{tot} - E_{dr})/l_{channel}$ is the average electric field strength in the microchannel.

The magnitude of ΔE_{elec} is most typically controlled by adjusting E_{tot}.

Importantly, eq 1.1 is only strictly true when the current through the BPE ($i_{BPE} = i_c = i_a$) is a small fraction of the total current through the microchannel (i_{tot}). In the case that i_{BPE} is a significant fraction of i_{tot}, the electric field strength in solution directly above the BPE decreases. To understand this, consider the simplified equivalent circuit diagrammed in Scheme 1.1c. The microchannel is represented by a set of resistors and can be divided into three segments: the anodic compartment (the solution between the anodic driving electrode and the BPE cathode), the BPE region (including both the BPE and the solution above it), and the cathodic compartment (the solution between the BPE anode and the cathodic driving electrode). In both the anodic and cathodic compartments all of the current is ionic current carried through solution (i_s) and $i_s = i_{tot}$. In the region of the BPE, however, i_{tot} is divided between ionic current (i_s') and electronic current (i_{BPE}) such that $i_{tot} = i_s' + i_{BPE}$. Therefore, $i_s > i_s'$, and assuming constant solution resistance (R_s) throughout the microchannel, Ohm's Law

dictates the following relationship between the field strengths in the channel segments.

$$V_c = V_a > V_{BPE} \quad (1.2)$$

$$V_c = V_a = i_s R_s \quad (1.3)$$

$$V_{BPE} = i_s' R_s \quad (1.4)$$

Here, V_c, V_a, and V_{BPE} are the electric field strength in the cathodic and anodic compartments and the region of the BPE, respectively. This decrease in V_{BPE} is called faradaic depolarization,[1] the degree of which is defined by the ratio i_{BPE}/i_{tot}. Faradaic depolarization causes prediction of ΔE_{elec} from eq 1.1 to be difficult. ΔE_{elec} will be overestimated unless depolarization is negligible ($i_{BPE} << i_{tot}$). Importantly, i_{BPE} cannot exceed i_{tot}.

In addition to estimating the degree of faradaic depolarization, measuring the value of i_{BPE} is essential for understanding faradaic reactions at the BPE unless they produce another form of signal (e.g. light emission or metal deposition).[2] This measurement can be accomplished using a split BPE having a gap at its center. When the two halves are interconnected by either a conductive wire or an ammeter, the split BPE carries out faradaic reactions in the same way as a continuous BPE. However, the gap in the BPE decreases the surface area in contact with the

electrolyte. The resulting decrease in current is negligible if the gap is small and if the gap is located close to x_0, which may or may not be at the center of the BPE depending on the distribution of i_c and i_a. If these conditions are met, then i_{BPE} in the split and continuous BPE are closely matched.[3]

In summary, faradaic reactions at BPEs are driven by a potential difference established between the BPE and the solution in contact with it. This potential difference is generated by application of an electric field across the solution containing the BPE while allowing the BPE potential to float. Both electrochemical oxidation and reduction reactions can occur at the BPE simultaneously but must proceed at equal rates, a requirement which is fulfilled by automatic adjustment of E_{elec} to modulate the relative magnitudes of η_c and η_a. The onset of these reactions is determined by ΔE_{elec} — the total potential available to drive both reactions — which is roughly a function of E_{tot}. Finally, the resulting current at the BPE ($i_{BPE} = i_c = i_a$) is determined by many parameters including ΔE_{elec}, mass transport, electron transfer kinetics, and i_{tot}.

1.2 Electrokinetics

Electrokinetics describes the movement of ions, particles, and liquids in response to an electric field. The two electrokinetic phenomena described here are electroosmosis and electrophoretic migration of ions.

Electroosmosis

Electroosmosis is the movement of an electrolyte solution along a charged surface in response to a tangentially applied electric field. For example, when a glass capillary is filled with an electrolyte solution, a fraction of the Si-OH groups on the surface of the glass in contact with the solution are deprotonated, and the capillary walls become negatively charged (Scheme 1.2a). In response to this, counter-ions (cations in this case) from the solution, migrate to the walls to shield the negative charge thus forming an electrical double layer (EDL) (Scheme 1.2b). The EDL is comprised of a layer of cations tightly bound to the surface (Stern layer) and a layer of mobile cations (diffuse layer). When an electric field is applied tangential to the capillary walls, the cations of the diffuse layer and their waters of solvation are drawn towards the cathodic (-) driving electrode (Scheme 1.2c). The movement of the diffuse layer drags the bulk solution

Scheme 1.2

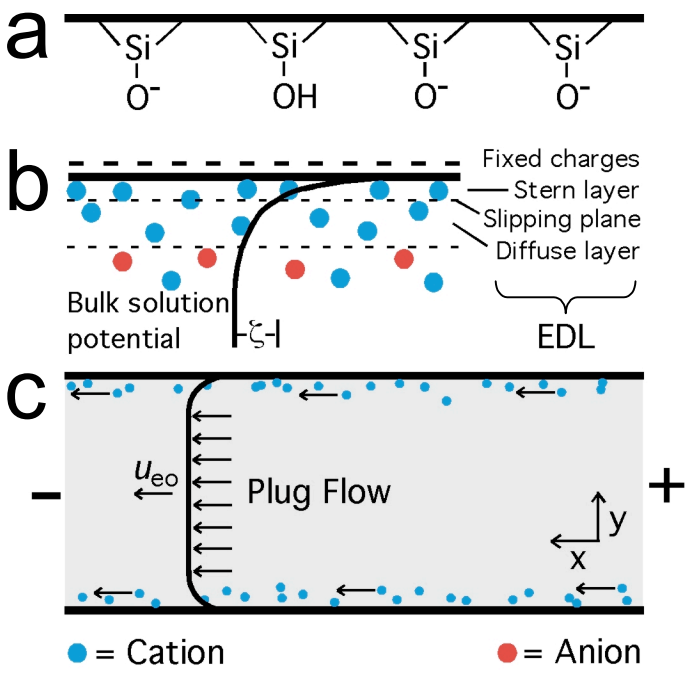
a
Si
O⁻
Si
OH
Si
O⁻
Si
O⁻
b
Fixed charges
Stern layer
Slipping plane
Diffuse layer
Bulk solution
potential
ζ-l
EDL
c
–
u_{eo}
Plug Flow
+
y
x
= Cation
= Anion

along by frictional force. Thus, a cathodic electroosmotic flow is established in the capillary. The flow profile is nearly flat (ie. uniform velocity in the x-direction across the entire capillary cross section) and is termed 'plug flow' (Scheme 1.2c). The average linear flow rate due to electroosmosis, u_{eo}, is described by eq 1.5 below.

$$u_{eo} = \mu_{eo} V \qquad (1.5)$$

Here, V is the electric field strength and μ_{eo} the electroosmotic mobility, a proportionality constant determined by the properties of the electrolyte solution and the capillary walls. The value of μ_{eo} can be calculated as is shown in eq 1.6.

$$\mu_{eo} = \varepsilon\zeta/\eta \qquad (1.6)$$

Here, ε is the permittivity of the solution, ζ the zeta potential (electric potential at the slipping plane between the Stern and diffuse layers, Scheme 1.2c) and η the dynamic viscosity of the solution. The zeta potential is defined relative to the bulk solution potential and is determined by several factors, including the density of fixed charges on the capillary walls and the ionic strength of the electrolyte solution. In general terms, a high density of fixed charges and a low ionic strength electrolyte both lead to a high value of ζ. Often in

practice, μ_{eo} is changed to a desired value by coating the capillary walls with charged or neutral polymers, lipids, or other surfactants, which alter the surface charge density and, ultimately, ζ.

Typically, the electroosmotic velocity, u_{eo}, is measured by injecting a plug of a neutral dye at the capillary inlet and then observing the transit time from the injection point to a downstream detector under electroosmotic flow. In a microfluidic channel, such as the ones used in the studies described in the following chapters, there is often not a convenient way in which to inject a discrete band of a neutral marker. Therefore, another method of measuring u_{eo} is employed called the current monitoring method.[4] In this method, u_{eo} is determined by observing the time required for an electrolyte solution of slightly lower ionic strength (~90% of initial ionic strength) to completely replace the electrolyte in the channel under electroosmotic flow. To measure cathodic electroosmotic flow, first, the microchannel is filled with the higher concentration electrolyte. Then, the lower ionic strength electrolyte is loaded into the anodic reservoir. Next, E_{tot} is applied, initiating electroosmotic flow. Finally, the progress of the front of the lower ionic

strength electrolyte is followed by monitoring i_{tot}. Initially, i_{tot} is at a maximum value, but as the front moves into the microchannel, the solution resistance increases until a minimum in i_{tot} – corresponding to the front reaching the cathodic reservoir – is reached. The value of u_{eo} is then simply calculated as follows.

$$u_{eo} = l_{channel}/t \qquad (1.7)$$

Here, t is the transit time (measured from the initial decrease in i_{tot} until it reaches a minimum). Diffusion of the electrolyte ions between the initial and lower ionic strength solutions tends to make the interface between solutions ill-defined. One solution to this problem is to use electrolyte solutions of very dissimilar concentrations. However, a large difference in electrolyte concentration will cause ζ to change over the course of the measurement. A superior solution to this problem of intermixing is to graphically estimate the intersection point as illustrated in Scheme 1.3.

Electrophoretic migration

Electrophoretic migration occurs when an ionic species, A, with charge, z_A, in a fluid medium is exposed to an electric field. The ion migrates towards the anodic or cathodic pole

Scheme 1.3

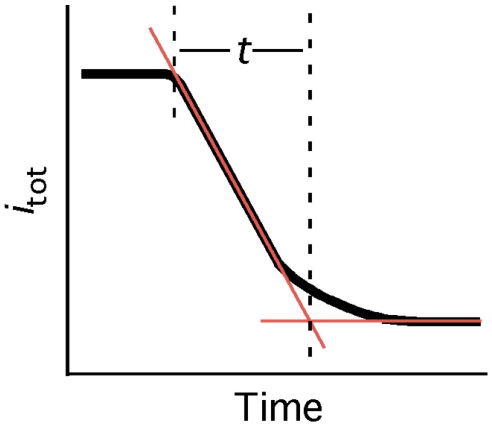

depending on the sign of its charge. The electrophoretic velocity, $u_{ep,A}$, is described by eq 1.8.

$$u_{ep,A} = \mu_{ep,A} V \quad (1.8)$$

Here, V is the strength of the electric field and $\mu_{ep,A}$ the electrophoretic mobility of species A, which is specific to the properties of A and the medium as shown in eq 1.9.

$$\mu_{ep,A} = D_A z_A / k_B T \quad (1.9)$$

Here, D_A is the diffusion coefficient of A, k_B is the Boltzmann constant, and T is the absolute temperature. Therefore, ions with higher diffusion coefficient and charge have a higher electrophoretic mobility and migrate faster in response to a given electric field strength. Importantly, properties of the electrolyte solution, including ionic strength and viscosity, affect the value of D_A, and therefore accurate determination of $\mu_{ep,A}$ requires separate measurement for each electrolyte solution employed.

The net velocity of an ion is the sum of the electroosmotic velocity of the fluid medium (u_{eo}) and $u_{ep,A}$. Therefore, $u_{ep,A}$ can be measured by comparing its migration velocity with that of a neutral species (for which $u_{ep} = 0$). This is accomplished experimentally by injecting a plug of the ion and neutral marker into the microchannel or

capillary (often by electroosmosis) and then applying an electric field. The time required for the ion (t_A) and neutral marker (t_{nm}) to migrate from the injection point to a detector is recorded and $u_{ep,A}$ calculated as follows.

$$u_{ep,A} = L/t_A - L/t_{nm} \quad (1.10)$$

Here, L is the distance from the injection point to the detector. $\mu_{ep,A}$ may then be calculated from $u_{ep,A}$ using eq 1.8.

In summary, when an electric field is applied across an electrolyte solution, both convective flow, driven by electroosmosis, and electrophoretic migration dictate the movement and distribution of ions. This subsection is a brief summary of the mathematical principles governing these electrokinetic phenomena and an introductory guide to their measurement.

1.3 Research Summary and Accomplishments

My dissertation discusses the development of bipolar electrode (BPE) focusing – a technique that locally enriches the concentration of charged analytes along an electric field gradient in the presence of a counter-flow Scheme 1.4. This field gradient is formed at the boundary of an ion depletion zone generated by faradaic processes at the end of a BPE in an electrolyte-filled microchannel.

Scheme 1.4

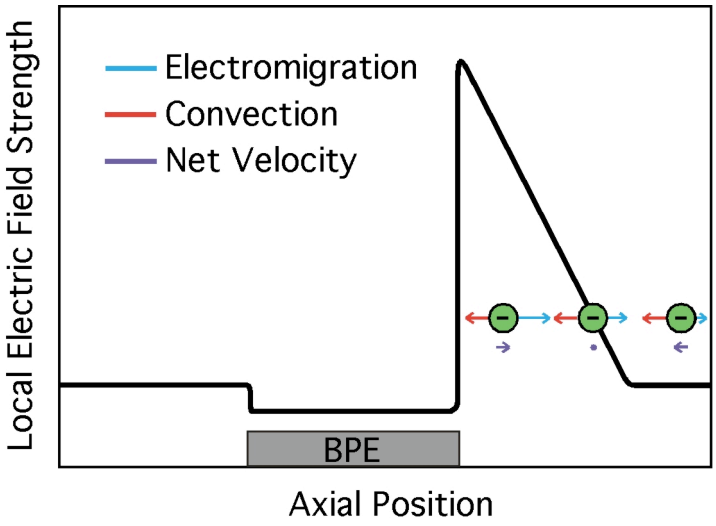
Electromigration
Convection
Net Velocity
Local Electric Field Strength
BPE
Axial Position

Here, the fundamental principles of BPE focusing are investigated and the results compared with numerical simulations, confirming the description given above. Specific advances made as a result of these studies include controlled transport of the focused band, greater control over focusing conditions, and enhanced concentration enrichment. The significance of this project is two-fold. First, BPE focusing is a convenient, broadly applicable technique for concentration enrichment and separation of ions in a simple device format, and through the research described above, has reached a level of functionality that makes it competitive with existing focusing techniques. Additionally, BPE focusing is an excellent tool for developing a better understanding of bipolar electrochemistry and electrokinetics in the presence of a non-linear and temporally changing electric field. These are complex and interesting topics at the forefront of both fields of study.

Chapter 3 describes the basic characterization of BPE focusing through measurement of i_{BPE} and the electric field profile along the microchannel under focusing conditions. Measurement of i_{BPE} indicate that BPE focusing conditions coincide with the onset of water electrolysis at the BPE

Electric field profile measurements confirm the existence of an electric field gradient adjacent to the BPE cathode, the magnitude and slope of which compare favorably with numerical simulations. Finally, controlled transport of a focused ion band is demonstrated.

Chapter 4 extends the investigation of BPE focusing to time-resolved studies in which the response of the electric field gradient to changes in experimental parameters is explored. The relationship between these parameters, the slope of the field gradient, and the rate and maximum extent of concentration enrichment is discussed. Guidelines are provided for tuning the properties of the electric field gradient.

Finally, these studies of the fundamental principles of BPE focusing culminate in Chapter 5, which describes both a 3-order of magnitude increase in the maximum extent of concentration enrichment (from 500- to 500,000-fold) and a 70-fold increase in enrichment rate. Furthermore, a new dual-channel device configuration is developed affording greater control over the experimental parameters affecting the enrichment process by decoupling E_{tot} and ΔE_{elec}. This dual-channel configuration is shown to generate concentration enrichment and depletion zones in two

separate microchannels linked only by a BPE in a manner similar to ion concentration polarization (ICP) at a micro-/nano-channel junction. This finding is significant because the dual-channel device is an excellent tool for understanding ICP and provides the same result as ICP with a more easily fabricated device.

In summary, the fundamental principles of BPE focusing are discussed, and measurements of i_{BPE} and the electric field profile are compared with numerical simulations. The impact of the slope and position of the electric field gradient on performance are uncovered, and methods for controlling the field gradient are described. The results of these studies allow significant improvements in the extent and rate of enrichment as well as greater control over the position of the focused ion band. Finally, BPE focusing is extended to a dual channel configuration, which both enhances concentration enrichment and generates ion concentration and depletion zones in a way that is similar to ICP.

Chapter 2: Experimental

2.1 Chemicals

All chemicals used in this work are described in the individual chapters.

2.2 Techniques

In this work, a technique for measuring the strength of the local axial electric field along a microfluidic channel was developed and then further extended to allow time-resolved measurements of the electric field profile using a scanning digital multimeter (SDMM).

Device fabrication. The devices were fabricated based on a previously described procedure,[5] and details can be found in the individual chapters of this dissertation. Briefly, the microfluidic channel was made by pouring poly(dimethylsiloxane) (PDMS) precursor over a photolithographically patterned photoresist mold on a Si wafer and curing at 65°C for 2 h. After curing, the PDMS monolith containing the microchannel pattern was peeled from the mold and 4.0 mm reservoirs were punched at the ends of the microchannel. Next, 100 nm-thick Au electrodes (no adhesion layer, Evaporated Metal Films, Ithaca, NY)

were microfabricated on glass slides using standard photolithographic techniques. Before sealing, the electrodes and PDMS microchannel were rinsed with copious amounts of acetone and ethanol, respectively, and dried with a stream of $N_{2(g)}$. Finally, the PDMS and electrodes were exposed to an O_2 plasma for 15 s on medium power (60 W, model PDC-32G, Harrick Scientific, Ossining, NY). The pieces were then aligned and brought into contact.

Steady state electric field profile measurement. The device design used to measure the steady state electric field gradient is shown in Figure 2.1a. An array of 15 Au microbands (40 μm lines and spaces) is located at the center of a 6.0 mm long, 100 μm wide, 21 μm high microchannel. The microbands are numbered 1-15 starting with the one nearest the anodic reservoir (right, Figure 2.1a). Each microband extends out from under the microchannel leading to a contact pad enabling electrical contact with a high impedance digital multimeter (DMM, Model 6517B, Keithley Instruments, Inc., Cleveland, OH). Any two of the microbands can be interconnected external to the microchannel by a conductive wire to form a BPE.[3, 6, 7] Two microbands with an outer-edge-to-edge distance (d) approximate a continuous BPE with length $l_{elec} = d$. That is,

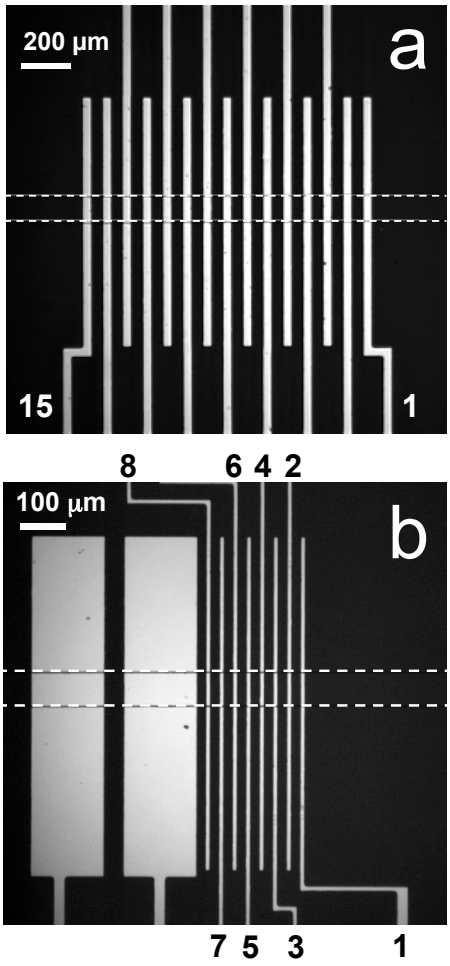

Figure 2.1 (a) Optical micrograph of an array of 15 Au microband electrodes (40 µm lines and spaces) at the center of a microfluidic channel (6.0 mm long, 100 µm wide, and 20 µm high). Microchannel indicated by white dashed lines. (b) Optical micrograph of a split BPE (225 µm wide halves with a 50 µm gap) and 8 microband electrodes (each 15 µm wide and spaced 40 µm apart on center). Dashed lines indicate microchannel.

the total potential available to drive faradaic reactions at the microband and continuous BPE (ΔE_{elec}) are the same and can be calculated from eq 1.1. The remaining microbands are then used to measure the electric field profile. The potential difference between each neighboring pair of microbands ($\Delta E_{n,m}$) was measured with the DMM and then divided by the distance between microbands (40 μm on center) to calculate the local electric field strength.

This microband array design is advantageous because there are microbands interior to the two microbands comprising the BPE thus allowing the field strength above the BPE to be measured. Several sets of electric field profile measurements were completed using different pairs of microbands to form the BPE for each set (1 and 7, 5 and 11, 6 and 12, or 9 and 15). Use of these multiple positions made it possible to obtain a more complete picture of the electric field. For instance, when microband 9 was the BPE cathode and microband 15 was the BPE anode, microbands 1 through 8 were available to measure the electric field extending far from the BPE cathode toward the anodic reservoir. Conversely, when microbands 1 and 7 formed the BPE, no other microbands were located between the BPE cathode and the anodic reservoir. Instead, microbands 8

through 15 measured the electric field adjacent to the BPE anode.

Measurement of the electric field profile proceeded as follows. First, the microfluidic channel was filled with buffer solution. Then, two microbands were selected to form the BPE and were interconnected by a conductive wire. Next, the DMM was connected to the two microbands nearest the BPE cathode. Finally, E_{tot} was applied and the potential difference between these two microbands ($\Delta E_{n,m}$) was measured until it attained a steady value (~200 s). This measurement was repeated for all other neighboring pairs of microbands while E_{tot} was maintained at a constant value. The potential difference between the original pair of microbands was periodically re-measured to ensure that its value remained constant during the experiment.

Monitoring the electric field gradient. The electric field profile evolves over the course of an enrichment experiment and can be impacted dynamically by changes in experimental parameters during enrichment. For this reason, temporal measurement of the electric field profile is desirable.

The device design used to monitor the electric field is a split BPE (225 μm long halves with a 50 μm gap at

center) with a set of 8 microband electrodes (each ~15 μm wide and having a center-to-center distance of 40.0 μm) located adjacent to the BPE cathode (Figure 2.1b). The 8 microband electrodes were placed here to measure the gradient portion of the electric field. The split BPE design was used to most closely approximate a continuous (500 μm long) BPE while still allowing the BPE to be activated and inactivated by interconnecting or disconnecting the halves, respectively. The 8 microbands were fabricated next to the BPE cathode because the field gradient used for enrichment is located there.

The axial electric field profile was monitored using a scanning digital multimeter (SDMM, Model 2700, Keithley Instruments, Inc., Cleveland, OH) equipped with a multiplexer module (Model 7701, Keithley) and connected to the 8 microband electrodes. The SDMM was controlled in Microsoft Excel via the software provided by the SDMM manufacturer (ExceLinx, Keithley). The SDMM was interfaced to the microband electrodes through a breakout board (screw terminals). The SDMM reads the potential difference between the two microbands farthest from the BPE first ($\Delta E_{1,2}$, Figure 2.1b), and then sequentially measures the potential between

the second and third microbands ($\Delta E_{2,3}$) and so forth until the last pair ($\Delta E_{7,8}$) is reached.

The multiplexer module is designed such that a single potential difference between two inputs (Channel (Ch) 1 Lo and Ch 1 Hi) can be measured at a time. After measuring Channel 1, internal switches are actuated, and Ch 2 Lo and Ch 2 Hi are interrogated. Now, when measuring the electric field profile with the 8 microband electrodes described above, this instrument design is limiting. For example, Scheme 2.1a shows the microbands interfaced directly to the multiplexer inputs such that microband 1 is electrically connected to Ch 1 Lo and microband 2 is connected to Ch 1 Hi. In this way $\Delta E_{1,2}$ is measured at Ch 1. However, $\Delta E_{2,3}$ cannot be measured because the multiplexer will not read the potential difference between Ch 1 Hi (microband 2) and Ch 2 Lo (microband 3). To solve this issue, the channel inputs were interfaced to a breakout board that was wired as shown in Scheme 2.1b. Microband 1 is connected to Ch 1 Lo while microband 2 is connected to both Ch 1 Hi and Ch 2 Lo. Microband 3 is then connected to Ch 2 Hi and Ch 3 Lo. This pattern is continued such that Ch 1 measures $\Delta E_{1,2}$, Ch 2 measures $\Delta E_{2,3}$, and so forth.

Scheme 2.1

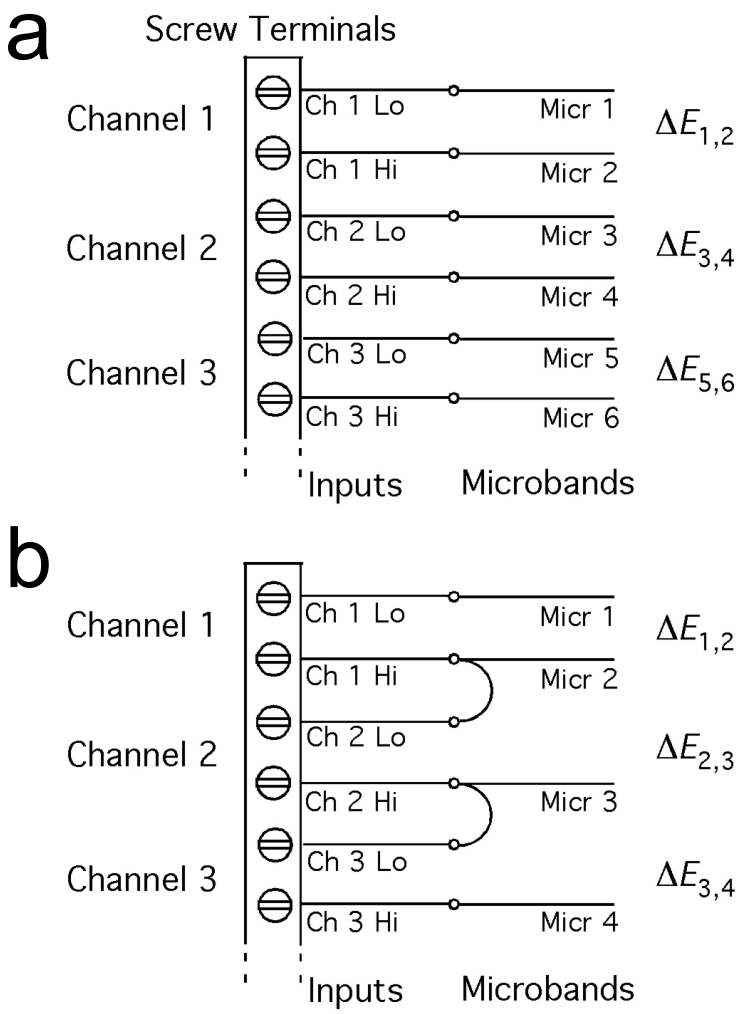
a
Screw Terminals
Channel 1
Channel 2
Channel 3
Ch 1 Lo
Ch 1 Hi
Ch 2 Lo
Ch 2 Hi
Ch 3 Lo
Ch 3 Hi
Micr 1
Micr 2
Micr 3
Micr 4
Micr 5
Micr 6
ΔE1,2
ΔE3,4
ΔE5,6
Inputs
Microbands
b
Channel 1
Channel 2
Channel 3
Ch 1 Lo
Ch 1 Hi
Ch 2 Lo
Ch 2 Hi
Ch 3 Lo
Ch 3 Hi
Micr 1
Micr 2
Micr 3
Micr 4
ΔE1,2
ΔE2,3
ΔE3,4
Inputs
Microbands

Another challenge of these electric field profile measurements is that the reading from Ch 1 is often skewed by the SDMM to higher potential readings and drifts over the course of an experiment (several minutes). This is most likely caused by the fact that there are no readings preceding Ch 1, and the instrument adjusts its range as it scans through the channels. This problem is most easily remedied by pinning the potential of Ch 1 and moving all of the microbands to higher numbered channels. The measurement at Ch 1 is then discarded. One way to do this is to attach microband 1 to both of the first two leads shown in Scheme 2.1b such that its potential is the input for Ch 1 Lo, Ch 1 Hi, and Ch 2 Lo. Then, Ch 1 will read zero volts, while Ch 2 will be $\Delta E_{1,2}$.

Chapter 3: Bipolar Electrode Focusing: The Effect of Current and Electric Field on Concentration Enrichment

3.1 Synopsis

Bipolar electrode focusing at discontinuous bipolar electrodes (BPEs) provides new insight into the faradaic current and electric field characteristics associated with the technique and allows for the controlled transport of a focused anionic tracer in a microfluidic channel. The findings described here corroborate simulation results, which indicate that the formation of an extended electric field gradient leads to concentration enrichment. This gradient has been attributed to the passage of faradaic current through a BPE affixed to the floor of the microchannel. These results demonstrate that the onset of faradaic current is coincident with the onset of concentration enrichment. Utilizing an array of microband electrodes, the tracer may be passed from one stationary position to another by instantaneously relocating the BPE. However, the tracer movement is limited to one direction, confirming the relative magnitude of opposing electrophoretic and electroosmotic forces acting on the tracer band in various microchannel segments.

3.2 Introduction

In this chapter we demonstrate concentration enrichment of an anionic tracer using discontinuous bipolar electrodes (BPEs) (Figure 3.1). The key finding is that these microband electrodes can be configured to induce analyte concentration,[8-10] but with some significant advantages compared to a single, continuous BPE design. Specifically, any two microband electrodes in a microchannel may be connected externally to yield a BPE.[6, 7] This makes it possible to simultaneously measure the current flowing through a BPE and the corresponding effect on the redistribution of the tracer in the microchannel. This correlation provides valuable insights into the role of faradaic reactions in the formation of electric field gradients and the onset of concentration enrichment. Additionally, arrays of microbands may be used to measure the electric field strength in solution at different locations in a microchannel. This provides a direct probe of the electric field and can, therefore, corroborate results obtained by numerical simulation. Finally, the accessibility of multiple BPE configurations within a microband array provides a means for controlled, unidirectional transport of the concentrated tracer.

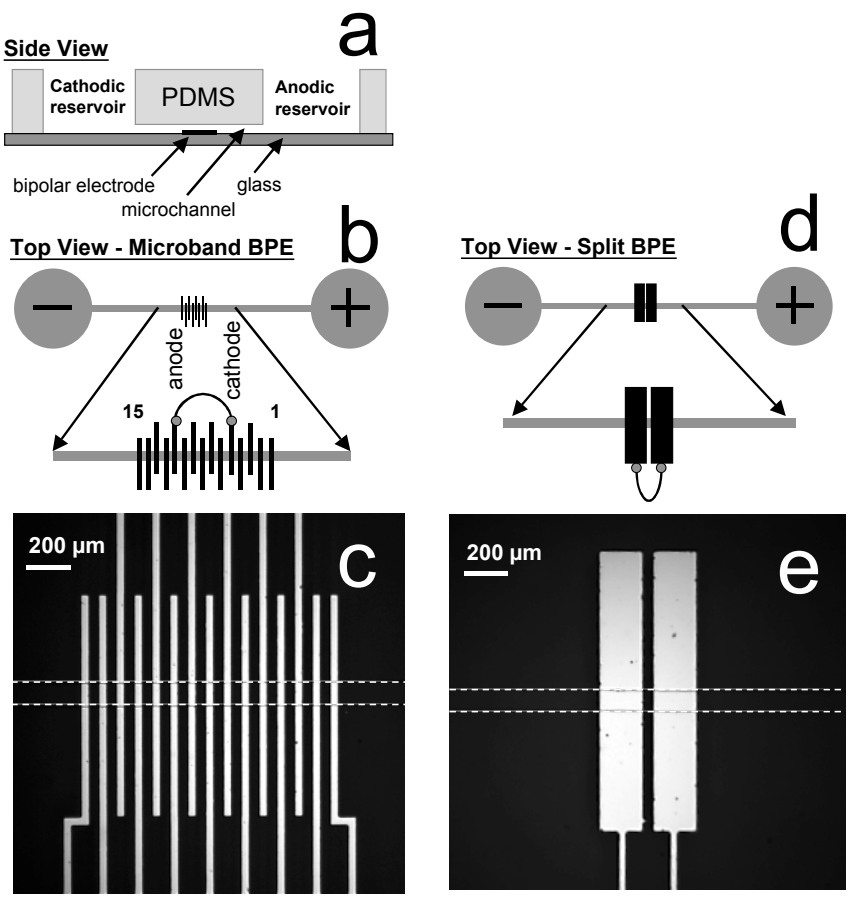

Figure 3.1. (a) The microfluidic device used in the experiments reported here. The PDMS microchannel measures 6.0 mm x 100 µm x ~20 µm with 4.0 mm diameter reservoirs. The PDMS channel is sealed to a glass slide with the gold BPE microfabricated at its center. (b) Top view schematic of the microfluidic channel showing detail of a microband array with a jumper wire connecting electrodes 5 and 11 to create a BPE. (c) An optical micrograph of the gold microband array (40 µm lines and spaces). (d) Top view schematic of the microfluidic channel showing a split BPE with a jumper wire connecting the two sides. (e) Optical micrograph of a gold split bipolar electrode. The electrode is 500 µm long with a 50 µm gap in the center.

Lab-on-a-chip devices are at the forefront of development of clinical diagnostic tools due to their ability to carry out rapid, integrated sample processing. In these devices, microfluidic channels allow transport and processing of nano- to microliter-scale samples. This attribute can be particularly advantageous in biomedical diagnostic applications in which sample volumes are often small. However, such small sample volumes, coupled with low analyte concentrations, lead to limited numbers of molecules being available for detection. Accordingly, ex-situ processing steps are frequently required to provide a more concentrated sample for chip-based analyses. However, for many applications, integration of a simple concentration enrichment module onto a lab-on-a-chip device is preferable to off-chip processing. This is the issue addressed here.

The majority of concentration enrichment methods presently used on microchips were originally developed for capillary electrophoresis. Many of these techniques rely on manipulation of the electrokinetic motion of an analyte. Some of the most well known of these are field-amplified sample stacking,[11, 12] isotachophoresis,[13-17] electric field gradient focusing (EFGF)[18-21] and isoelectric focusing

(IEF).[22-26] Some newer techniques that were specifically designed for microchip applications include concentration enrichment by electrostatic exclusion at nanochannels and nanoporous membranes[27-41] and temperature gradient focusing (TGF) within microchannels.[42-45] Techniques such as IEF, EFGF, and TGF have the added advantage of focusing individual analytes at particular locations along a gradient. Indeed, opposing forces may act to counter diffusional band broadening, therefore allowing enhanced enrichment and simultaneous high-resolution separations.[10]

The most widely used focusing technique is IEF due to its applicability to protein separations. IEF employs a pH gradient to focus each analyte at a specific location based on its isoelectric point (pI). The major limitations of IEF are the necessity to generate a high-quality static pH gradient and the fact that proteins have low solubility in their net-neutral state (where pH = pI).[46] The appeal of newly developed techniques, such as TGF and EFGF, is that charged (and hence more soluble) analytes can be enriched 1,000 to 10,000-fold.[46] One EFGF technique called dynamic field gradient focusing (DFGF) utilizes an array of electrodes to directly control the shape of the electric field.[47]

We recently reported electrokinetic focusing of anions in a microchannel using a BPE to control the local electric field.[8, 9] The BPE is a conductive material that is not connected to an external power supply, and therefore it is free to float to an equilibrium potential. If there is a sufficient potential dropped across the solution above a BPE, it can act as an electrode at which cathodic and anodic reactions occur simultaneously at opposite ends. By providing a low resistance path for the passage of current, the BPE results in less ionic current being carried by the solution above the electrode. Therefore, the electric field in the vicinity of the electrode is suppressed. The diversion of current through the BPE is termed faradaic depolarization.[48] The ratio of the current passing through the BPE (i_{BPE}) to the total current passing through the fluidic channel (i_{tot}) defines the degree of depolarization. As discussed in detail later, the faradaic reactions taking place at the BPE lead to the formation of an extended electric field gradient that can be used for concentration enrichment. During enrichment, anions entering the channel from the anodic reservoir via cathodic electroosmotic flow (EOF) encounter an increasing electric field that eventually becomes strong enough to exactly counteract the

EOF. Accordingly, anions focus at a unique position where the electrophoretic and electroosmotic velocities of the analyte sum to zero. We call this phenomenon bipolar electrode focusing, and it has the advantage of being applicable to all anionic analytes under the appropriate conditions. It is also a simple technique that is capable of simultaneously concentrating and separating analytes.[10]

Here, experimental results and interpretive simulations are presented that provide new fundamental and applied insights into bipolar electrode focusing. Specifically, discontinuous BPEs replace the continuous BPEs used in our previous reports.[8-10] This advance makes it possible to directly correlate the extent of concentration enrichment to in-situ amperometric and potentiometric measurements. The results of these studies indicate that concentration enrichment is coincident with the onset of faradaic electrochemistry at the BPE. Moreover, by measuring the potential between neighboring microband electrodes, it is possible to map the intrachannel electric field gradient and compare it to results derived from numerical simulations. Finally, the use of discontinuous microband electrodes makes it possible to control transport of a focused analyte band. This finding is important

because it represents a rare example of removing a concentrated analyte band from a crude sample without the need for additional channels or mechanical switches, and then moving it to a desired location for further processing.

3.3 Experimental

Chemicals. BODIPY disulfonate ($BODIPY^{2-}$, Molecular Probes, Eugene, OR) was used as a fluorescent tracer to quantitate the degree of concentration enrichment. Molecular biology grade 1.0 M Tris–HCl buffer (Fisher Biotech, Fair Lawn, NJ, USA) was diluted to 5.0 mM (pH 8.0) with deionized water (18.0 MΩ•cm, Milli-Q Gradient System, Millipore) and used as background electrolyte in all experiments. The silicone elastomer and curing agent (Sylgard 184) used to prepare the poly(dimethylsiloxane) (PDMS) microfluidic devices were obtained from K. R. Anderson, Inc. (Morgan Hill, CA, USA).

Device Fabrication. The hybrid PDMS/glass microfluidic devices and gold electrodes were prepared by a previously published procedure.[5] Briefly, a microfluidic channel (6.0 mm long, 100 μm wide, and ~20 μm high) spanning two 4.0 mm-diameter reservoirs was fabricated from PDMS. Next, 100-nm

thick gold electrodes (no adhesion layer, Evaporated Metal Films, Ithaca, NY) were microfabricated on glass slides by standard photolithographic techniques. Finally, the PDMS and glass were exposed to an O_2 plasma (60 W, model PDC-32G, Harrick Scientific, Ossining, NY) for 15 s and then bonded together. The microband electrodes were positioned at the center of the channel and protruded from beneath the PDMS monolith so they could be interconnected via an external jumper wire.

Three distinct new electrode designs were used in these experiments (Figure 3.1). The split BPE (Figures 3.1d and 3.1e) is most similar to the 500 μm-long continuous BPEs used in our previous studies.[8-10] The outer edges of the split BPE are separated by 500 μm and there is a 50 μm gap at its center. The total electrode area exposed to the solution is 4.5×10^{-4} cm^2. This design was used to determine the current passing through the BPE. The second type of BPE is an array of 15 gold microband electrodes consisting of 40 μm lines and spaces (Figures 3.1b and 3.1c). Current measurements at a pair of these microbands, which have an outer edge-to-edge distance of 520 μm and a total exposed area of 0.8×10^{-4} cm^2, were compared with those obtained using the split BPE to confirm that the current in the

microbands (and the corresponding effect on the electric field) is not significantly affected by the smaller exposed electrode area. This design was also used for all electric field profiling measurements. The third design consists of 15 microbands, but in this case the electrodes are 20 μm wide and the spaces between electrodes are 80 μm. This design was used solely for analyte transport experiments in which the wider gaps between electrodes provided a clearer view of the focused analyte movement.

Concentration enrichment experiments. Prior to each experiment, the microfluidic channel was rinsed by introducing 40.0 μL of 5.0 mM Tris buffer (pH 8.0) into the anodic reservoir and 15.0 μL into the cathodic reservoir. The buffer solution was allowed to flow through the microchannel for 20 min in response to the solution height differential (~2 mm). Next, the rinsing solution in each of the reservoirs was replaced with 40.0 μL of 0.1 μM $BODIPY^{2-}$ in 5.0 mM Tris. Additional microliter increments of the same solution were added to each reservoir in individual experiments as indicated in the Results and Discussion section.

Concentration enrichment experiments were carried out as follows. First, two microband electrodes having the

desired separation were connected via a conductive wire. Second, a driving voltage (E_{tot} = 35.0 V) was applied across the microchannel using a high-voltage power supply (LLS9120, TDK-Lambda Americas, Inc., San Diego, CA) connected to the microfabricated gold driving electrodes spanning the bottoms of the reservoirs. Finally, the extent of enrichment was determined by fluorescence microscopy.

Fluorescence measurements. Enrichment of the $BODIPY^{2-}$ tracer dye was monitored using a fluorescence microscope (Multizoom AZ100, Nikon, Japan) fitted with a CCD camera (QuantEM 512SC, Photometrics, Tucson, AZ, USA). An inverted epifluorescence microscope (Eclipse TE 2000-U, Nikon) fitted with a CCD camera (Cascade 512B, Photometrics) was only used to obtain images during controlled analyte transport experiments. Values of the enrichment factor were determined by comparing the region of maximum intensity in the concentrated band of dye to calibrated fluorescence intensities. All measurements were corrected for the background intensity.

Current measurements. Current flowing through the BPEs was measured by connecting pairs of microbands via an ammeter (Model 6517B Electrometer, Keithley Instruments, Inc., Cleveland, OH). As previously mentioned, the split

BPE design more closely mimicked the electrode area of a continuous BPE,[8-10] and therefore it provided a point of comparison for the current measured using the microband BPEs. Data were processed using LabView software (National Instruments, Austin, TX, USA). Simultaneous measurement of the total current through the microfluidic channel was achieved by monitoring the voltage drop across a 523 kΩ resistor in series with the microchannel. These measurements were made with a hand-held, digital multimeter equipped with PC-Link software (VA18B, Sinometer Instruments, ShenZhen, China).

Electric field profile measurements. The electric field profile within a buffer-filled channel was measured as follows. First, a pair of microbands having an appropriate spacing was connected to form a BPE. Second, the Keithley electrometer (set in voltage measurement mode) was connected between the pair of microband electrodes adjacent to the BPE on the anodic side of the channel. Third, 35.0 V was applied across the microchannel via the driving electrodes. When the measured voltage attained a constant value (~200 s), $\Delta E_{n,m}$ for all other neighboring pairs of microbands was measured. The voltage between the original pair of microbands was periodically re-measured to

ensure that its value remained constant during the experiment. Finally, this process was repeated several times using different pairs of microbands to define the BPE.

3.4 Results and Discussion

Concentration enrichment. Concentration enrichment is initiated by connecting two of the band electrodes in the microarray with a jumper wire, and then applying a suitable potential (E_{tot}) between the two driving electrodes (Figure 3.1b). In this configuration, the connected pair of microband electrodes behaves as a single, discontinuous BPE. When E_{tot} attains a sufficiently high value, water electrolysis is induced at the ends of the BPE. The resulting anodic and cathodic reactions are given in eqs 3.1 and 3.2, respectively.

$$2H_2O - 4e^- \rightarrow O_2 + 4H^+ \qquad E^\circ = 0.40\ V \qquad (3.1)$$

$$2H_2O + 2e^- \rightarrow H_2 + 2OH^- \qquad E^\circ = -0.83\ V \qquad (3.2)$$

$$TrisH^+ + OH^- \rightarrow Tris + H_2O \qquad (3.3)$$

A consequence of these processes is the neutralization of the buffer cation ($TrisH^+$) by OH^- generated at the cathode

end of the BPE (eq 3.3). This homogeneous reaction results in a region of low conductivity that starts at the cathode end of the BPE (right side, Figure 3.1) and extends into the anodic compartment of the microchannel. An extended electric field gradient results, which provides a region for analyte focusing.[8, 9]

The fluorescence micrograph shown in Figure 3.2a demonstrates concentration enrichment of $BODIPY^{2-}$ using a continuous BPE 800 s after the driving voltage (E_{tot} = 35.0 V) was applied. This result is consistent with our previous reports.[8, 9] Comparable behavior is observed at an array of microband electrodes (Figure 3.2b). In this experiment, electrodes 5 and 11 were externally connected, as shown schematically in Figure 3.1b, to form the BPE. The approximate potential drop across the BPE, ΔE_{elec}, is given by eq 3.4.

$$\Delta E_{elec} = \frac{E_{tot} \bullet l_{elec}}{l_{channel}} \qquad (3.4)$$

Here, $l_{channel}$ is the length of the channel (6 mm), l_{elec} is the effective length of the bipolar electrode (0.52 mm), and E_{tot} = 35.0 V. For this experiment, ΔE_{elec} = 3.0 V. Note that this simple analysis assumes all of E_{tot} is dropped within the channel and that the potential profile across the channel

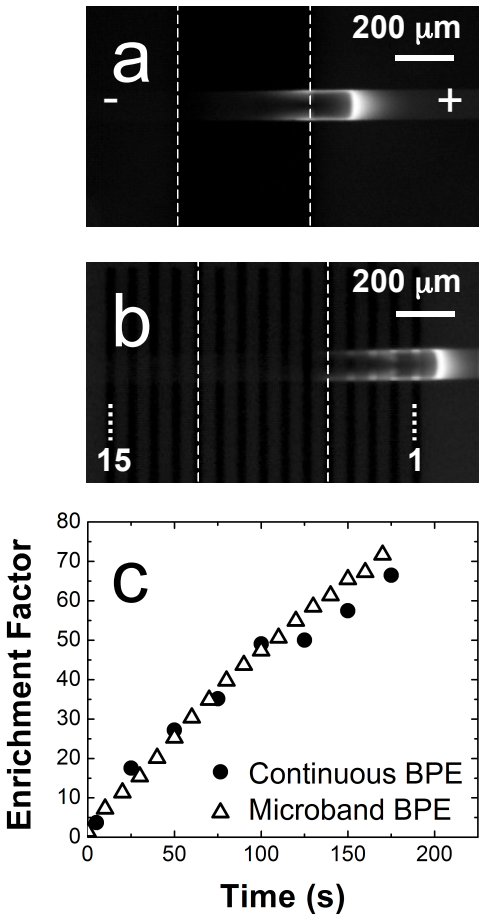

Figure 3.2. Fluorescence micrographs demonstrating concentration enrichment of BODIPY disulfonate after enriching for (a) 800 s at a continuous BPE of total length 500 μm and (b) 160 s at a microband array consisting of 40 μm lines and spaces in which electrodes 5 and 11 are connected to form a BPE of ~520 μm total length. Initial concentration of $BODIPY^{2-}$ is 0.1 μM in 5.0 mM Tris buffer (pH 8.0); E_{tot} = 35.0 V. (c) Comparison of the enrichment factor for $BODIPY^{2-}$ at the microband array BPE and a solid BPE. Enrichment factor is determined by dividing the maximum $BODIPY^{2-}$ concentration attained by the initial concentration.

is linear. However, we are mindful that this is just a useful approximation and that the real situation is slightly more complex.[3] For example, a fraction of E_{tot} is dropped at the driving electrodes.[49] Nevertheless, as will be explicitly demonstrated later, E_{tot} = 35.0 V is sufficient to drive the electrochemical reactions represented by eqs 3.1 and 3.2, even though they do not occur at their thermodynamic potentials. This results in the extended field gradient in solution that is required for analyte concentration. Indeed, $BODIPY^{2-}$ concentrates ~350 μm to the right of electrode 5, thereby exhibiting behavior very similar to that observed at the continuous BPE (compare Figures 3.2a and 3.2b).

Figure 3.2c is a plot of measured enrichment factor versus time for both the continuous and microband BPEs. The important point is that the time course of the enrichment is essentially independent of the electrode design. Specifically, both configurations result in an enrichment factor of ~70 after 180 s. The correspondence between the behavior of the two types of electrodes highlights the suitability of the microband array as a tool for developing a better understanding of continuous BPEs.

BPE current measurement. An important parameter that affects bipolar electrode focusing is the magnitude of the current passing through the BPE. Here, we compare this faradaic current for the split (Figure 3.1e) and microband (Figure 3.1b) BPE designs, and correlate these values to the onset of concentration enrichment. For these experiments, the two halves of the BPEs were connected in series with an ammeter external to the channel. We have previously shown that the presence of the ammeter does not significantly affect the current passing through the electrode.[3] The steady-state current (i_{BPE}) was measured in split and microband BPEs having similar total lengths (l_{elec} = 500 μm and 520 μm, respectively) during focusing of 0.1 μM $BODIPY^{2-}$ in 5.0 mM Tris buffer with E_{tot} = 35.0 V. For the split BPE, i_{BPE} = 271 nA and i_{tot} = 328 nA. For the microband array, i_{BPE} = 225 nA and i_{tot} = 285 nA. Importantly, ~80% of the total channel current is diverted through the BPE regardless of design. As discussed below, it is this high value of i_{BPE}/i_{tot} that is responsible for the modulation of the local electric field and hence focusing of the tracer. This relationship between the magnitude of the faradaic current and the onset of concentration enrichment is clearly observed at the very start of an experiment in a

newly prepared microfluidic device. Under these conditions, i_{BPE} is low when E_{tot} is first applied (i_{BPE}/i_{tot} < 20%). However, after a few minutes, i_{BPE} increases rather suddenly (i_{BPE}/i_{tot} > 80%). Importantly, this increase is accompanied by the onset of enrichment.

Because of the relationship between faradaic processes at the BPE and the onset of enrichment, it is important that E_{tot} be high enough to drive the necessary faradaic reactions. Accordingly, the split BPE configuration was used to measure the fraction of the total current that is carried by the BPE (i_{BPE}/i_{tot}) as a function of E_{tot} (Figure 3.3). Simultaneous measurement of i_{BPE} and i_{tot} is achieved by connecting the two halves of the BPE through an ammeter and monitoring the voltage drop across a resistor in series with the microchannel (inset of Figure 3.3). Measurements of i_{BPE}/i_{tot} at each value of E_{tot} were made at t = 1500 s which, in all cases, is several hundred seconds after this ratio achieved a constant value. The results in Figure 3.3 show that a threshold value of the driving voltage of between E_{tot} = 20.0 V and 25.0 V must be reached before a significant fraction of channel current is diverted through the BPE. Using eq 3.4, these values of E_{tot} correlate to ΔE_{elec} = ~1.7 V and ~2.0 V, respectively, which is consistent

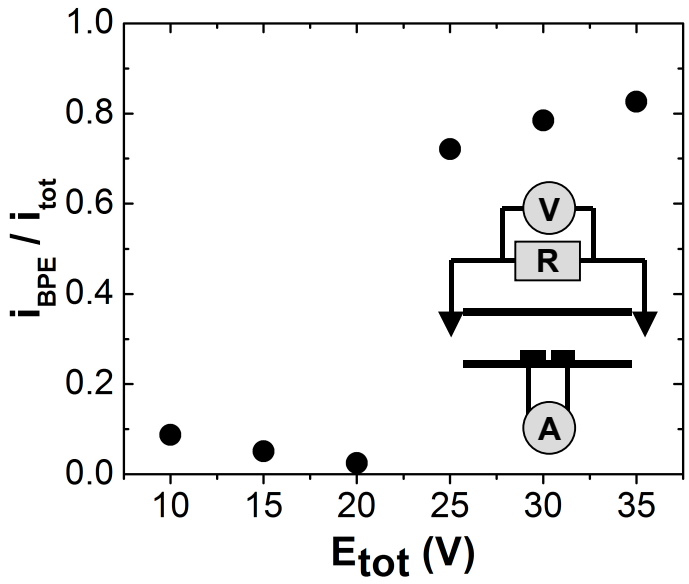

Figure 3.3. Steady-state ratio of BPE current (i_{BPE}) to total current (i_{tot}) obtained for several values of E_{tot} with 5.0 mM Tris (pH 8.0) and no $BODIPY^{2-}$. Values were recorded after driving voltage was applied >1500 s. Measurements were made with a split BPE configured as represented schematically in the inset.

with our earlier contention that electrolysis of water is responsible for i_{BPE}. This threshold provides a lower bound for the selection of E_{tot} while the upper bound is defined by the onset of O_2 and H_2 bubble formation at the BPE (eqs 3.1 and 3.2). The formation of bubbles is dependent not only on E_{tot} (and the associated heterogeneous reaction rate), but also on the rate of diffusive and convective transport, which prevent accumulation of the gases. A larger accessible range of E_{tot} allows greater breadth of control during the optimization of electric field characteristics.

Microchannel electric field profile measurements. The shape of the electric field gradient in the microchannel determines the extent and location of concentration enrichment. In this section, we show how the microband array can be used to map the field gradient, and then we compare the experimental results to numerical simulations. These experiments were carried out in several steps. First, the microchannel was filled with 5.0 mM Tris buffer (no $BODIPY^{2-}$) with an excess (8 μL, which corresponds to a 0.2 mm height difference) in the cathodic reservoir. Although an excess volume in the *anodic* reservoir tends to prevent concentration enrichment, excess volume in the *cathodic* reservoir is found to stabilize both enrichment and the

observed electric field profile. This might be due to a slight counterflow opposing the electroosmotic flow. Second, one pair of electrodes was connected via an external jumper wire to yield a bipolar electrode. Third, E_{tot} = 35.0 V was applied to initiate the formation of the electric field gradient used for focusing. Simultaneously, the voltage drop between the pair of electrodes adjacent to the BPE cathode was monitored until it reached steady state (~200 s). Fourth, the potential between the remaining electrode pairs (except those acting as the BPE) was sequentially measured to map out the electric field. Because the sensing microband electrodes are connected by a high-impedance voltmeter, they are not able to function as BPEs.

Figure 3.4a shows the steady-state electric field profile measured under enrichment conditions, but in the absence of the $BODIPY^{2-}$ tracer. Measured voltages are divided by the center-to-center distance between microbands to obtain the average field strength for each 80 μm segment. The results (and error bars) shown in Figure 3.4a represent data from several sets of measurements on two separate devices. Each set of measurements was taken using a different pair of electrodes to form the BPE (1 and 7, 5

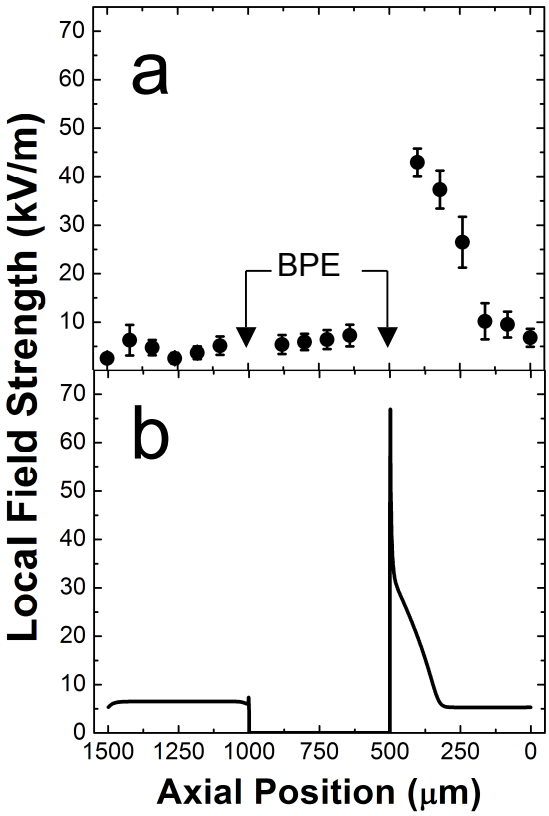

Figure 3.4. (a) Steady state electric field strength averaged over 80 μm distances between neighboring microband electrodes. The data is averaged over two separate devices. In each case, several maps of the electric field were obtained by using a different pair of microbands to define the BPE during each set of measurements. No $BODIPY^{2-}$, 5.0 mM Tris, E_{tot} = 35.0 V. (b) Simulated axial electric field at y = 3.5 μm at t = 60 s after application of driving voltage (at 5.83 kV/m). The 2D simulated geometry is 1500 μm long with a 3 μm tall BPE from x = 500 to 1000 μm. The zeta potential on the channel walls is assumed to be -85 mV. The initial condition is a uniform distribution of 5.0 mM Tris.

and 11, 6 and 12, or 9 and 15). The arrows in this figure indicate the location of the microbands comprising the BPE. The results indicate that there is a marked increase in the field strength to the right of the BPE cathode. The extended field gradient is at a maximum of ~40 kV/m at the BPE edge and gradually decreases to 10 kV/m at a distance of 400 μm from the electrode. The field strength continues to decrease at farther distances, but at a lower rate. It is also apparent that the electric field between the outer edges of the BPE is essentially unchanged. Finally, the electric field in the cathodic compartment does not reveal any defining features, but rather appears to be somewhat suppressed (4.0 kV/m average).

These findings compare favorably to numerical simulations with a continuous BPE. Complete details regarding the conditions used for the simulations have been provided previously.[9] Briefly, a 1500 μm segment of the microchannel with the 500 μm BPE at the center (x = 500 to 1000 μm) was approximated by a two dimensional model (Figure 3.4b). The time-dependent redistribution of ions in solution was modeled taking into consideration convection and diffusion, buffer reactions, faradaic processes, and the effects of the applied electric field (5.8 kV/m)

including electromigration of ions and electroosmotic flow. The initial condition is a uniform distribution of 5.0 mM Tris buffer. Figure 3.4b shows the resulting electric field profile at t = 60 s for a cross section 0.5 μm above the BPE surface. The magnitude of the electric field is zero over the interior of the BPE and close to 6.5 kV/m in the cathodic compartment. Most significantly, the results reveal the extended field gradient required for bipolar electrode focusing in the anodic compartment with a maximum field strength located at the edge of the BPE cathode and decreasing to the right.

There are two main differences between the simulated and experimental results. First, the simulation leads to a somewhat smaller magnitude and extension of the electric field gradient. This difference is most likely due to the ambiguity involved in selecting diffusion coefficients and reaction rates from the literature for simulation parameters. Taking this into consideration, along with the sensitivity of the system to small changes in conditions, the agreement of the resulting electric field gradient to within 30-40% of the measured magnitude is remarkably good. Second, in the simulation, the electric field in the region directly above the BPE is near zero. The absence of

complete suppression of the electric field over the BPE in the experimental results is unexpected considering the high magnitude of i_{BPE}/i_{tot}. When ~80% of the ionic current is diverted through the BPE, it is expected that the electric field in solution over the BPE will be ~80% weaker due to a simple Ohm's Law argument. However, this argument assumes that the solution resistance in the region over the BPE remains constant. If there is extensive depletion of ions above the BPE, increased solution resistance will proportionally augment the electric field in that region. While the simulations do account for some ion depletion in solution over the BPE, our electric field measurements indicate further depletion.

Unidirectional band motion. Microband arrays permit positional control of the focused tracer band within the microchannel. In this section, we describe the controlled transport of the enriched tracer zone between two locations, depending on which microbands are connected. We used a microband array having 20 μm lines and 80 μm spaces for these experiments. The wider spaces in this version of the microarray provide a clearer view of the focused analyte movement than the 40 μm spaces used for the just-described field profiling measurements. Positional control

of the enriched band was carried out as follows. First, 30.0 μL of 0.10 μM $BODIPY^{2-}$ and 5.0 mM Tris solution was added to each reservoir. Second, E_{tot} = 30.0 V was applied across the microchannel (ΔE_{elec} = 3.6 V). Third, to generate band movement, a switch was used to alternately connect two separate pairs of electrodes (1 with 8 and 7 with 14). Switching between the two configurations results in analyte focusing just to the right of either electrode 1 or electrode 7 (Figure 3.5a and 3.5b, respectively). These are referred to hereafter as positions 1 and 7. These fluorescent micrographs demonstrate the formation of a tracer band after switching to each position for 50 s and 25 s, respectively.

We observe that upon switching from position 1 to position 7, the band is transferred from right to left and stopped at position 7. However, upon switching back to position 1, the original band continues in the direction of the EOF, out of the channel, while a new band begins to form at position 1. Movie 1 (available in the Supplemental Materials to this dissertation), which plays at a frame rate 10x real time, demonstrates this phenomenon when the switch is triggered at 25 s, and thereafter at 50 s intervals. The mechanism for band relocation from 1 to 7 is

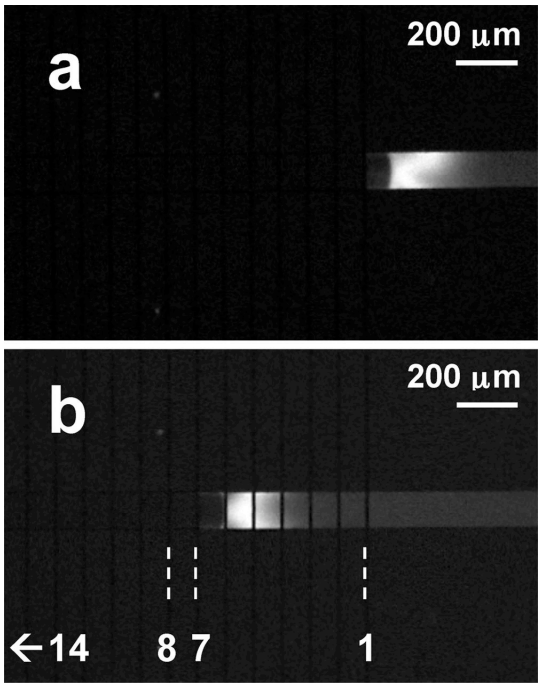

Figure 3.5. Fluorescence micrographs showing the concentrated band of $BODIPY^{2-}$ at two locations. The position is controlled by connecting different pairs of microbands to form the BPE. BPE comprised of electrodes (a) 1 and 8 (b) 7 and 14. The bands are enriched for 50 and 25 s respectively. 5.0 mM Tris, 0.1 μM $BODIPY^{2-}$, E_{tot} = 30 V.

explained by the redevelopment of the extended field gradient “downstream” (left) of the initial band location. The inability of the band to return from left to right is a consequence of reformation of the extended field gradient “upstream” in an area inaccessible to the band. This is strong evidence that electroosmosis dominates band motion except at the focusing location. This behavior also demonstrates that the electric field gradient forms very rapidly. After switching from position 1 to 7, the new field gradient must form at position 7 within ~2 s to ‘catch’ the concentrated tracer band. Contrast this time interval with that discussed earlier for the very first enrichment experiment carried out using a freshly prepared microfluidic device (a few minutes).

3.5 Summary and Conclusion

We have demonstrated bipolar electrode focusing at continuous and discontinuous BPEs in a microfluidic device. Three discontinuous designs, two microband arrays and a split BPE, provide an approximation of the continuous BPE system we have reported previously.[8-10] These new designs provide important insights into the focusing process. Measurement of the BPE current reveals an onset of

electrolysis above E_{tot} = 20.0 V ($\Delta E_{elec} \approx$ 1.7 V), and confirms that these faradaic reactions must proceed at an appreciable rate for enrichment to occur. Further investigation by mapping of the electric field in the vicinity of the BPE provides support for previously reported simulation results,[9] highlighting in particular the development of an extended field gradient in the anodic compartment.

Experiments and simulations reveal a 5 to 7—fold increase in the electric field adjacent to the BPE cathode relative to the strength of the average applied electric field. Finally, a novel means of analyte band transport has been developed that takes advantage of the flexibility of the microband array design. This approach might prove useful for extraction and subsequent delivery of discrete, concentrated packets of analytes to remote on-chip processing modules without the need for additional hardware or mechanical switches. More refined, bi-directional control over analyte band location may soon be achieved using a combination of microband arrays and pressure driven flow.

In ongoing research, we aim to use microband arrays for the simultaneous concentration, separation, and

electrochemical detection of analytes by employing additional bands for amperometric purposes. In the following chapters we demonstrate how electric field mapping can be used to correlate experimental conditions to the shape of the electric field.

Chapter 4: Bipolar Electrode Focusing: Tuning the Electric Field Gradient

4.1 Synopsis

Bipolar electrode (BPE) focusing is a developing technique for enrichment and separation of charged analytes in a microfluidic channel. The technique employs a bipolar electrode that initiates faradaic processes that subsequently lead to formation of an ion depletion zone. The electric field gradient resulting from this depletion zone focuses ions on the basis of their individual electrophoretic mobilities. The nature of the gradient is of primary importance to the performance of the technique. Here, we report dynamic measurements of the electric field gradient showing that it is stable over time and that its axial position in the microchannel is directly correlated to the location of an enriched tracer band. The position of the gradient can be tuned with pressure-driven flow. We also show that a steeper electric field gradient decreases the breadth of the enriched tracer band and therefore enhances the enrichment process. The slope of the gradient can be tuned by altering the buffer concentration: higher concentrations result in a steeper gradient. Coating the

channel with the neutral block co-polymer Pluronic also results in a steeper field gradient and more rapid enrichment.

4.2 Introduction

In this chapter, we report time-resolved measurements of the electric field gradient responsible for bipolar electrode (BPE) focusing in microchannels,[50] and correlate the location and slope of the gradient to the position and breadth of an enriched band of a fluorescent tracer. The results provide important information about the fundamental parameters that affect the focusing process. These include the buffer concentration, flow rate, applied field strength, and the effect of a neutral, polymeric coating on the microchannel walls. These observations are significant, because they provide a basis for understanding and optimizing concentration enrichment driven by BPE focusing. The key findings of this study are threefold. First, when left unperturbed, the electric field gradient remains stable over long periods of time (hundreds of seconds). This is consistent with previously published numerical simulations for this system.[9] Second, the location and slope of the electric field gradient, which control the position

and breadth of the enriched band, can be tuned by adjusting the flow rate and buffer concentration, respectively. Finally, addition of a neutral polymeric coating to the microchannel walls enhances enrichment by reducing Taylor dispersion and preventing bubble formation at the BPE even at high average field strength (V_m). This results in a steeper slope of the electric field gradient and therefore a higher degree of enrichment.

We have previously reported that a BPE can be used to alter the local electric field within a microchannel in a predictable way, and that the resulting field gradient can be used to concentrate and separate charged analytes.[8-10, 50] Specifically, when a voltage is applied to driving electrodes situated in reservoirs at the ends of a microchannel filled with an electrolyte solution, but lacking a BPE, the applied voltage (E_{tot}) is dropped approximately linearly over the length of the channel. The resulting electric field is illustrated by the dashed line in Scheme 4.1d. However, when a BPE is present in the channel (Schemes 4.1a and 4.1b), faradaic reactions may take place at its ends (Scheme 4.1c). This provides an alternative path for current flow, and hence distorts the distribution of electrolyte ions within the channel. This

Scheme 4.1

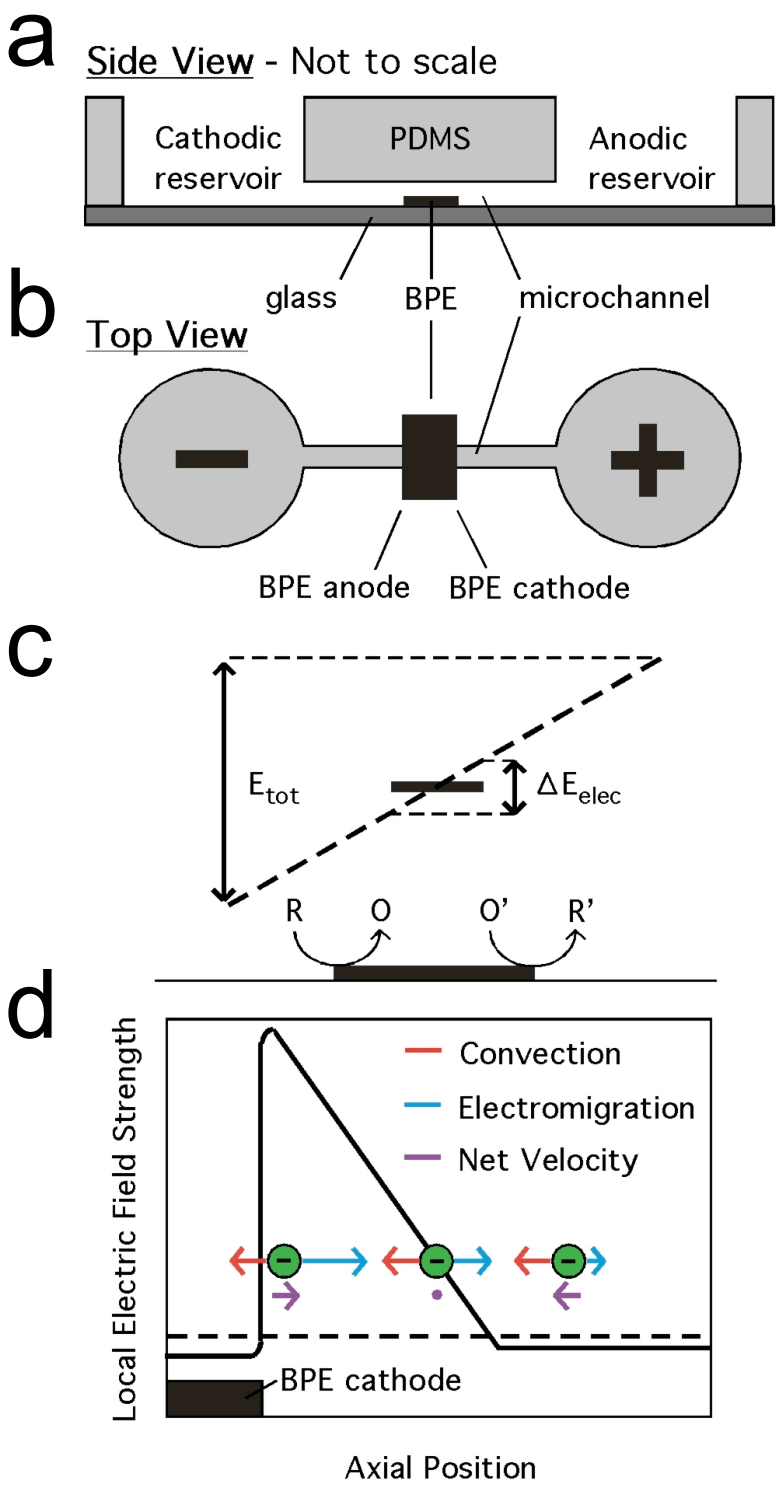
a
Side View - Not to scale
Cathodic reservoir
PDMS
Anodic reservoir
b
Top View
glass
BPE
microchannel
BPE anode
BPE cathode
c
E_{tot}
ΔE_{elec}
R
O
O'
R'
d
Local Electric Field Strength
Convection
Electromigration
Net Velocity
BPE cathode
Axial Position

in turn causes the simple linear voltage drop to adopt a more complex shape and gives rise to a gradient in the electric field. To illustrate this point, the solid line in Scheme 4.1d shows a typical field profile (confirmed by experimental measurements and simulations)[50] in the region adjacent to the BPE cathode and depicts the resulting enrichment of a fluorescent anionic tracer. As discussed later, enrichment is driven by the interplay between bulk flow and electrophoretic migration.

Analyte preconcentrators are a key component of lab-on-a-chip devices (LoCs).[46] One of the many advantages of LoCs is that they are capable of rapidly processing minute sample volumes (nanoliters) using networks of microchannels.[46] Many LoC applications, such as medical diagnostics, require analysis of analytes present at low concentrations. However, detection limit often suffers because the small cross-sectional area interrogated by the detector, coupled with low analyte concentration, translates to a small total number of analyte molecules. Therefore, local enrichment of the analyte in the detection volume is often desirable. Many methods have been developed to accomplish preconcentration in LoCs.[46] A recent review article summarizes the fundamental principles of BPE

focusing and describes its relationship to other concentration enrichment methods.[2] Briefly, BPE focusing falls under the category of electrokinetic equilibrium techniques, which also includes isoelectric focusing (IEF),[22, 25, 51] field amplified sample stacking,[12, 52] isotachoporesis,[15, 53] and counter-flow gradient focusing (CFGF) methods.[8, 54] BPE focusing is a CFGF method. CFGF methods balance electromigration velocity against a counterflow. In these methods, there is a gradient in electric field strength along a microchannel, and each analyte is focused at a unique location based on its electrophoretic mobility. Prominent examples include temperature gradient focusing (TGF),[42-45] electric field gradient focusing (EFGF),[55-60] and dynamic field gradient focusing (DFGF).[47, 61, 62] A very steep electric field gradient can also form at the boundary of a zone depleted of ions in an electrolyte-filled channel. Such depletion zones can be produced at junctions between micro- and nano-scale channels in a process termed ion concentration polarization (ICP).[39, 41, 63, 64] Han and coworkers exploited ICP to focus 33 fM green fluorescent protein 10 million-fold in 35 min (4760-fold/s).[39] The extent and rate of enrichment were found to be highly dependent on initial protein

concentration. For example, enrichment fell to 100-fold and a rate of 0.11-fold/s when the initial GFP concentration was increased from 33 fM to 33 nM. Others have observed a similar enrichment dependence on the initial concentration of analyte.[9, 35]

Previously we reported enrichment at an ion depletion zone formed by BPE focusing.[8-10, 50] In this chapter, the relationship between the electric field profile and enrichment behavior in BPE focusing is described, and we present guidelines for tuning the electric field properties to maximize enrichment. Specifically, we demonstrate that the slope of the field gradient increases with the concentration of the buffer, and this in turn leads to a narrower tracer band and more rapid enrichment. Decreasing the flow velocity (cathodic electroosmotic flow (EOF)) in the microchannel, through the addition of opposing pressure-driven flow, extends the ion depletion zone boundary further from the BPE and is accompanied by a corresponding shift of the enriched tracer location. Coating the channel walls with a non-ionic hydrophilic surfactant suppresses bubble formation at the BPE, thereby allowing the use of higher applied voltages and this leads to higher enrichment factors. The wall coating also

decreases non-uniform flow and associated Taylor dispersion. Finally, the strength and slope of an electric field gradient are shown to be stable over at least 400 s of continuous enrichment of an anionic fluorescent tracer, and the field strength at the focusing point can be predicted from simple electrokinetic equations.

4.3 Experimental

Chemicals. 4,4-difluoro-1,3,5,7,8-pentamethyl-4-bora-3a,4a-diaza-*s*-indacene-2,6-disulfonic acid ($BODIPY^{2-}$, Molecular Probes, Eugene, OR) was used as a fluorescent tracer to quantitate the degree of concentration enrichment. Molecular biology grade 1.0 M Tris—HCl buffer (Fisher Biotech, Fair Lawn, NJ) was diluted to concentrations of 1.0, 5.0, or 10.0 mM (pH 8.1) with deionized water (18.0 MΩ•cm, Milli-Q Gradient System, Millipore) and used as background electrolyte. The silicone elastomer and curing agent (Sylgard 184) used to prepare the poly(dimethylsiloxane) (PDMS) microfluidic devices were obtained from K. R. Anderson, Inc. (Morgan Hill, CA). Pluronic F108 (ethylene-oxide/propylene-oxide block copolymer) was obtained from BASF (Florham Park, NJ).

Device Fabrication. The hybrid PDMS/glass microfluidic devices and Au electrodes were fabricated by a previously published procedure.[5] Briefly, a microfluidic channel (6.0 mm long, 100 μm wide, and ~20 μm high) spanning two 4.0 mm-diameter reservoirs was fabricated from PDMS. Next, 100 nm-thick Au electrodes (no adhesion layer, Evaporated Metal Films, Ithaca, NY) were microfabricated on glass slides using standard photolithographic techniques. Finally, the PDMS and glass were exposed to an O_2 plasma (60 W, model PDC-32G, Harrick Scientific, Ossining, NY) for 15 s and then bonded together. The BPE was centered at the midpoint of the channel.

Two different electrode configurations were used in this study. For experiments in which enrichment alone was quantified, focusing was carried out using a continuous, 500 μm-long BPE that spanned the width of the channel. The BPE used for electric field measurements was of a split design (Figure 4.1a). Each half of the BPE was 225 μm long, and there was a 50 μm gap between them. Leads from the two halves of the split BPE extended outside of the microchannel and could be connected externally by a conductive wire so that they acted like a single, 500 μm-long BPE.[3, 6, 7, 50] This design simplified negative control

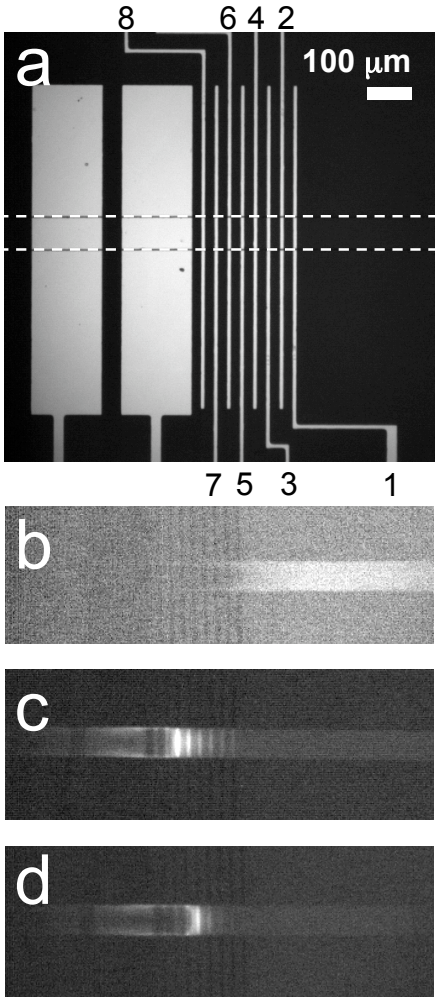

Figure 4.1. (a) Optical image of a split Au BPE and 8 Au microband electrodes used for measuring the electric field gradient. The split BPE has a total length of 500 μm and is interrupted by a 50 μm gap. The microbands are ~15 μm wide and are 40 μm on center. All electrodes span the 100 μm-wide microchannel (indicated by the dashed white lines). (b – d) Fluorescence micrographs showing enrichment of 100 nM $BODIPY^{2-}$ at E_{tot} = 35.0 V in (b) 1.0, (c) 5.0, and (d) 10.0 mM Tris (pH 8.1) with 8.5, 3.5, and 2.5 μL excess buffer solution in the cathodic reservoir, respectively. The images were obtained (b) 1500, (c) 800, and (d) 290 s after enrichment was initiated.

experiments, because the BPE was deactivated when the external connection was removed. To measure the electric field adjacent to the split BPE, 8 microband electrodes (each ~15 μm wide and having a center-to-center distance of 40.0 μm) were situated next to the cathodic pole of the BPE (Figure 4.1a). The microband electrodes also extended from beneath the PDMS monolith so they could be connected to a digital multimeter.

Concentration enrichment experiments. Prior to each experiment, the microfluidic channel was rinsed with buffer (1.0, 5.0, or 10.0 mM Tris, pH 8.1) by introducing a solution height differential (~2 mm) between the reservoirs, and allowing the buffer solution to flow through the microchannel for 20 min. Next, the rinsing solution in each of the reservoirs was replaced with 40.0 μL of buffer containing either 5.0 or 100 nM $BODIPY^{2-}$. In some cases, additional microliter increments of the same solution were added to each reservoir in individual experiments as indicated in the Results and Discussion section.

Concentration enrichment experiments were carried out by applying a driving voltage (E_{tot} = 35.0 or 60.0 V) across the microchannel using a high-voltage power supply

(LLS9120, TDK-Lambda Americas, Inc., San Diego, CA) connected to the microfabricated Au driving electrodes spanning the bottoms of the reservoirs. Simultaneously, the extent of enrichment was monitored by fluorescence microscopy.

Fluorescence measurements. Enrichment of the $BODIPY^{2-}$ tracer dye was monitored using a fluorescence microscope (Multizoom AZ100, Nikon, Japan) fitted with a CCD camera (QuantEM 512SC, Photometrics, Tucson, AZ, USA). Images were recorded at 1 s intervals by a CCD camera and analyzed by image processing software. Values of the enrichment factor were determined by comparing the region of maximum intensity in the concentrated band of dye to calibrated fluorescence intensities. Intensity traces showing the band profile along the channel length were obtained by averaging the fluorescence intensity across the middle 70 μm of the 100 μm-wide microchannel. All measurements were corrected for the background fluorescence intensity.

Removal of peaks in the fluorescence profiles caused by reflection of light. For experiments in which fluorescence intensity and electric field profiles were monitored simultaneously, an electrode arrangement having 8 Au microband electrodes (~15 μm wide and 40 μm on center)

adjacent to the BPE cathode was employed (Figure 4.1a). Reflection of fluorescence from the microbands resulted in evenly space peaks in the fluorescence intensity profiles, as shown in the black curve in Figure 4.2. For all such experiments, these spikes were removed from the data to clarify the position and shape of the enriched tracer band (red curve, Figure 4.2). This was done by deleting the data points comprising the reflection peaks and then interpolating between the remaining data points using graphing software (Origin 8.0, OriginLab Corporation, Northampton, MA). Specifically, the deleted data points were replaced using a cubic spline function, which interpolated based on the trajectory of the data points preceding and following the spike.

Electric field monitoring. The axial electric field profile was monitored using a scanning digital multimeter (SDMM, Model 2700, Keithley Instruments, Inc., Cleveland, OH) equipped with a multiplexer module (Model 7701, Keithley) and connected to the 8 microband electrodes described in the previous subsection. The SDMM was controlled in Microsoft Excel via the software provided by the SDMM manufacturer (ExceLinx, Keithley). The SDMM was interfaced to the microband electrodes through a breakout

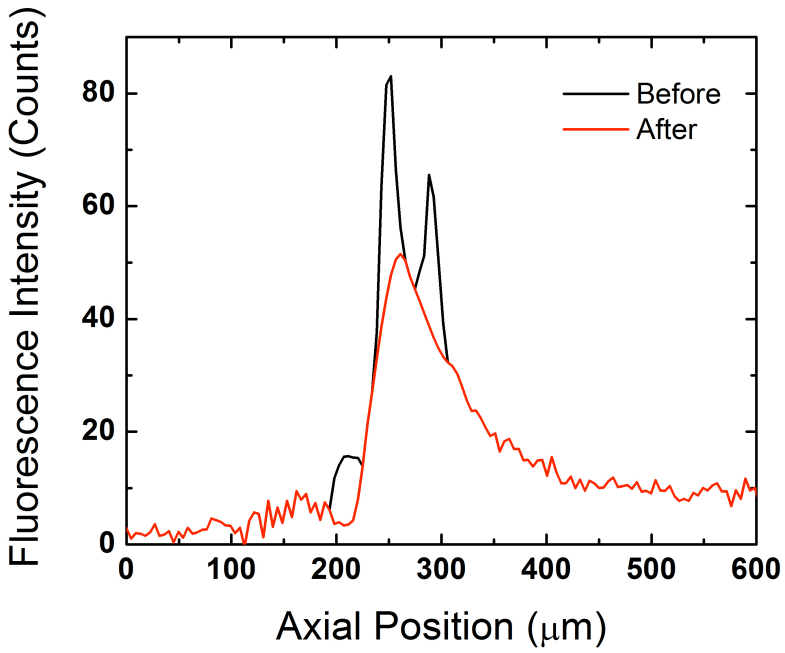

Figure 4.2. Background-subtracted fluorescence intensity as a function of position along the microfluidic channel (axial position = 0 at the cathodic edge of the BPE). The black spectrum was obtained before removing intensity spikes caused by reflection of fluorescence from the Au microband electrodes. The red spectrum was obtained after removal of the reflected intensity. The data shown here is taken from Figure 4.3c at t = 200 s.

board (screw terminals). The SDMM reads the difference between the two microbands farthest from the BPE first ($\Delta E_{1,2}$, Figure 4.1a), and then sequentially measures the potential between the second and third microbands ($\Delta E_{2,3}$) and so forth until the last pair ($\Delta E_{7,8}$) is reached. The acquisition time for each voltage measurement was ~0.1 s, and the voltage between pairs of microbands was read every 2 s. Electric field monitoring experiments proceeded as follows. First, the two halves of the BPE were connected via a conductive wire. Second, the SDMM was placed into scan mode. Third, a driving voltage (E_{tot} = 35.0 or 60.0 V) was applied across the microchannel via the driving electrodes. Scans were stored and plotted in real-time in Excel.

4.4 Results and Discussion

Electric field profile measurements. The local axial electric field strength in a microchannel can be visualized by recording the potential difference between neighboring pairs of Au microband electrodes fabricated on the bottom of the microchannel (Figure 4.1a). If the two halves of the split BPE are not connected, and E_{tot} = 35.0 V, then the calculated electric field strength throughout the

microchannel is V_m = 5.8 kV/m. If the two halves of the BPE are connected, then the resulting ΔE_{elec} ($\Delta E_{elec} \approx E_{tot}(l_{elec}/l_{channel})$ = 2.9 V, where l_{elec} is the length of the BPE, and $l_{channel}$ is the length of the microchannel) is sufficient to initiate the coupled faradaic reactions given in eqs 4.1 and 4.2 at the anodic and cathodic poles, respectively.[9, 50] This results in formation of an electric field gradient having the general characteristics of the solid line in Scheme 4.1d.

$$2H_2O - 4e^- \rightarrow O_2 + 4H^+ \qquad E^\circ = 0.40 \text{ V} \qquad (4.1)$$

$$2H_2O + 2e^- \rightarrow H_2 + 2OH^- \qquad E^\circ = -0.83 \text{ V} \qquad (4.2)$$

$$TrisH^+ + OH^- \rightarrow Tris + H_2O \qquad (4.3)$$

A consequence of the electrochemical reactions taking place at the BPE is that OH^- generated at the cathodic pole neutralizes $TrisH^+$ (eq 4.3).[9, 50] This results in a low conductivity zone near the cathodic pole of the BPE that is depleted of buffer cations, and therefore the local electric field in this region increases (Scheme 4.1d). Buffer anions migrate through this high-field, depletion zone faster than elsewhere in the channel, and therefore the concentration of Cl^- in the depletion zone decreases

too.[9, 50] The resulting enhanced electric field is observed to have a gradient shape, and it is this gradient that is measured in our experiments. During an experiment, as an anion (such as $BODIPY^{2-}$) is carried from the anodic toward the cathodic reservoir by electroosmotic flow (EOF), its average axial transport velocity is the sum of its mean velocity due to convection (u_m) and opposing electromigration (u_{ep}). As the molecule approaches the cathodic edge of the BPE, it encounters an increasing electric field strength, resulting in increased anodic u_{ep}. The molecule slows, ultimately focusing at a location where $u_m = -u_{ep}$ (Scheme 4.1d). Focusing behavior at the split BPE (Figure 4.1a) has been shown to be similar to that observed at a continuous BPE,[50] and typical enriched bands formed in 1.0, 5.0, and 10 mM Tris buffer are shown in Figures 4.1b-4.1d.

Temporal evolution of the electric field gradient. This subsection describes the formation of the electric field gradient and the subsequent enrichment of the anionic fluorescent tracer $BODIPY^{2-}$. The experiments were carried out as follows using the electrode design shown in Figure 4.1a. First, the reservoirs were filled with 40.0 μL of 5.0 mM Tris (pH 8.1) containing 100 nM $BODIPY^{2-}$. An additional

4.0 μL of the same solution was pipetted into the cathodic reservoir. This additional volume adjusts the flow in the microchannel to an optimal rate for enrichment in 5.0 mM Tris. Specifically, it ensures that enrichment begins within 10 s after application of the driving voltage and that the electric field gradient remains stable over time. Second, the two halves of the BPE were connected. Finally, a driving voltage (E_{tot} = 35.0 V) was applied to initiate enrichment.

Figures 4.3a and 4.3c show the location of the enriched tracer band upon application of the driving voltage on short and long time scales, respectively. Corresponding measured electric field profiles are provided in Figures 4.3b and 4.3d. Figure 2a reveals a slight enrichment of the tracer near the cathodic edge of the BPE (axial position = 0). During this initial stage of enrichment, the electric field gradient responsible for enrichment is not detectable (Figure 4.3b). This is because the depletion zone has not yet extended from the BPE cathode into the region monitored by the microbands. As shown in Figures 4.3c and 4.3d, an increase in field strength is first clearly observed at t = 100 s between the two pairs of microband electrodes closest to the BPE edge

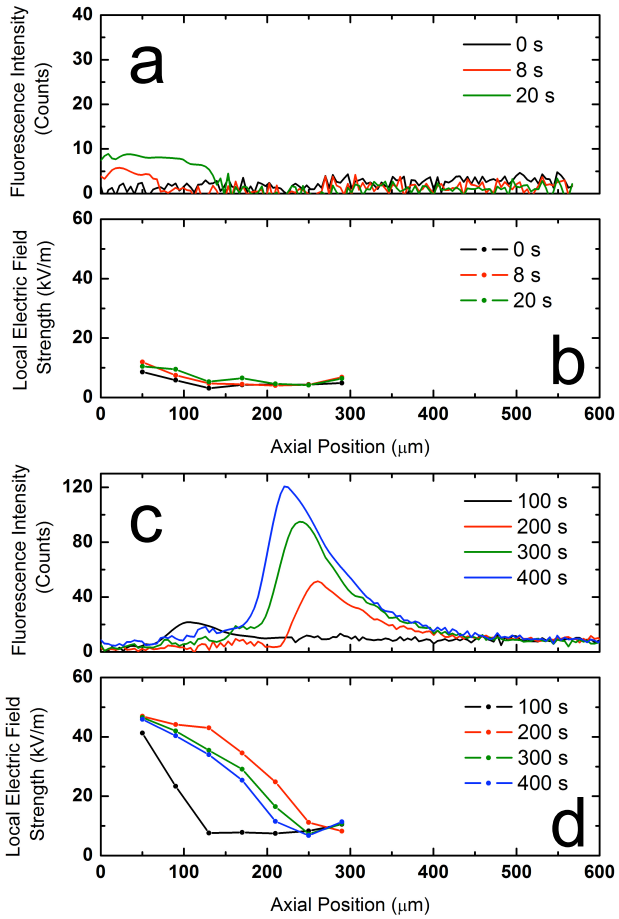

Figure 4.3. (a and c) Background-subtracted fluorescence intensity as a function of position along the microfluidic channel (axial position = 0 at the cathodic edge of the BPE). (b and d) Local axial electric field strength as a function of position. The microchannel was filled with 5.0 mM Tris (pH 8.1) containing 100 nM $BODIPY^{2-}$ and E_{tot} = 35.0 V. Pressure-driven flow was initiated by adding 4.0 μL of excess solution to the cathodic reservoir. Fluorescence and electric field profiles were collected every 1 s and 2 s, respectively, and selected time points are shown here to illustrate the evolution of the field on the (a and b) short time scale (0, 8, and 20 s), and (c and d) long time scale (100 - 400 s). The electrode arrangement shown in Figure 1a was used for these experiments.

($\Delta E_{7,8}$ and $\Delta E_{6,7}$). In Figure 4.3d, these positions are 50 μm and 90 μm away from the edge of the BPE, respectively. This evolving gradient in the field corresponds to a small peak in fluorescence intensity centered at ~100 μm (Figure 4.3c). Between 100 and 200 s the depleted ion region grows, the electric field gradient extends closer to the anodic reservoir, and the tracer band moves away from the BPE. The field gradient and the location of the enriched band begin to stabilize at t > 200 s, but both the height and width of the tracer peak continue to increase. Both of these peak characteristics are a consequence of $BODIPY^{2-}$ enrichment. That is, as the ionic strength in the region of $BODIPY^{2-}$ enrichment increases, the electric field gradient is reduced.[9] This latter point is important, because it suggests this focusing method will be most effective for low concentrations of analytes. It also implies that there is an upper limit to the local concentration of enriched tracer under a given set of conditions, which include the applied field strength and the ionic strength of the buffer.

As discussed earlier, the centroid of the tracer band is located at the lateral position where $u_m = -u_{ep}$ (Scheme 4.1d). Its position can be attributed to the *local* electric

field strength (V_l) at the focusing point, which is observed to be ~10 kV/m in this particular experiment. In the following calculation, this observed value will be compared with the theoretical value. Given the experimentally determined electrophoretic mobility, μ_{ep} = (-4.2 ± 0.2) x 10^{-4} $cm^2/V\bullet s$,[10] eq 4.4 can be used to calculate that u_{ep} = (-4.2 ± 0.2) x 10^{-2} cm/s for $BODIPY^{2-}$ when V_l = 10 kV/m.

$$u_{ep} = \mu_{ep} V_l \qquad (4.4)$$

The convective fluid velocity, u_m, can be approximated by measuring the electroosmotic velocity (u_{eo}) and subtracting the average velocity due to the opposing pressure driven flow. Recall that pressure driven flow was introduced by adding 4.0 μL of solution to the cathodic reservoir. The experimentally determined value of u_{eo} is (4.1 ± 0.2) x 10^{-2} cm/s. Numerical simulation indicates that the addition of 4.0 μL of solution to the cathodic reservoir reduces the average flow velocity by only 0.17 x 10^{-2} cm/s. Therefore, the calculated value of u_m ((3.9 ± 0.2) x 10^{-2} cm/s) is approximately equal and opposite in sign to the value of u_{ep} ((-4.2 ± 0.2) x 10^{-2} cm/s) when the experimentally determined V_l = 10 kV/m at the focusing point.

It should be noted that the value of the electroosmotic velocity (u_{eo}) used in the foregoing discussion was measured

in a channel containing a BPE and corresponds to an electroosmotic mobility (μ_{eo}) that is higher than that reported previously for a PDMS/glass microchannel under similar conditions. For instance, Hellmich et al. reported μ_{eo} = (2.3 ± 0.04) x 10^{-4} $cm^2/V\bullet s$ for 20.0 mM phosphate buffer (pH 8.2) in a hybrid PDMS/glass device which had been treated with an O_2 plasma prior to assembly in a manner similar to the devices used in our study.[65] The value of μ_{eo} can be calculated from the measured u_{eo} using the relationship given in eq 4.5.

$$\mu_{eo} = \frac{u_{eo}}{V_m} \qquad (4.5)$$

Here, V_m is the *mean* electric field strength (5.8 kV/m), which is used because variations in the local electric field, V_l, (and associated u_{eo} values) along the channel are mitigated by mass conservation in incompressible fluid flow and effectively averaged. The calculated value of μ_{eo} is (7.1 ± 0.4) x 10^{-4} $cm^2/V\bullet s$ in the presence of a BPE, which is significantly larger than the value we measure in the absence of a BPE (μ_{eo} = (5.3 ± 0.4) x 10^{-4} $cm^2/V\bullet s$) under similar conditions. This finding will be discussed in more detail later, but briefly, the increased apparent electroosmotic mobility is observed only in the presence of

a BPE and is due to the formation of the ion depletion zone. The local mobility ($\mu_{eo,l}$) is much higher in this zone due to the decreased ionic strength. The locally high mobility increases the average fluid flow velocity in the entire channel causing the measured u_{eo} and apparent μ_{eo} to be higher than expected.

Effects of buffer concentration and flow rate. The electric field gradient can be manipulated by exerting control over the experimental conditions. For example, the effect of Tris buffer concentration and flow rate on the field gradient is illustrated by the results shown in Figure 4.4. These two variables are considered together, because enrichment for each buffer concentration is optimized at a different convective flow rate. These experiments were carried out as follows. First, 40.0 μL of Tris buffer (1.0, 5.0, or 10.0 mM, pH 8.1) containing 100 nM $BODIPY^{2-}$ was added to each reservoir. Second, the BPE halves were connected. Third, E_{tot} = 35.0 V (V_m = 5.8 kV/m) was applied to initiate enrichment. Simultaneously, the fluorescence intensity and electric field profiles were recorded.

Figure 4.4a shows fluorescence intensity profiles obtained during enrichment of 100 nM fluorescent tracer in

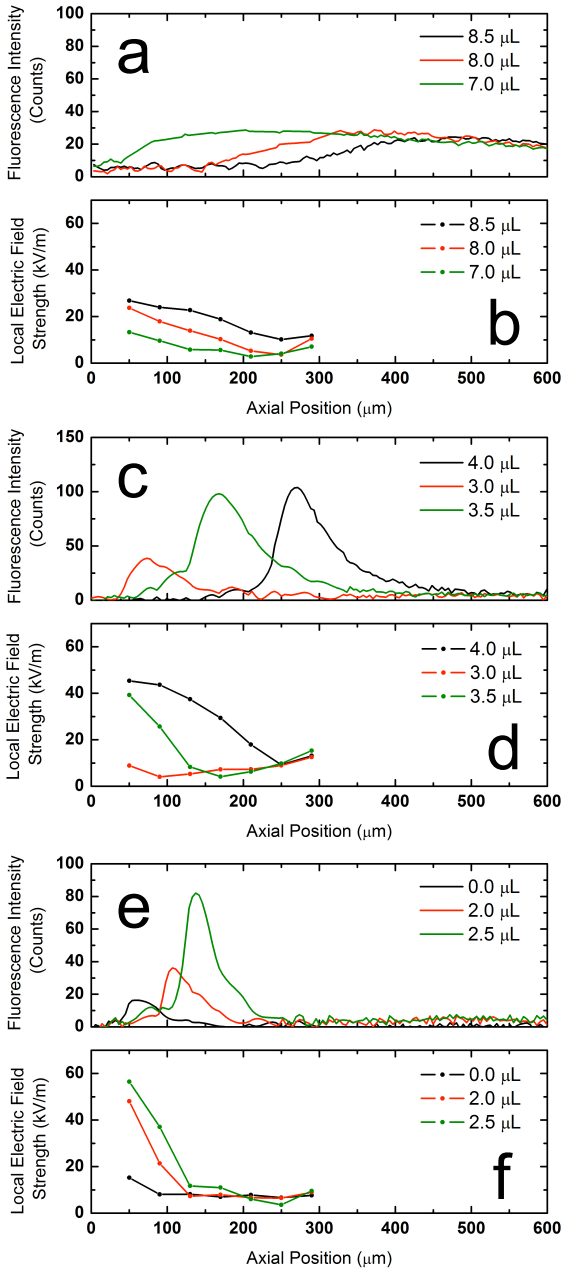

Figure 4.4. (a, c, and e) Background-subtracted fluorescence intensity as a function of position along the microfluidic channel (axial position = 0 at the cathodic edge of the BPE). (b, d, and f) Local axial electric field strength as a function of position. The microchannel was filled with 100 nM $BODIPY^{2-}$ plus (a and b) 1.0 mM, (c and d) 5.0 mM, and (e and f) 10.0 mM Tris (pH 8.1). Pressure-driven flow was initiated by adding the indicated volumes of excess solution to the cathodic reservoir. E_{tot} = 35.0 V.

1.0 mM Tris. In this experiment, enrichment did not begin immediately, but rather it was induced by addition of 8.0 μL of buffer/$BODIPY^{2-}$ solution to the cathodic reservoir. After enrichment began, the volume in the cathodic reservoir was increased and decreased multiple times in 0.5, 1.0, or 2.0 μL increments to change the position of the enriched band. These volume additions and removals were randomized to decouple total enrichment time from band position. Figure 4.4a shows fluorescence profiles for tracer enriched in 1.0 mM Tris with excess volumes of 8.5, 8.0, and 7.0 μL in the cathodic reservoir. These steps are reported in chronological order during a sequence in which volume was being removed in 0.5 μL increments. For each removal of 0.5 μL from the 4.0 mm-diameter cathodic reservoir, the solution height decreases by 0.04 mm, which is estimated by numerical simulations to increase the flow velocity (towards the cathodic reservoir) by 2.1×10^{-4} cm/s. As seen in Figure 4.4a, although this change is small, its effect on the position of the enriched band is marked. When a greater excess volume is present in the cathodic reservoir (on the left-hand side with respect to Figure 4.4a), the enriched band is located further from the BPE (i.e., to the right). Note that although 8.0 μL excess volume in the

cathodic reservoir was required to initiate enrichment, the focused band was maintained with an excess volume of just 7.0 μL.

The local electric field strength corresponding to the data in Figure 4.4a is plotted in Figure 4.4b. The most notable characteristics of these field gradients are that they have both low magnitudes and shallow slopes, which correlate to the broad, low-intensity tracer bands. The specific positions of the enriched tracer bands also correlate to the shape of the field gradients. Specifically, enrichment is excluded from regions in which V_1 is > ~10 kV/m. Note that the measured value of u_{eo} for 1.0 mM Tris (pH 8.1) in the presence of a BPE is 5.1 x 10^{-2} cm/s. The decrease in average linear flow velocity resulting from 8.0 μL excess solution in the cathodic reservoir is estimated to be 0.34 x 10^{-2} cm/s. Under these conditions, the band is expected to form at V_1 = 11.6 kV/m based on eq 4.4.

In contrast to the enrichment behavior observed for 1.0 mM buffer, the fluorescence line profiles for 5.0 mM Tris (Figure 4.4c) exhibit better-defined peaks. In this case, the experiment was initiated with 4.0 μL of excess solution in the cathodic reservoir, and this resulted in

formation of an enriched band centered ~270 μm to the right of the BPE edge. Next, 1.0 μL was removed from the cathodic reservoir (3.0 μL total excess), which results in the enriched band shifting toward the BPE. During this adjustment, the degree of enrichment decreased. This loss of fluorescence intensity is a consequence of leakage of the tracer over the BPE and toward the cathodic reservoir. That is, some of the tracer escapes from the concentrated band as it nears the edge of the BPE. Finally, 0.5 μL of buffer solution was added to the cathodic reservoir (3.5 μL total excess) restoring the band to an intermediate position. The fluorescence intensity profile shown in Figure 4.4c was obtained 100 s after addition of the buffer, and during this period it re-enriched to nearly the level observed with 4.0 μL excess buffer present.

Figure 4.4d demonstrates a locally enhanced maximum electric field ($V_{l,max}/V_m \approx 7$) in 5.0 mM Tris with the field strength exceeding 40 kV/m close to the BPE. Because the field gradient is steep, the tracer band is narrower compared to those observed for 1.0 mM Tris. Comparison of the location of the peak fluorescence intensity with the electric field profile at 3.5 μL excess solution (Figures 4.4c and 4.4d) reveals that the enriched band is focused in

a region where V_1 ~ 10 kV/m. Under these conditions, the theoretical value of the field strength at the focusing location is V_1 = 9.6 kV/m.

Finally, the data shown in Figures 4.4e and 4.4f, obtained in 10.0 mM Tris buffer, show a continuation of the trends described for the two lower concentrations. In this experiment, enrichment began immediately (no addition of buffer to the cathodic reservoir required) when E_{tot} = 35.0 V (Figure 4.4e). Once enrichment began, aliquots of 2.0 μL and then an additional 0.5 μL of buffer were added to the cathodic reservoir. This resulted in the enriched band moving to the right, and becoming more intense and narrower. The narrowness and location of the tracer bands (Figure 4.4e) correlate well with the steep slope and positioning of the electric field gradient (Figure 4.4f). Again, the band is focused at a location for which V_1 ~ 10 kV/m. Note that the calculated value of V_1 at the focusing location is 9.0 kV/m (based on the measured u_{eo} = 3.7 x 10^{-2} cm/s) when no pressure driven flow is added. The close correspondence between the measured and theoretical V_1 values for all three Tris buffer concentrations provides confidence in the model embodied by Scheme 4.1d.

It is important to examine the underlying principles responsible for the trends in the data presented in Figure 4.4. The first notable trend is that the slope of the field gradient is directly related to the concentration of the Tris buffer (Figures 4.4b, 4.4d, and 4.4f). This is because at higher concentrations, OH^- produced at the cathodic edge of the BPE reacts quickly, resulting in a narrow ion-depletion zone. For this reason, the tracer bands form close to the BPE in 10.0 mM Tris. Furthermore, the difference in conductivity in the depletion zone and elsewhere in the channel is greater in 10.0 mM Tris than at lower buffer concentrations. Taken together with the narrowness of the depletion zone, this difference in conductivity results in high local electric field strength (up to nearly 60 kV/m, $V_{l,max}/V_m \approx 10$). Perhaps the obvious question is why all enrichment experiments are not carried out in 10.0 mM Tris buffer (or even higher). The disadvantage of higher buffer concentration is that it increases the faradaic current at the BPE, leading to more rapid production of gas (eqs 4.1 and 4.2), and hence bubbles at the BPE.[50]

The second trend is that the amount of excess volume required in the cathodic reservoir to optimize enrichment

during a given experiment is lower at higher buffer concentrations. This is because the excess volume slows the flow rate, and at high buffer concentrations, the EOF is already slower due to a decrease in zeta potential at the microchannel walls. Therefore, the EOF alone is already optimal for enrichment. Furthermore, if too much excess volume is added to the cathodic reservoir during enrichment in 10.0 mM Tris, the electric field gradient collapses and the enriched band dissipates. This collapse is demonstrated in Figures 4.5a and 4.5b, which show the same data as was presented in Figures 4.4e and 4.4f with additional fluorescence and electric field profiles measured after adding a total of 3.0 and 3.5 μL of excess volume.

Quantitation of enrichment factor as a function of buffer concentration. Figure 4.6a shows typical enrichment factors (EFs) achieved within the first 900 s after applying E_{tot} = 35.0 V across unmodified (no Pluronic, vide infra) PDMS/glass microchannels containing 1.0, 5.0, and 10.0 mM Tris and 100 nM $BODIPY^{2-}$. These data were obtained using a microchannel having a continuous 500 μm BPE situated at the center and no microband electrodes. This simplified design is ideal for determination of EFs, because otherwise reflection of the tracer fluorescence from microband

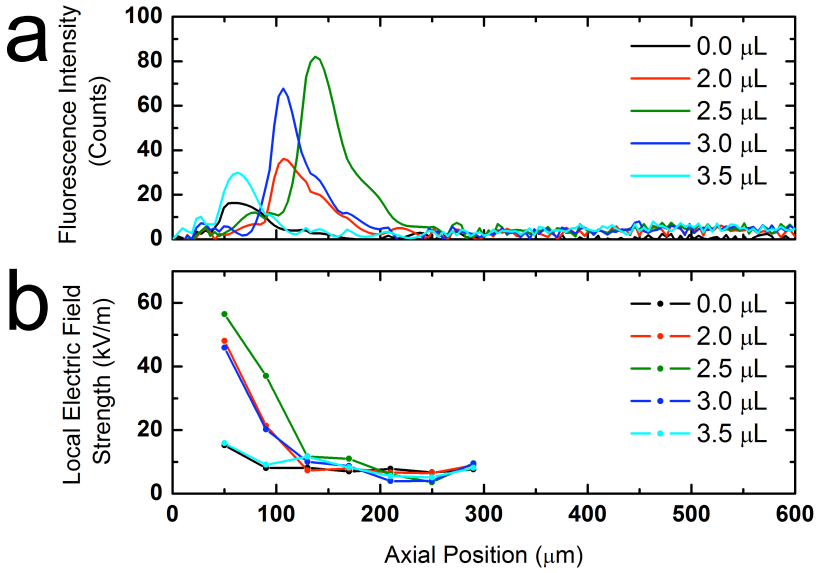

Figure 4.5. (a) Background-subtracted fluorescence intensity as a function of position along the microfluidic channel (axial position = 0 is at the cathodic edge of the BPE). (b) Local axial electric field strength as a function of axial position. The microchannel contained 100 nM $BODIPY^{2-}$ plus 10.0 mM Tris (pH 8.1). Pressure-driven flow was initiated by adding the indicated volumes of excess solution to the cathodic reservoir. E_{tot} = 35.0 V.

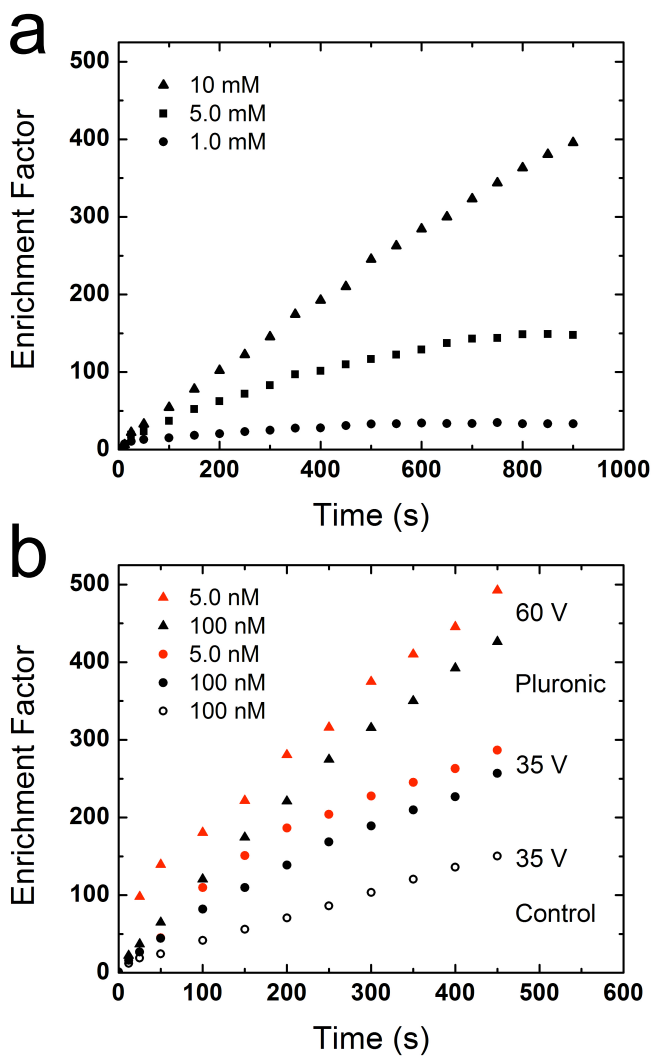

Figure 4.6. Plot of enrichment factor vs. time. (a) The enrichment experiments were carried out using solutions containing 100 nM $BODIPY^{2-}$ and 1.0, 5.0, or 10.0 mM Tris (pH 8.1). Pressure-driven flow was initiated by adding 8.0, 4.0, and 0 μL, respectively, of excess solution to the cathodic reservoirs. E_{tot} = 35.0 V. (b) The enrichment experiments were carried out in microchannels modified with Pluronic (see main text) and using solutions containing 5.0 mM Tris (pH 8.1) and either 5.0 or 100 nM $BODIPY^{2-}$. E_{tot} = 35.0 or 60.0 V as indicated in the figure. No pressure-driven flow was required to initiate concentration enrichment. The control experiment was identical to the others carried out at E_{tot} = 35.0 V, but the channel was not modified with Pluronic. The 500 μm split BPE (no microband electrodes) was used for this experiment.

electrodes interferes with the analysis. To obtain EFs, the reservoirs are first filled with 40.0 μL of Tris buffer solution containing the $BODIPY^{2-}$ tracer. The 1.0, 5.0, and 10.0 mM Tris enrichment experiments began with 8.0, 4.0, and 0.0 μL of excess volume in the cathodic reservoir, respectively, to optimize and stabilize the enriched band. Second, E_{tot} = 35.0 V was applied across the microchannel, and the subsequent enrichment of the tracer was monitored by fluorescence microscopy. EFs were determined by comparing the maximum fluorescence intensity in the enriched band to calibration curves of fluorescence intensity versus tracer concentration.

The results in Figure 4.6a show that enrichment proceeds more rapidly as the Tris concentration is increased. The rate of enrichment from t = 25 s to 300 s is linear for 1.0, 5.0, and 10.0 mM Tris and is measured to be 0.05-fold/s, 0.23-fold/s, and 0.46-fold/s, respectively. The maximum EF also increases with buffer concentration. The maximum enrichment achieved in 1.0 mM and 5.0 mM Tris were 33-fold and 145-fold, respectively. The EF did not plateau in 10.0 mM Tris and continued to increase past 400-fold at 900 s. To understand these results, recall that the enhancement of the electric field in the depleted-ion

region is caused by a disparity in conductivity between the ion-depletion region and the rest of the channel. The magnitude of the field enhancement ($V_{l,max}/V_m$) is proportional to the ratio of the conductivities inside and outside the depletion region. This ratio is larger at higher buffer concentration. For instance, $V_{l,max}/V_m \approx 7$ and 10 for 5.0 and 10.0 mM Tris, respectively (Figure 4.4). Furthermore, as the local concentration of $BODIPY^{2-}$ increases, it augments the local ionic strength, which, as we have already discussed, negatively impacts the slope of the electric field gradient. That is, when the enriched band concentrates sufficiently, the boundary between the depletion zone and the buffer becomes less distinct and a maximum EF obtains. This causes the EF-versus-time plot (Figure 4.6a) to plateau. The effect of this enrichment saturation is two-fold. First, as already mentioned, the maximum achievable EF is higher for higher buffer concentrations. Second, for a given buffer concentration, a lower initial tracer concentration results in higher enrichment. We have reported and discussed this trend previously.[9] Higher EFs for analytes initially present at lower concentrations was also observed by Han and

coworkers.[39] Though they did not address this trend, it was pointed out subsequently by Shackman and Ross.[54]

Enrichment in a microchannel coated with a neutral surfactant and at a higher driving voltage (E_{tot}). Previously, we reported enhanced enrichment of 100 nM $BODIPY^{2-}$ (~600-fold in 200 s, 3-fold/s) during separation experiments when the microchannel was coated with the neutral block copolymer Pluronic.[10] In this subsection, we compare enrichment in coated and uncoated microchannels, and correlate the EF to the electric field characteristics. The enrichment of $BODIPY^{2-}$ in a Pluronic-coated microchannel is shown in Figure 4.6b. In these experiments, the channel walls were coated by introducing a 3.0 μM solution of Pluronic in 10.0 mM Tris (pH 8.1) and allowing it to stand for 20 h. As a control, a second microchannel was similarly filled with Pluronic-free buffer solution. After coating, the microchannels were thoroughly rinsed with 5.0 mM Tris (pH 8.1) by introducing a ~2 mm height differential between the reservoirs and allowing the solution to flow for 5 min. This was repeated once more with fresh buffer. Next, the reservoirs were emptied, and then 40.0 μL of 5.0 mM Tris (pH 8.1) containing 5.0 or 100 nM $BODIPY^{2-}$ was added to each

reservoir. Finally, a driving voltage was applied across the channel to initiate enrichment (E_{tot} = 35.0 or 60.0 V).

The resulting EF versus time plots (Figure 4.6b) have three distinct characteristics. First, under all conditions, a slightly higher enrichment factor was achieved with the lower $BODIPY^{2-}$ concentration. Second, for a particular set of experimental conditions, enrichment occurs more rapidly in the coated channels. This point will be discussed in more detail in the next subsection. Third, bubble formation at the BPE is suppressed in the Pluronic-coated channels, and therefore it is possible to use higher values of E_{tot} which lead to higher EFs. As discussed later, this enhancement is attributed to a steeper electric field gradient and faster transport of the tracer to the enrichment zone. For example, Pluronic coating alone increases the rate of enrichment of 100 nM $BODIPY^{2-}$ from 0.36-fold/s to 0.57-fold/s, reaching over 250-fold enrichment in 450 s. Increasing the driving voltage to E_{tot} = 60.0 V brings the enrichment rate to 0.96-fold/s, nearing 450-fold in 450 s.

Electric field profile measurements in a microchannel coated with a neutral surfactant (E_{tot} = 35.0 and 60.0 V). Here we describe the nature of the electric field profile

in Pluronic-coated channels. These measurements were carried out exactly as described for the uncoated channels. Briefly, the electroosmotic mobility of the buffer solution was suppressed by coating the PDMS microchannels with Pluronic as described in the previous subsection. Second, the microchannel reservoirs were each filled with 40.0 μL of 100 nM $BODIPY^{2-}$ in 5.0 mM Tris (no pressure-driven flow). Third, the two halves of the BPE were connected via a conductive wire. Fourth, the SDMM was activated to scan the potential difference between neighboring microband electrodes. Finally, E_{tot} = 35.0 or 60.0 V was applied across the channel to initiate enrichment.

Figures 4.7a and 4.7b show the fluorescence intensity traces and corresponding electric field profiles, respectively, obtained during a typical enrichment of 100 nM $BODIPY^{2-}$ in 5.0 mM Tris at E_{tot} = 35.0 V. Comparison of this enrichment behavior with that shown in Figures 4.3c and 4.3d under the same conditions, but in an uncoated channel, reveals three important characteristics. First, no pressure-driven flow was required to reach conditions appropriate for enrichment, which is consistent with the fact that the electroosmotic flow velocity is slower in a Pluronic-coated channel. Second, the enrichment of the dye

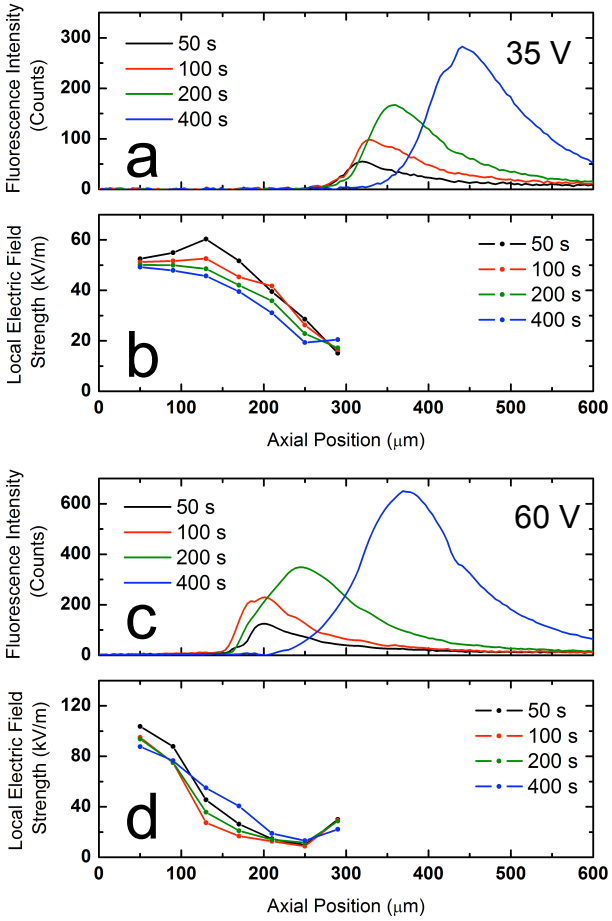

Figure 4.7. Evolution of the (a, c) background-subtracted fluorescence intensities and (b, d) local axial electric field strengths as a function of time in the absence of pressure-driven flow. The walls of the microchannel were coated with Pluronic, and the channel was filled with a solution containing 5.0 mM Tris and 100 nM $BODIPY^{2-}$. (a and b) E_{tot} = 35.0 V, and (c and d) E_{tot} = 60.0 V. The axial position = 0 at the cathodic edge of the BPE.

is significantly enhanced in the coated channel: within 400 s of applying E_{tot}, the EF is ~180 versus ~75 in the uncoated channel. Third, the electric field profile is not markedly different in the coated and uncoated channels, having a similar maximum value of ~50 kV/m and extending 250-300 μm to the right of the BPE.

Despite the presence of similar electric field gradients in coated and uncoated channels at E_{tot} = 35.0 V, enrichment is significantly enhanced in the coated channels. This can be attributed to a reduction in electroosmotic mobility differentials along the channel. As mentioned earlier, the width of the enriched band is determined mainly by the steepness of the electric field, but it can be greatly increased by Taylor dispersion. The electroosmotic velocity in the ion-depleted region ($u_{eo,l}$) is significantly increased due to *both* the enhanced electric field and the low ionic strength, which results in increased zeta potential at the channel walls. If the driving force for EOF in the depletion zone becomes significantly greater than in neighboring channel segments, parabolic backflow, and even vortex flow, can develop.[64, 66, 67] The band broadening due to these phenomena is worse than Taylor dispersion arising from simple laminar flow.[68] Maynes

et al. derived a useful relationship (eq 4.6) for estimating the width of a peak focused along an electric field gradient when taking electroosmotic velocity differentials into account.[68]

$$s = \sqrt{\frac{D_{im} + \left(\frac{u_{eo,l}}{u_m} - 1\right)^2 \frac{a^2 u_m^2}{52.5 D_{im}}}{\left|\mu_{ep} m\right|}} \qquad (4.6)$$

Here, s is the standard deviation of the width of a focused band, D_{im} the diffusion coefficient of the focused species, a the half-height of a 2-D (parallel plate) rectangular channel, and m the local slope of the electric field gradient.[68] Importantly, in the absence of electroosmotic velocity differentials ($u_{eo,l} = u_m$), eq 4.6 simplifies to include only three parameters determining the peak width: the molecular diffusivity (D_{im}), the electrophoretic mobility (μ_{ep}), and the electric field gradient slope (m). Note that, in this case of uniform flow, a steeper slope of the electric field gradient is the only experimental variable (related to Taylor dispersion) providing access to improved enrichment. More significantly, eq 4.6 suggests two possible solutions for limiting dispersion induced by the non-uniform EOF. Taylor dispersion will lessen with

suppression of the EOF (decreasing $u_{eo,1}$) while maintaining the same u_m, or with a reduction in channel dimensions (a).

This mathematical treatment (eq 4.6) explains the enhanced enrichment observed in Pluronic coated channels. The coating protocol used here[10] suppresses the EOF by decreasing the wall charge. To understand this enhancement, consider the limiting case in which the charge on the channel walls is zero, and all flow (u_m) is pressure driven. In this case, variations in ionic strength and V_1 along the channel will no longer have an adverse effect on the uniformity of flow.

Finally, we consider the effect of increasing E_{tot} on the enrichment process. Figures 4.7c and 4.7d show the outcome of an experiment conducted under the same conditions used to obtain the results shown in Figures 4.7a and 4.7b, but here E_{tot} = 60.0 V. As before, no pressure-driven flow was used. Two important comparisons may be made between the results obtained at E_{tot} = 35.0 and 60.0 V. First, the extent of enrichment at 400 s increased from EF ~180 to ~410. Second, the maximum field strength and the slope of the gradient are both increased at the higher value of E_{tot}. At E_{tot} = 35.0 V the maximum field strength measured at t = 400 s is ~48.0 kV/m and the slope of the

gradient is 1.50 x 10^5 kV/m^2. By comparison, at E_{tot} = 60.0 V (t = 400 s), these quantities are ~87 kV/m and 4.18 x 10^5 kV/m^2.

There are three reasons for the improvement in EF at higher values of E_{tot}. First, transport of the tracer to the focusing zone is faster. Recall that the dominance of convective flow (driven by EOF) over electromigration is responsible for moving the tracer from the anodic reservoir to the focusing location. Therefore, it is necessary that $\mu_{eo} > \mu_{ep}$. The corresponding dominance of electroosmotic over electrophoretic velocity ($u_{eo} > u_{ep}$) between the anodic reservoir and focusing location is magnified at higher field strengths, resulting in faster enrichment. Second, the electric field gradient is steeper. This may be due to higher faradaic current passing through the BPE leading to faster production of OH^- and subsequent neutralization of $TrisH^+$. A steeper field gradient signifies a sharper transition in ionic strength inside and outside the depletion zone. A third reason for enhanced enrichment is the increase of both sequestering forces, convection (u_{eo}) and opposing electromigration (u_{ep}) of the tracer, at the focusing location at higher E_{tot}.

4.5 Summary and Conclusion

In conclusion, we have reported simultaneous measurements of the evolution of the electric field gradient and an enriched tracer band during BPE focusing. These studies have provided insight into the factors affecting the location of the band and extent of enrichment. We also correlated the location of the band to the position of the field gradient and the specific local electric field strength at which the convective and electrophoretic velocities of the tracer balanced. These findings make it possible to tune the slope of the electric field gradient and its position by modulating the concentration of the buffer, the flow velocity, and the applied electric field strength. More rapid enrichment is achieved at higher buffer concentrations and higher applied fields, both of which increase the slope of the electric field gradient. Coating the channel with the neutral surfactant Pluronic does not have a significant impact on the magnitude or slope of the electric field gradient, but nevertheless the coated channels lead to a significant increase in enrichment rate. This enhancement is understood to be the result of decreased Taylor dispersion.

Specifically, the neutral coating suppresses non-uniform EOFs throughout the channel.

The following chapter describes how the findings reported here were used to achieve even greater enrichment. Ongoing research will focus on measurement of the electric field gradient during separation experiments. These measurements will be especially interesting, because our previous studies indicated that mixed analytes concentrate in different locations compared to the individual components.[10] This finding implies a complex and dynamic electric field profile in the case of mixed analytes.

Chapter 5: Bipolar Electrode Focusing: Significantly Enhanced Focusing in a Dual Channel Configuration

5.1 Synopsis

Bipolar electrode (BPE) focusing locally enriches charged analytes along an electric field gradient against an opposing counter-flow. In this chapter, we demonstrate significantly enhanced enrichment (up to 500,000-fold) of an anionic fluorescent tracer and introduce a dual-channel configuration allowing more rapid enrichment (up to 71-fold/s). These improvements are accomplished using a device design that is simpler than that used for similar techniques. Finally, we discuss similarities between the formation of an ion depletion zone at a BPE to depletion at a micro-/nano-channel junction by ion concentration polarization.

5.2 Introduction

In this chapter, we describe the use of bipolar electrodes (BPEs) for focusing and concentrating analytes by up to 500,000-fold in a microfluidic channel (Scheme 5.1).[8–10, 50, 69] Additionally, enrichment rates as high as 71-fold/s were reached in a dual-channel fluidic configuration (Scheme

Scheme 5.1

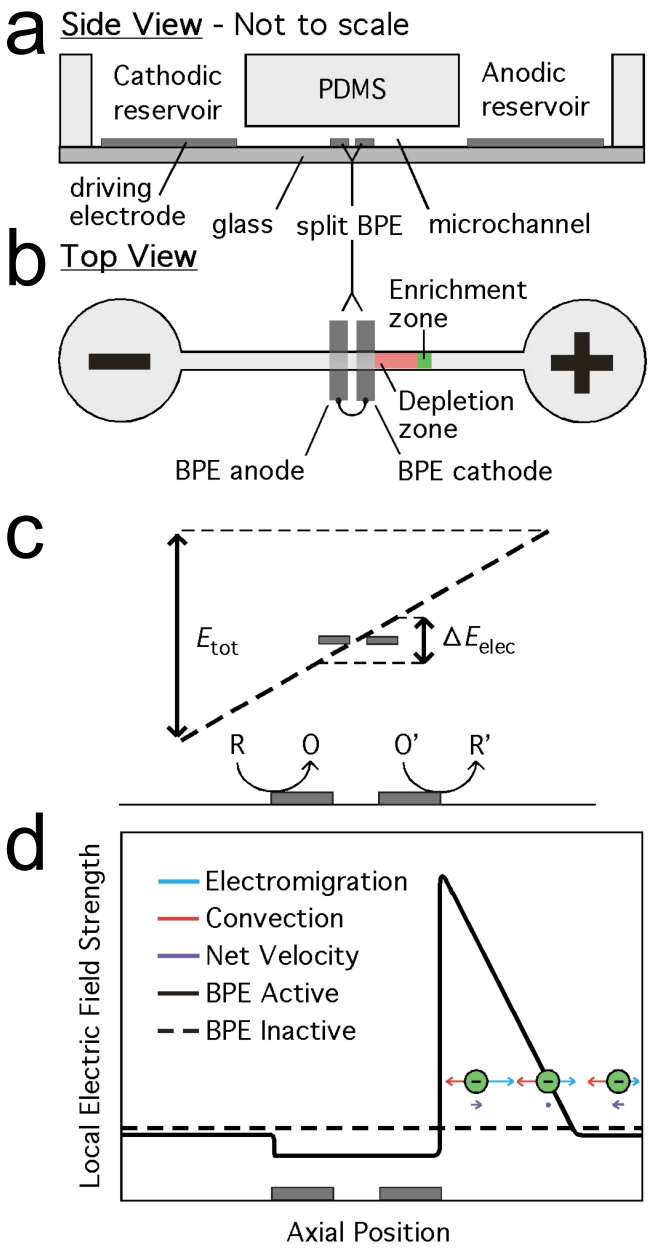
a
Side View - Not to scale
Cathodic reservoir
PDMS
Anodic reservoir
driving electrode
glass
split BPE
microchannel
b
Top View
Enrichment zone
Depletion zone
BPE anode
BPE cathode
c
E_{tot}
ΔE_{elec}
R
O
O'
R'
d
Local Electric Field Strength
Electromigration
Convection
Net Velocity
BPE Active
BPE Inactive
Axial Position

5.2) that decouples the applied driving voltage, which is required for focusing, from the potential drop across the BPE. Importantly, we show that faradaic electrochemistry at a BPE can be used to generate ion depletion and enrichment zones at the BPE ends in a way that is analogous to ion concentration polarization (ICP) at micro-/nano-channel junctions. This is a significant finding, because our 'faradaic ICP' method produces the same type of ion depletion zone as ICP but without the need for fabricating channels having nanometer-scale features.

Lab-on-a-chip devices (LoCs) offer many opportunities for new sensing and sample processing strategies including: high resolution separation,[70, 71] single-cell manipulation,[70, 72] nanoscale transport investigation,[73, 74] and microdroplet chemistry[75, 76] among many others.[77] The advantages of LoC technology lie in the characteristic micro- to nanoscale fluidic components, which enable precise handling of very small volume (pL – nL) samples while also introducing transport phenomena unique to this size scale. However, detection of analytes in LOCs can be challenging due to the combination of small detection volumes and low concentration of analytes frequently encountered.

Scheme 5.2

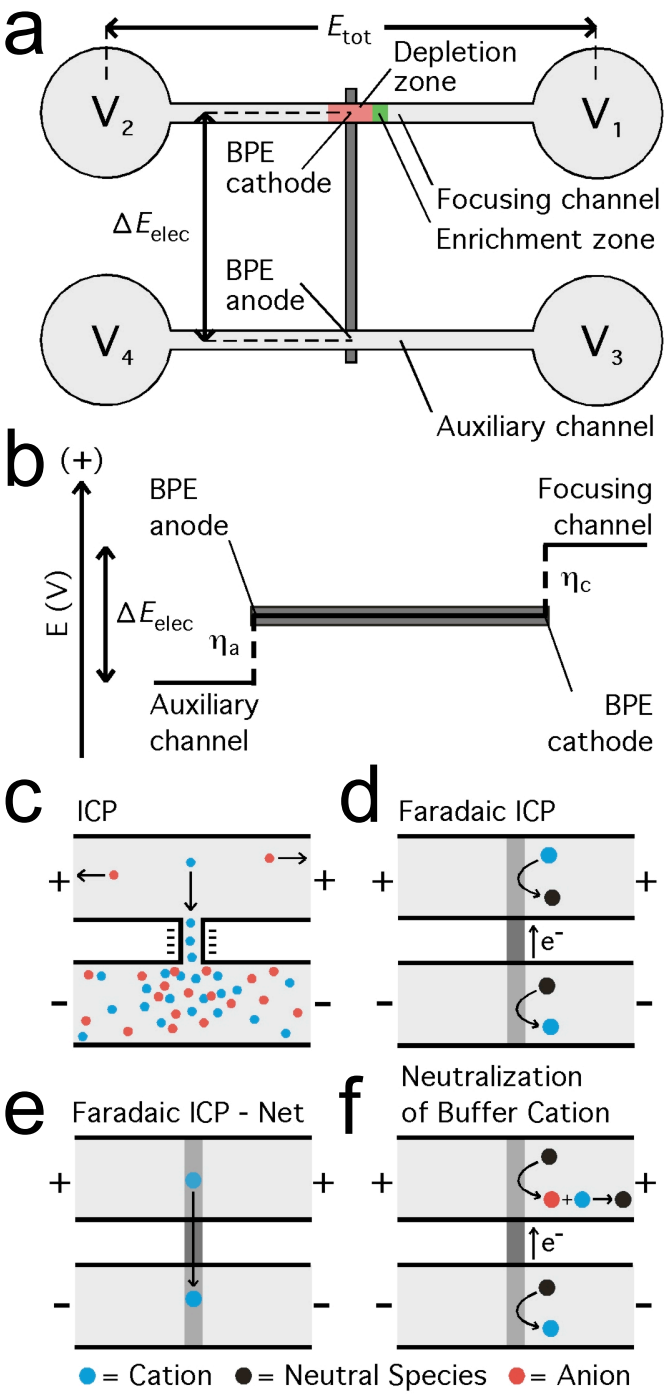
a
E_{tot}
Depletion zone
V_2
V_1
BPE cathode
ΔE_{elec}
Focusing channel
Enrichment zone
BPE anode
V_4
V_3
Auxiliary channel
b
(+)
BPE anode
Focusing channel
E (V)
ΔE_{elec}
η_c
η_a
Auxiliary channel
BPE cathode
c
ICP
d
Faradaic ICP
e
Faradaic ICP - Net
f
Neutralization of Buffer Cation
= Cation
= Neutral Species
= Anion

Therefore, local enrichment of analyte concentration in the detection volume is highly desirable.

Many methods have been developed to accomplish analyte enrichment in LoCs.[46] One of these was developed by us, and we refer to it as BPE focusing.[2] Briefly, BPE focusing is a counter-flow gradient focusing (CFGF) method in which electromigration velocity is balanced against a counter-flow.[8, 54] CFGF methods have in common a gradient in electric field strength along which each analyte focuses at a unique location based upon its electrophoretic mobility. CFGF methods fall under the broader category of electrokinetic equilibrium techniques, which also includes isoelectric focusing (IEF),[22, 25, 51] field amplified sample stacking,[12, 52] and isotachophoresis.[15, 53] Other CFGF methods include temperature gradient focusing (TGF),[42, 43, 45] electric field gradient focusing (EFGF),[55-60] and dynamic field gradient focusing (DFGF).[47, 61, 62]

If concentration enrichment, rather than separation, is the primary goal of a CFGF method, then the steepest possible local electric field gradient is desirable. Such a gradient can form at the boundary of a zone depleted of ions in an electrolyte-filled channel. Just such a depletion zone can be produced at a micro-/nano-channel

junction in a process called ion concentration polarization (ICP).[35, 39, 41, 63] This approach results in very rapid enrichment. For example, Wang et al. enriched 33 pM green fluorescent protein at a depletion zone boundary 100,000-fold in just 60 min (28-fold/s).[39] The authors reported further enrichment, up to 10^7-fold in 40 min using a lower initial concentration (33 fM) of green fluorescent protein.[39]

BPE focusing also enriches analytes at a depletion zone boundary, but in this case the electric field gradient forms near a BPE (Scheme 5.1d). Previously, we reported using this method to concentrate a fluorescent anionic tracer by a factor of ~500.[10, 69] Here we report 500,000-fold enrichment of a tracer, present at an initial concentration of 10.0 pM, within 150 min (56-fold/s) using a BPE in a single microchannel. We also introduce a dual-channel arrangement, which leads to more rapid enrichment, reaching 130,000-fold in just 30 min (72-fold/s). These performance gains result from a better fundamental understanding of the experimental parameters affecting enrichment in BPE focusing. Specifically, a 12.5-fold reduction of the height of the microchannel relative to our previous fluidic design leads not only to reduction in Taylor dispersion,[68, 69] but

also provides access to higher applied field strength and higher buffer concentration, both of which increase the slope of the electric field gradient (Scheme 5.1d).[69] The further performance gain observed in the dual-channel arrangement is due to decoupling of the driving voltage (E_{tot}) from the voltage drop over the BPE (ΔE_{elec}) (Scheme 5.2a). This makes it possible to use higher values of E_{tot}, which in turn leads to enhanced enrichment. Finally, we show that the electric field gradient formed at a BPE is equivalent to that obtained at the micro-/nano-channel junction in ICP.

5.3 Experimental

Chemicals. 4,4-difluoro-1,3,5,7,8-pentamethyl-4-bora-3a,4a-diaza-*s*-indacene-2,6-disulfonic acid ($BODIPY^{2-}$, Molecular Probes, Eugene, OR) was used as a fluorescent tracer to quantitate the degree of concentration enrichment. A 1.0 M stock solution of Tris•$HClO_4$ (pH 8.0) was prepared from reagent grade Tris(hydroxymethyl)aminomethane (Sigma-Aldrich, Inc., St. Louis, MO) by dissolution in deionized water (18.0 MΩ•cm, Milli-Q Gradient System, Millipore) and subsequent titration with 2.0 N $HClO_4$ (Ricca Chemical Co., Arlington, TX). This stock solution was diluted to

concentrations of 10.0 or 100.0 mM (pH 8.0) and used as background electrolyte. The silicone elastomer and curing agent (Sylgard 184) used to prepare the poly(dimethylsiloxane) (PDMS) microfluidic devices were obtained from K. R. Anderson, Inc. (Morgan Hill, CA).

Device Fabrication. The hybrid PDMS/glass microfluidic devices and Au electrodes were fabricated by a previously published procedure.[5] Briefly, a microfluidic channel spanning two 4.0 mm-diameter reservoirs was fabricated from PDMS. The microchannel was 6.0 mm-long and either 100 μm wide and 21 μm high or 10 μm wide and 1.6 μm high. Next, 100 nm-thick Au electrodes (no adhesion layer, Evaporated Metal Films, Ithaca, NY) were microfabricated on glass slides using standard photolithographic techniques. Finally, the PDMS and glass were exposed to an O_2 plasma (60 W, model PDC-32G, Harrick Scientific, Ossining, NY) for 15 s and then bonded together. The BPE was centered at the midpoint of the channel.

Two principal device configurations were used in this study. Single-channel focusing experiments and current measurements were carried out using a split, 100 μm-long BPE that spanned the width of the channel (Schemes 5.1a and 5.1b and Figure 5.1a). Each half of the BPE was 35 μm long,

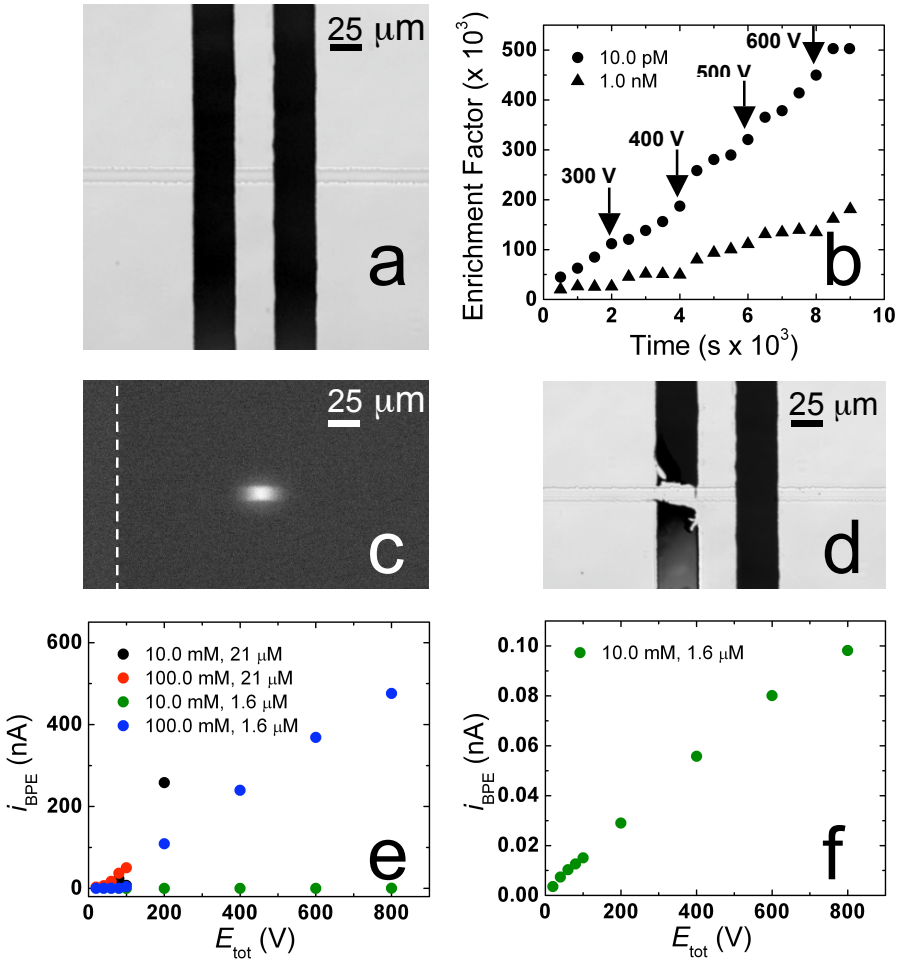

Figure 5.1. (a and d) Optical micrograph of a 10 μm wide, 1.6 μm high PDMS microchannel crossing a 100 μm wide Au split BPE (a) before and (d) after a 150 min enrichment experiment. (b) EF (thousands) obtained over time for initial concentrations of 10.0 pM (circles) and 1.0 nM (triangles) $BODIPY^{2-}$ in 100 mM Tris•$HClO_4$ (pH 8.0) after application of E_{tot} = 200 V and increasing by 100 V at 2000 s intervals. Arrows indicate time of each increase in E_{tot}. (c) Fluorescence micrograph of an enriched band of $BODIPY^{2-}$ with an initial concentration of 1.0 nM in 100 mM Tris•$HClO_4$ (pH 8.0). The band was enriched for 1000 s at E_{tot} = 200 V to ~30,000-fold (30 μM). The dashed white line indicates the cathodic edge of the BPE. (e and f) Plots of i_{BPE} (through 100 μm-wide Au split BPE) versus E_{tot} for both a 100 μm wide, 21 μm high channel and a 10 μm wide, 1.6 μm high channel filled with either 10.0 mM or 100 mM Tris•$HClO_4$ (pH 8.0).

and there was a 30 μm gap between them. Leads from the two halves of the split BPE extended outside of the microchannel and could be connected externally by a conductive wire so that they acted like a single, 100 μm long BPE.[3, 6, 7, 50] This design allowed the current flowing through the BPE (i_{BPE}) to be measured by connecting the two halves of the electrode with an ammeter (Model 2700 electrometer, Keithley Instruments, Inc., Cleveland, OH). Driving electrodes consisted of a microfabricated Au electrode spanning the bottom of each reservoir (Scheme 5.1a). For dual-channel experiments, two 1.6 μm high and 10 μm wide channels, formed from two separate PDMS monoliths, were placed into electrochemical contact at their center with a 12.0 mm long, 50 μm wide BPE (Scheme 5.2a). Driving electrodes for the dual channel experiment consisted of a coiled Au wire immersed in each of the four reservoirs.

In addition to the two principal configurations described in the previous paragraph, two modified dual-channel devices were also used: one to measure i_{BPE}, the current through the BPE, and another to measure ΔE_{elec} (Scheme 5.2b), the difference in solution potential between its ends. The first design was the same as that shown in Scheme 5.2a with the exception that the BPE was split at

the center with the two halves connected with an ammeter (Scheme 5.3). This design allowed i_{BPE} to be measured. The second design was also like that in Scheme 5.2a, except two 20 μm wide Au bands were spaced 65 μm away from the edges of one end of the BPE and connected to external leads (Scheme 5.4, not to scale). This design makes it possible to estimate ΔE_{elec}. In this case, the potential experienced by each of the two microbands versus V_2 (ground, Schemes 5.4a and 5.4b) was measured via a digital multimeter (Model 2700 electrometer, Keithley Instruments, Inc.). The two measurements were averaged to estimate the potential of the solution directly contacting the BPE. This measurement was carried out independently for both ends of the BPE using just one pair of microbands by taking the measurement at one end and then interchanging the roles of the focusing and auxiliary channels (Schemes 5.4c and 5.4d). The difference in solution potential measured at the two ends of the BPE was taken to be ΔE_{elec}.

Concentration enrichment experiments. Prior to each experiment, the microfluidic channel was rinsed with buffer (100.0 mM Tris, pH 8.0). In the single-channel configuration this was carried out by applying E_{tot} = 50.0 V, and allowing the buffer solution to flow through the

Scheme 5.3

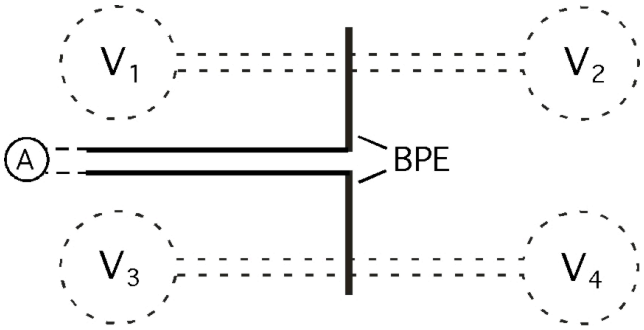

Scheme 5.4

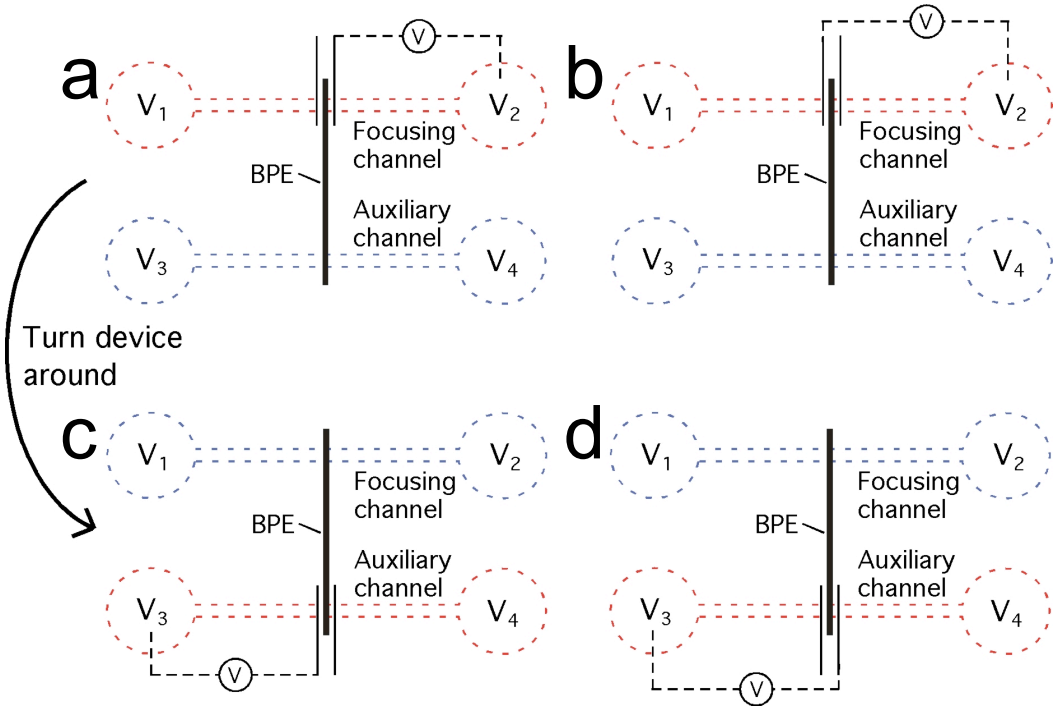
a
b
c
d
V
V1
V2
V3
V4
BPE
Focusing channel
Auxiliary channel
Turn device around

microchannel for 5 min by electroosmosis. In the dual-channel configuration, four separate potentials (V_1, V_2, V_3, and V_4 in Scheme 5.2a) were applied using voltage pattern (VP) 1 (Table 5.1). Finally, the rinsing solution in each of the reservoirs of both device configurations was replaced with 40.0 μL of buffer containing either 10.0 pM or 1.0 nM $BODIPY^{2-}$.

For single-channel experiments, concentration enrichment was carried out by applying a driving voltage (E_{tot} = 200 V to 600 V) across the microchannel using a custom-built, high-voltage power supply that incorporated a high-power, C-series voltage source (Ultra Volt, Ronkonkoma, NY) connected to the microfabricated Au driving electrodes spanning the bottoms of the reservoirs. In dual-channel experiments, concentration enrichment was carried out by applying the VPs shown in Table 5.1 and discussed in the Results and Discussion section. Simultaneously, the extent of enrichment was monitored by fluorescence microscopy.

Fluorescence measurements. Enrichment of the $BODIPY^{2-}$ tracer dye was monitored using an inverted epifluorescence microscope (Eclipse TE 2000-U, Nikon) fitted with a CCD camera (Cascade 512B, Photometrics). Images were recorded

Table 5.1 Voltage patterns employed in the dual-channel configuration.

Voltage Pattern	V_1 (V)	V_2 (V)	V_3 (V)	V_4 (V)
1	50.0	Ground	50.0	Ground
2	200	Ground	Ground	Ground
3	300	Ground	50.0	50.0

at 5 or 10 s intervals and analyzed by image processing software (V++ Precision Digital Imaging, Digital Optics Limited, Auckland, New Zealand). Values of the enrichment factor (EF) were determined by comparing the region of maximum intensity in the concentrated band of dye to calibrated fluorescence intensities. All measurements were corrected for the background fluorescence intensity.

5.4 Theory and Background

Ion concentration polarization at micro-/nano-channel junctions. Many excellent review articles exist on the topic of ICP.[63, 67, 78] Briefly, for ICP to occur, ionic current flowing between two compartments, across which a potential bias is applied, must be carried by a significant majority of either cations or anions. In the case that cations are the majority charge carrier, a depletion zone forms in the anodic (+) compartment and enrichment of both cations and anions occurs in the cathodic (-) compartment (Scheme 5.2c). This scenario may be induced by connecting two microchannels by a nanochannel having walls with fixed negative charges. Counter-ions (cations in this case) shield the charge on the wall, forming an electrical double layer (EDL). If the EDLs on opposing walls overlap, then

there will be selective transport of cations through the nanochannel. If, however, the EDLs do not overlap, ionic current will be carried by both cations through the EDL (i_{EDL}) and cations and anions through the bulk solution (i_b). In the latter case, ICP may still occur if a large majority of the current is carried through the EDL.[78] The magnitudes of i_{EDL} and i_b are determined by the EDL (σ_{EDL}) and bulk (σ_b) conductivities, respectively, the ratio of which is defined as the Dukhin number (D_u) as shown in eq 5.1.

$$D_u = \sigma_{EDL}/\sigma_b \qquad (5.1)$$

Santiago and coworkers have shown that ICP is best characterized by an inverse Dukhin number ($1/D_u$) such that in the case of complete double layer overlap eq 5.2 applies.[78]

$$1/D_u = \sigma_b/\sigma_{EDL} = 0 \qquad (5.2)$$

Comparison of traditional ICP and faradaic ICP between two microchannels. An important result reported here is that a BPE connecting two microchannels can also lead to ion depletion and enrichment zones by way of faradaic reactions. This situation is illustrated in Scheme 5.2d. Here, the reduction of a cation to a neutral species proceeds at the BPE cathode. The reverse process occurs at the BPE anode. These two processes, which must occur at the

same rate to maintain electroneutrality, are equivalent to selective transport of cations from the anodic (+) microchannel to the cathodic (-) microchannel (Scheme 5.2e). This situation is analogous to perfectly selective cation transport through a negatively charged nanochannel (that is, $1/D_u = 0$), and can likewise result in the formation of ion depletion and enrichment zones in the anodic and cathodic microchannels, respectively. Note that in faradaic ICP the challenge of fabricating nanochannels is eliminated.

Despite the analogy between 'faradaic ICP' and traditional ICP alluded to in the previous paragraph, there are also some important differences. First, the charge of ions generated and consumed (neutralized) at the ends of the BPE is determined by the identity of the faradaic reactions. For example, instead of 'transporting' a cation from the anodic to cathodic microchannel, as shown in Schemes 5.2d and 5.2e, two different faradaic reactions could occur at the BPE ends. For example, a cation could be neutralized (reduced) at the BPE cathode while an anion could be neutralized (oxidized) at the BPE anode. In this case, the result would be generation of an ion depletion zone in each channel. This flexibility is significant,

because it provides greater control over charge transport than traditional ICP. Second, the transport process is mediated by faradaic reactions. If faradaic ICP is used as a model to study traditional ICP, the rate of the faradaic reactions employed must be limited by mass transport and not electron-transfer kinetics. This is true because traditional ICP is entirely mass transport controlled. Third, the BPE introduces selectivity that is not available in traditional ICP. Specifically, a nanochannel transports ions based on charge (and size in the case of sterically hindered transport), while the BPE generates or neutralizes ions selectively on the basis of the interfacial potential and the reduction potential of the redox molecule. This selectivity requires that ΔE_{elec} be maintained at the magnitude necessary to drive the desired half reactions at the BPE ends. Finally, the BPE results in perfectly selective charge transport, which can only be approached in traditional ICP.

Faradaic ICP configuration. Scheme 5.2f depicts the reaction sequence used for faradaic ICP in the present study. Cations are generated by the oxidation of neutral species at the BPE anode in the bottom channel of Scheme 5.2f. This is accomplished by the reaction shown in eq 5.3.

$$2H_2O - 4e^- \rightarrow 4H^+ + O_2 \qquad E^\circ = 0.40\ V \qquad (5.3)$$

Anions are generated by the reduction of neutral species at the BPE cathode (top channel). The anion then goes on to neutralize a buffer cation. These two reactions are governed by eqs 5.4 and 5.5.

$$2H_2O + 2e^- \rightarrow 2OH^- + H_2 \qquad E^\circ = -0.83\ V \qquad (5.4)$$

$$OH^- + TrisH^+ \rightarrow Tris + H_2O \qquad (5.5)$$

The net result of eqs 5.3-5.5 is the same as that shown in Scheme 5.2e: 'transport' of a cation from the anodic to cathodic microchannel and corresponding formation of ion depletion and enrichment zones. Importantly, the rate of water electrolysis (eqs 5.3 and 5.4) is not limited by mass transfer, but rather by electron-transfer kinetics. In this respect, the behavior of this particular faradaic ICP configuration is unlike traditional ICP in which the transfer of charge is limited by the rate of mass transfer of ions to the micro-/nano-channel intersection. This is important, because it impacts the rate of formation of ion enrichment and depletion zones. Furthermore, because water is a neutral molecule, its transport to the BPE is not affected by the electric field as is the case in traditional ICP for cation transport to the nanochannel inlet.

Faradaic ICP in a single microchannel. The previous two subsections addressed faradaic ICP with a BPE connecting two microchannels. This is analogous to traditional ICP with $1/D_u = 0$. If the anodic and cathodic compartments are connected by both an electrolyte solution and a BPE, a situation arises which is analogous to traditional ICP where $1 > 1/D_u > 0$. That is, there is some bulk ionic conductance. We have previously observed that an ion depletion zone forms when a large majority of the total current flowing between the anodic and cathodic reservoirs (i_{tot}) passes through the BPE (i_{BPE}).[50] For example, we reported the formation of an ion depletion zone at a 500 μm-long BPE situated at the center of a single microchannel having uniform dimensions (100 μm wide x 21 μm high) along its length (6.0 mm).[50] In that channel geometry, and under conditions in which a depletion zone formed, $i_{BPE}/i_{tot} \approx 0.8$.[50] In other words, in the segment of the microchannel containing the BPE, 80% of the current flowed through the BPE and 20% through the electrolyte solution above it. Of course, 100% of the current in the remaining length of the channel was ionic. This is analogous to ICP in which $i_{EDL}/(i_{EDL} + i_b) = 0.8$. This is significant, because such a dominance of i_{EDL} over i_b in traditional ICP requires a

nanochannel. In contrast, the same effect is observed in a micron-scale channel outfitted with a BPE.

5.5 Results and Discussion

BPE focusing in a single-channel configuration. Enrichment of the fluorescent tracer ($BODIPY^{2-}$) was carried out as follows in a 1.6 μm high single-channel device containing a 100 μm wide split BPE (Figure 5.1a). First, the channel was rinsed as described in the Experimental Section. Second, the buffer in the reservoirs was replaced with either 10.0 pM or 1.0 nM $BODIPY^{2-}$ in 100 mM Tris buffer (pH = 8.0). Finally, E_{tot} = 200 V was applied to initiate enrichment, and then the driving voltage was increased by 100 V every 2000 s up to a maximum of 600 V. A fluorescence image of a typical enriched band (EF = 30,000 after 1000 s at E_{tot} = 200 V) is shown in Figure 5.1c.

Figure 5.1b shows the effect of voltage and time on the concentration enrichment of 10.0 pM and 1.0 nM $BODIPY^{2-}$ tracer. Tracer at an initial concentration of 10.0 pM enriches at an average rate of 56-fold/s reaching 500,000-fold enrichment in 150 min, while the 1.0 nM tracer enriches at 19-fold/s to 180,000-fold over the same period of time. During the course of these enrichment experiments,

the Au BPE slowly degraded starting from the anodic edge of the BPE (Figure 5.1d). This shortens the length of the BPE over which potential is dropped, and this has the effect of gradually decreasing ΔE_{elec}. Electrode degradation can be prevented by enriching at lower E_{tot}, but the associated lower electric field strength, and correspondingly shallower field gradient, results in a lower EF.[69]

To maximize enrichment, E_{tot} was increased every 2000 s (indicated by arrows in Figure 5.1b). This increase was necessary because, for both of the initial concentrations of tracer used here, the EF was found to reach a plateau when E_{tot} was held constant. For example, in the enrichment of 1.0 nM $BODIPY^{2-}$ at E_{tot} = 200 V, a plateau at EF = 25,000 is apparent after 1000 s (Figure 5.1b). A similar plateau is observed with an initial concentration of 10.0 pM tracer, however, it is typically reached just after 2000 s of enrichment. A control experiment was performed using the same conditions as described above for enrichment of 10.0 pM tracer but maintaining E_{tot} = 200 V. The resulting enrichment of the tracer over time is plotted in Figure 5.2. The EF of the focused band reaches ~60,000-fold within approximately 2000 s and does not increase further. The plateau is avoided by increasing E_{tot}. Note however that

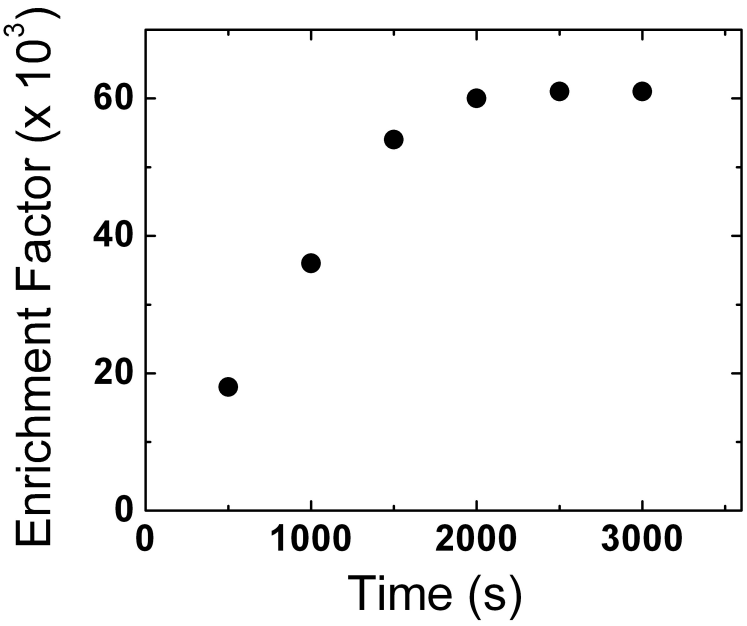

Figure 5.2. Enrichment factor achieved over time during enrichment of 10.0 pM $BODIPY^{2-}$ tracer in 100 mM Tris (pH 8.0) at E_{tot} = 200 V.

increasing E_{tot} too rapidly results in formation of gas bubbles at the BPE cathode.

The EF observed under these conditions is three orders of magnitude higher than what has been reported for BPE focusing thus far.[8, 10, 50, 69] The conditions used here were optimized based on our previously published study of the fundamental parameters affecting the enrichment process.[9, 69] Specifically, an increase in E_{tot} and buffer concentration were found to increase the slope of the electric field gradient (m),[69] which in turn narrows the focused band of tracer. Eq 5.6 incorporates several experimental parameters determining the standard deviation (s) of the width of the focused band.[68]

$$s = \sqrt{\frac{D_{im} + \left(\frac{u_{eo,l}}{u_m} - 1\right)^2 \frac{a^2 u_m^2}{52.5 D_{im}}}{\left|\mu_{ep} m\right|}} \qquad (5.6)$$

Here, a is the half-height of a 2-D (parallel plate) rectangular channel, u_m is the mean axial convective flow velocity of the solution, $u_{eo,l}$ is the local electroosmotic flow velocity in the depletion zone, and D_{im} and μ_{ep} are, respectively, the diffusion coefficient and electrophoretic mobility of the focused species. The EFs in Figure 5.1b are orders of magnitude higher than previously reported for the

following reasons. First, the channel height (a) was decreased from 21 μm to 1.6 μm, which directly decreases s. Second, a higher buffer concentration was employed, which has been shown to increase m and the enrichment rate.[69] High buffer concentrations were not possible to use in channels with higher cross sectional areas due to high current densities in the BPE and corresponding gas bubble formation. In the 1.6 μm high channel, however, the current density at the BPE is greatly decreased (vide infra), which supresses bubble formation. Finally, the BPE was shortened allowing use of higher E_{tot}, thereby further increasing m and the enrichment rate.[69]

Determination of faradaic current in a single-channel configuration. In the preceding subsection, we alluded to a decrease in current density at the BPE in channels having a smaller cross sectional area. Here we quantitatively address the relationship between i_{BPE} and E_{tot} for channels having dimensions of 21 μm high by 100 μm wide and 1.6 μm high by 10 μm wide. Current measurement experiments proceeded as follows. First, the reservoirs were each filled with 40 μL of 10.0 or 100 mM Tris (pH 8.0) and E_{tot} = 20.0 V (21 μm high channel) or 50.0 V (1.6 μm high channel) was applied to rinse the channel for 5 min by

electroosmosis. Next, the reservoirs were filled with fresh buffer solution. Then, the two halves of the 100 μm long split BPE were interconnected via an ammeter. Finally, a driving voltage (E_{tot} = 20.0 V to 800 V) was applied for 30 s while i_{BPE} was recorded. This procedure was repeated three times for each value of E_{tot} allowing 30 s between measurements. Values of i_{BPE} taken at the end of each of the three cycles (at which time i_{BPE} had attained a stable value) were then averaged.

Figures 5.1e and 5.1f show the resulting i_{BPE} vs. E_{tot} behavior. Consider the data taken at 100 mM Tris in a 1.6 μm high channel (the same conditions as those used for enrichment in Figure 5.1b). At low values of E_{tot}, ΔE_{elec} is not sufficiently high to drive water electrolysis at the ends of the BPE and i_{BPE} increases linearly. This linear increase is most likely due to O_2 reduction at the BPE cathode and water oxidation (eq 5.3) at the BPE anode. However, between E_{tot} = 100 V and 200 V (ΔE_{elec} = 1.6 and 3.3 V), i_{BPE} steps to a higher value. This corresponds to the onset of water electrolysis. Above E_{tot} = 200 V, i_{BPE} continues to increase approximately linearly.

The value of i_{BPE} is determined by several factors including the total current in the microchannel (limited by

ionic strength). Therefore, at low buffer concentration (10 mM Tris, 1.6 μm high channel), the current at all values of E_{tot} is less than 0.1 nA. Conversely, for the 21 μm high channel containing 10.0 mM Tris it was not possible to obtain values for i_{BPE} for E_{tot} > 200 V because gas bubbles formed at the BPE under these conditions. Such was also the case at high buffer concentration (100 mM Tris, 21 μm high channel) with bubble formation at $E_{tot} \geq 200$ V.

The i_{BPE} results for the two channel heights qualitatively demonstrate that lower current density observed in the smaller channels. To quantitatively compare the average current densities at the BPEs in the 21 and 1.6 μm high channels, values of i_{BPE} obtained under similar conditions must be considered. Both systems are stable when E_{tot} = 200 V and the channel is filled with 10.0 mM Tris, so these conditions were chosen for direct comparison. For the 21 μm high channel (Figure 5.1e), i_{BPE} = 258 ± 5 nA, and for the 1.6 μm high channel (Figure 5.1f), i_{BPE} = 29.0 ± 0.3 pA. These currents correspond to current densities of 2.58 mA/cm^2 and 2.90 μA/cm^2, respectively. Therefore, in the larger channel, the current density is estimated to be 1000 times higher than in the smaller channel under the same

conditions. For this reason, gas bubble formation is suppressed in the 1.6 μm high channel.

Note that division of i_{BPE} by the total BPE area provides only a rough estimate of the current density. The actual distribution of current along the BPE is non-uniform with the majority of current density at the edges and decreasing exponentially towards the center of the BPE.[3]

Finally, under conditions used for focusing (1.6 μm high channel, 100 mM buffer, and E_{tot} = 200 V), i_{BPE} is ~75% of i_{tot}. In this case where 75% of the total current through the microchannel flows through the BPE and only 25% through the solution above it, the system is analogous to ICP where $i_{EDL}/(i_{EDL} + i_b) = 0.75$.

Enrichment of $BODIPY^{2-}$ in a dual-channel configuration. The enrichment of 10.0 pM and 1.0 nM $BODIPY^{2-}$ was carried out using the dual-channel configuration described earlier (Scheme 5.2a). For these experiments, both microchannels were 6.0 mm long, 10.0 μm wide, and 1.6 μm high with 4.0 mm-diameter reservoirs at either end. A single 50 μm wide Au strip (12.0 mm long) crossed the center of both microchannels. Prior to enrichment, both channels were rinsed as described in the Experimental Section. Then, the contents of the reservoirs were replaced with fresh 100 mM

Tris (pH 8.0) containing 10.0 pM or 1.0 nM $BODIPY^{2-}$. Finally, either VP 2 or VP 3 (Table 5.1) was applied to initiate enrichment and the VP was maintained for 2000 s.

The time-dependent enrichment of the resulting focused band of tracer is shown in Figure 5.3. With an initial tracer concentration of 1.0 nM, and using VP 2, enrichment reaches 23,000-fold in 2000 s at an average rate of 9.3-fold/s. This rate of enrichment is similar to that observed for the same tracer concentration during the first 2000 s of enrichment in the single-channel configuration (Figure 5.1b). Using VP 3, but otherwise the same conditions, the tracer enriches 55,000-fold at an average rate of 27-fold/s. An additional increase in EF is observed for both VP 2 and VP 3 when the initial concentration of tracer is lowered to 10.0 pM. For example, VP 2 results in 71,000-fold enrichment (35.5-fold/s), and VP 3 leads to 142,000-fold enrichment (71-fold/s). The latter is the highest rate of enrichment we have reported thus far.[8, 10, 50, 69] Typical EFs and rates reported for some other CFGF methods are EF = 10,000 at 1.7-fold/s for TGF[45] and EF = 10,000 at 4.17-fold/s for EFGF.[55] Wang et al. achieved widely varied results dependent on the initial analyte concentration with

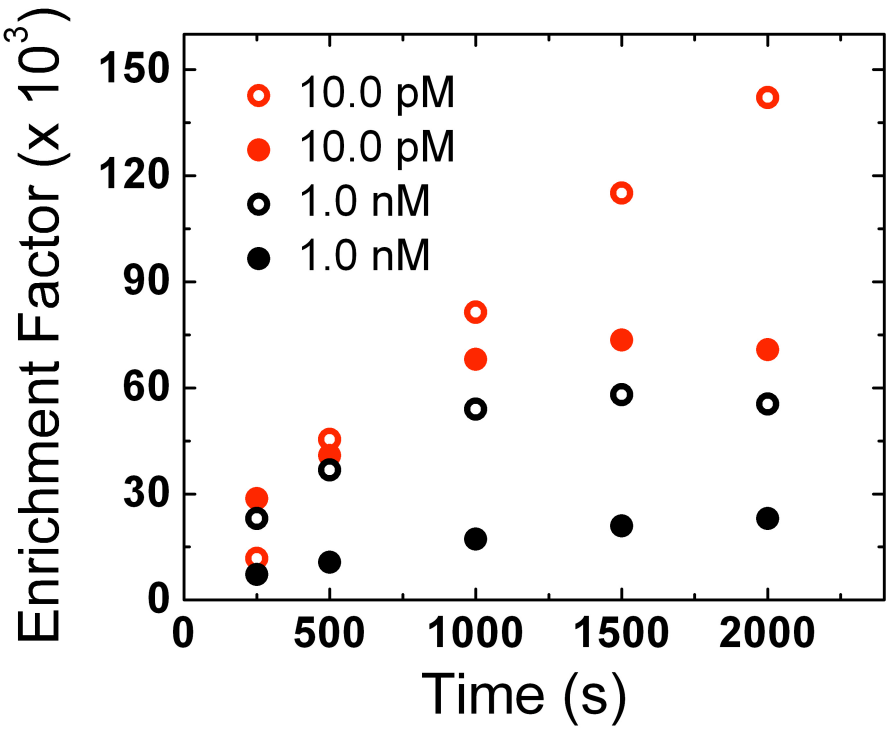

Figure 5.3. Enrichment versus time plots for enrichment of 10.0 pM (open circles) and 1.0 nM (solid circles) $BODIPY^{2-}$ fluorescent tracer in 100 mM Tris•$HClO_4$ (pH 8.0) in a dual-channel device. VP 2 (black) and VP 3 (red) were applied to drive enrichment.

EFs ranging from 300 to 10^7 in 40 min for 33 nM to 33 fM analyte, respectively.[39]

The increase in the rate of enrichment observed for lower initial tracer concentrations has been reported and discussed previously by us[9, 69] and others.[39] Briefly, the higher tracer concentration contributes to the ionic strength at the depletion zone boundary, degrading the electric field gradient.[9, 69] The gain in enrichment rate observed for VP 3 compared to VP 2 is due to the increase in E_{tot}. This dependence on E_{tot} is similar to that described earlier for the single-microchannel arrangement.[69] That is, an increase in the electric field strength in the focusing channel speeds up transport of the tracer from the anodic reservoir to the focusing location, increases both forces responsible for focusing (electromigration of the tracer and opposing convective flow driven by electroosmosis, Scheme 5.1d), and increases the slope of the electric field gradient.[69] Most importantly, in the dual-channel configuration, E_{tot} can be increased while maintaining ΔE_{elec} at a sufficiently low value to prevent gas bubble formation and degradation of the BPE. In the single-channel configuration, as E_{tot} increases, ΔE_{elec} increases proportionaly (Scheme 5.1c).

Characterization of i_{BPE} and ΔE_{elec} in the dual-channel configuration. In the dual-channel system, i_{BPE} and ΔE_{elec} were measured using two device designs, which are described in the Experimental Section. In all experiments, the microchannels were rinsed by filling the reservoirs with 100 mM Tris (pH 8.0), applying VP 1 for 5 min, and then filling the reservoirs with fresh buffer solution.

To measure i_{BPE}, a device with a split BPE was employed and the experiment proceeded as follows. First, the halves of the BPE were connected by an ammeter. Then, VP 2 or VP 3 (Table 5.1) was applied. The resultant current at the BPE was measured for 3 intervals of 30 s each with 30 s between measurements. The value of i_{BPE} at the end of each of the three intervals was averaged and is reported here.

Using VP 2, i_{BPE} = 188 ± 3 nA and with VP 3, i_{BPE} = 386 ± 4 nA. Two important conclusions can be drawn from these results. First, the existence of a stable, non-zero i_{BPE} supports the discussion provided earlier regarding the underlying phenomena governing the behavior of the dual channel system. Specifically, a potential difference (ΔE_{elec}) is established across the BPE between the focusing and auxiliary channels (Schemes 5.2a and 5.2b), leading to faradaic reactions at the BPE ends and current flow (i_{BPE})

between the channels. Second, the magnitude of the current (hundreds of nanoamps) is similar to that observed for a single-channel system having the same channel height (1.6 μm) and buffer concentration (100 mM Tris) used here (blue circles, Figure 5.1e). This is important, because the magnitude of i_{BPE} is a measure of the rate of faradaic reactions governing the formation of the ion depletion zone.

The value of ΔE_{elec} (Schemes 5.2a and 5.2b) was measured using a device having microband electrodes on either side of one end of the BPE as described in the Experimental Section. First, the device was oriented such that the two microbands were in the focusing channel (Scheme 5.2a). Then, a digital multimeter was connected between one of the microbands and V_2 (ground, Scheme 5.2a). Then, VP 2 or VP 3 was applied and the measured voltage recorded. This measurement was repeated for both microbands. Then the device was turned to interchange the roles of the focusing and auxiliary channels, such that the microbands were in the auxiliary channel. The potential of each microband was measured versus V_3 (Scheme 5.2a), which for VP 2 and VP 3 was ground and 50 V, respectively. In this way, the solution potential on either side of both ends of the BPE

was measured allowing ΔE_{elec} to be estimated as discussed next.

The measured values of ΔE_{elec} are provided in Table 5.2. Consider first the voltage measurements for VP 2. In this case, when the microbands are in the focusing channel, the microband farthest from V_2 is at 31.0 V versus ground while the microband closest to V_2 is at 3.0 V. Since these microbands are on either side of the BPE, the solution potential directly above the BPE must be between 31.0 V and 3.0 V, and it is reasonable to take the average, 17.0 V, as the solution potential. When the microbands are in the auxiliary channel, the picture is different because the potential profile is symmetrical about the BPE. Therefore, the potential measured at the two microbands is the same (6.0 V). Finally, the value of ΔE_{elec} can be estimated from the difference in the average potential measured at each end of the BPE such that ΔE_{elec} = 17.0 V - 6.0 V = 11.0 V.

The largest error in this estimate results from taking the average of the voltage measurement at the two microbands in the focusing channel. Averaging here assumes a linear potential drop between the two microbands. Assuming that the slope of the potential profile in each half of the channel is continued between each microband and

Table 5.2 Solution potential near the BPE ends in the dual channel arrangement.

		Measured voltage (V)					
Channel	Microband	VP 2	Avg	ΔE_{elec}	VP 3	Avg	ΔE_{elec}
Focus.	Near V_2	3	17	11	50	61	8
	Far from V_2	31			72		
Aux.	Near V_3	6	6		4* (54)	3* (53)	
	Far from V_3	6			2* (52)		

*Value was measured versus 50 V (V_3, voltage pattern 3). The value in parentheses indicates the value versus ground

the BPE, the potential above the BPE would be lower than 17.0 V and therefore ΔE_{elec} would be < 11.0 V.

For VP 3, ΔE_{elec} = 61.0 V - 53.0 V = 8.0 V. The key point is that the estimated value of ΔE_{elec} is maintained at a similar value at the two VPs. This is the advantage of the dual-channel arrangement, that E_{tot} can be increased (leading to improved focusing) without significantly impacting ΔE_{elec}.

5.6 Summary and Conclusion

We have demonstrated significantly more rapid enrichment of an anionic fluorescent tracer then previously reported for BPE focusing.[8-10, 50, 69] This improvement is a result of optimizing the experimental parameters affecting enrichment.[69] The rate of enrichment is higher (71-fold/s vs. 28-fold/s) for a given initial concentration of analyte (~10 pM) in the dual-channel configuration than has been reported for the most closely related technique — focusing at the boundary of a depletion zone formed by ICP.[39] Additionally, the depletion zone is formed here using a much more easily fabricated device in which a single strip of Au replaces the nanochannel. Furthermore, we have shown that a BPE connecting two microchannels can form enrichment

and depletion zones at its ends through faradaic processes in a way that is analogous to ICP at a micro-/nano-channel junction. This work will be extended to investigate various pairs of faradaic reactions at the BPE which more closely mimic ICP behavior in an effort to more clearly understand fundamentals of ICP currently under study by other research groups such as the propagation of the enrichment and depletion zones as they form.[79]

Chapter 6: Summary and Conclusion

This dissertation describes the development of bipolar electrode (BPE) focusing as a concentration enrichment technique. The mechanism responsible for BPE focusing has been investigated, and the relationship between individual experimental parameters and the enrichment process has been revealed.

Chapter 3 described how the mechanism for BPE focusing was confirmed. Specifically, the use of split and microband BPEs for focusing was established. These device designs were used to probe the electric field profile as well as the magnitude of current through the BPE (i_{BPE}). Results of these studies showed that an electric field gradient was required for focusing to occur and that i_{BPE} had to be a significant fraction of the total current through the microchannel (i_{tot}). Finally, an array of microband electrodes enabled controlled transport of the enriched tracer band by simply switching the pair of microbands acting as the BPE. This had the additional benefit of demonstrating that the electric field gradient could form rapidly upon activating a BPE. This rapid formation allowed

the enriched band to be transported rapidly and smoothly from location to location.

Chapter 4 described the central role of the electric field gradient in BPE focusing, demonstrating that a steeper gradient led to higher enrichment factors (EFs). The effect of experimental parameters on the shape of the electric field gradient was described, and guidelines were provided for optimizing the buffer concentration, surface charge density on the microchannel walls, flow rate, and the total potential applied across the microchannel (E_{tot}). Additionally, the location of an enriched band was correlated to the location of the electric field gradient in real time.

Chapter 5 described the vast improvements to BPE focusing that result from the fundamental understanding gained in Chapters 3 and 4. A three-order-of-magnitude increase in maximum enrichment factor and an increase in enrichment rate were attained by selecting experimental conditions for which the electric field gradient was predicted to be steepest and by reducing causes of band broadening. Furthermore, a dual-channel design was developed allowing greater control over focusing conditions. Importantly, this dual-channel design generates

ion depletion and enrichment zones at each end of the BPE in a manner that is analogous to ion concentration polarization (ICP) at micro-/nano-channel junctions.

In conclusion, as a result of the research described in this dissertation, BPE focusing is much better understood on a fundamental level, and it has become a competitive alternative to current concentration enrichment techniques. BPE focusing provides many avenues for future research including integration of BPE focusing into a micro-total analysis device, optimization of multi-analyte focusing (separation) experiments using electric field profile monitoring as a guide, and further investigation of faradaic ICP in the dual-channel configuration.

Major Symbols

Symbol	Meaning	Unit
a	Half height of a rectangular channel	m
d	Outer-edge-to-edge distance between two microband electrodes	m
D_A	Diffusion coefficient of species A	m^2/s
D_{im}	Molecular diffusivity	m^2/s
D_u	Dukhin number	*unitless*
E_{dr}	Potential dropped at the driving electrodes	V
E_{elec}	Potential of the BPE	V
ΔE_{elec}	Potential difference between two ends of the bipolar electrode	V
E^o	Standard reduction potential	V
$\Delta E_{n,m}$	Potential difference between microband electrodes n and m	V
E_{tot}	Applied voltage between the driving electrodes	V
ε	Permittivity of the solution	F/m
η	Dynamic viscosity	kg/m•s
η_a	Anodic overpotential	V
η_c	Cathodic overpotential	V
i_a	Anodic current	A

i_b	Ionic current through the bulk solution	A
i_{BPE}	Current through the BPE	A
i_c	Cathodic current	A
i_{EDL}	Ionic current through the EDL	A
i_s	Ionic current through the solution	A
i_s'	Ionic current through the solution above the BPE	A
i_{tot}	Total current through the microchannel	A
k_B	Boltzmann constant	J/K
L	Length of capillary from the injection point to the detector	m
$l_{channel}$	Length of the microchannel	m
l_{elec}	Length of the bipolar electrode	m
m	Slope of the electric field gradient	kV/m^2
μ_{eo}	Electroosmotic mobility	$cm^2/V•s$
$\mu_{eo,l}$	Local electroosmotic mobility	$cm^2/V•s$
μ_{ep}	Electrophoretic mobility	$cm^2/V•s$
$\mu_{ep,A}$	Electrophoretic mobility of species A	$cm^2/V•s$
R_s	Solution resistance	Ω
s	Standard deviation of the width of a focused band	m

σ_b	Ionic conductance of the bulk solution	S
σ_{EDL}	Ionic conductance of the EDL	S
T	Absolute temperature	K
t	Time required for microchannel volume to be displaced by electroosmotic flow	s
t_A	Time required for species *A* to travel from the injection point to the detector	s
t_{nm}	Time required for a neutral marker to travel from the injection point to the detector	s
u_{eo}	Electroosmotic velocity	cm/s
$u_{eo,l}$	Local electroosmotic velocity	cm/s
u_{ep}	Electrophoretic velocity	cm/s
$u_{ep,A}$	Electrophoretic velocity of species *A*	cm/s
u_m	Mean convective flow velocity	cm/s
V_a	Electric field strength in the anodic compartment	kV/m
V_{BPE}	Electric field strength in the region above the BPE	kV/m
V_c	Electric field strength in the	kV/m

	cathodic compartment	
V_l	Local electric field strength	kV/m
$V_{l,max}$	Maximum measured local electric field strength	kV/m
V_m	Mean electric field strength	kV/m
x_0	Lateral position on the BPE at which $\eta_c = \eta_a = 0$	m
z_A	Charge of species *A*	*unitless*
ζ	Zeta potential	V

References

1. Duval, J. F. L.; Huijs, G. K.; Threels, W. F.; Lyklema, J.; van Leeuwen, H. P., Faradaic Depolarization in the Electrokinetics of the Metal-Electrolyte Solution Interface. *J. Colloid Interface Sci.* **2003**, *260*, 95-106.

2. Mavré, F.; Anand, R. K.; Laws, D. R.; Chow, K.-F.; Chang, B.-Y.; Crooks, J. A.; Crooks, R. M., Bipolar Electrodes: A Useful Tool for Concentration, Separation, and Detection of Analytes in Microelectrochemical Systems. *Anal. Chem.* **2010**, *82*, 8766-8774.

3. Mavré, F.; Chow, K.-F.; Sheridan, E.; Chang, B.-Y.; Crooks, J. A.; Crooks, R. M., A Theoretical and Experimental Framework for Understanding Electrogenerated Chemiluminescence (ECL) Emission at Bipolar Electrodes. *Anal. Chem.* **2009**, *81*, 6218-6225.

4. Huang, X.; Gordon, M. J.; Zare, R. N., Current Monitoring Method for Measuring the Electroosmotic Flow Rate in Capillary Zone Electrophoresis. *Anal. Chem.* **1988**, *60*, 1837-1838.

5. McDonald, J. C.; Duffy, D. C.; Anderson, J. R.; Chiu, D. T.; Wu, H.; Schueller, O. J. A.; Whitesides, G. M.,

Fabrication of Microfluidic Systems in Poly(dimethylsiloxane). *Electrophoresis* **2000**, *21*, 27-40.

6. Arora, A.; Eijkel, J. C. T.; Morf, W. E.; Manz, A., A Wireless Electrochemiluminescence Detector Applied to Direct and Indirect Detection for Electrophoresis on a Microfabricated Glass Device. *Anal. Chem.* **2001**, *73*, 3282-3288.

7. Ordeig, O.; Godino, N.; del Campo, J.; Munoz, F. X.; Nikolajeff, F.; Nyholm, L., On-Chip Electric Field Driven Electrochemical Detection Using a Poly(dimethylsiloxane) Microchannel with Gold Microband Electrodes. *Anal. Chem.* **2008**, *80*, 3622-3632.

8. Dhopeshwarkar, R.; Hlushkou, D.; Nguyen, M.; Tallarek, U.; Crooks, R. M., Electrokinetics in Microfluidic Channels Containing a Floating Electrode. *J. Am. Chem. Soc.* **2008**, *130*, 10480-10481.

9. Hlushkou, D.; Perdue, R. K.; Dhopeshwarkar, R.; Crooks, R. M.; Tallarek, U., Electric Field Gradient Focusing in Microchannels with Embedded Bipolar Electrode. *Lab Chip* **2009**, *13*, 1903-1913.

10. Laws, D. R.; Hlushkou, D.; Perdue, R. K.; Tallarek, U.; Crooks, R. M., Bipolar Electrode Focusing: Simultaneous Concentration Enrichment and Separation in a Microfluidic

Channel Containing a Bipolar Electrode. *Anal. Chem.* **2009,** *81*, 8923-8929.

11. Chien, R. L., Sample Stacking Revisited: A Personal Perspective. *Electrophoresis* **2003,** *24*, 486-497.

12. Lichtenberg, J.; Verpoorte, E.; de Rooij, N. F., Sample Preconcentration by Field Amplification Stacking for Microchip-Based Capillary Electrophoresis. *Electrophoresis* **2001,** *22*, 258-271.

13. Chen, L.; Prest, J. E.; Fielden, P. R.; Goddard, N. J.; Manz, A.; Day, P. J. R., Miniaturised Isotachophoresis Analysis. *Lab Chip* **2006,** *6*, 474-487.

14. Gebauer, P.; Thormann, W.; Bocek, P., Sample Self-Stacking in Zone Electrophoresis : Theoretical Description of the Zone Electrophoretic Separation of Minor Compounds in the Presence of Bulk Amounts of a Sample Component with High Mobility and Like Charge. *J. Chromatogr. A* **1992,** *608*, 47-57.

15. Jung, B.; Bharadwaj, R.; Santiago, J. G., On-Chip Millionfold Sample Stacking Using Transient Isotachophoresis. *Anal. Chem.* **2006,** *78*, 2319-2327.

16. Kohlheyer, D.; Eijkel, J. C. T.; van den Berg, A.; Schasfoort, R. B. M., Miniaturizing Free-Flow

Electrophoresis - A Critical Review. *Electrophoresis* **2008,** *29*, 977-993.

17. Xu, Z. Q.; Nishine, T.; Arai, A.; Hirokawa, T., Performance of Electrokinetic Supercharging for High-Sensitivity Detection of DNA Fragments in Chip Gel Electrophoresis. *Electrophoresis* **2004,** *25*, 3875-3881.

18. Kelly, R. T.; Li, Y.; Woolley, A. T., Phase-Changing Sacrificial Materials for Interfacing Microfluidics with Ion-Permeable Membranes To Create On-Chip Preconcentrators and Electric Field Gradient Focusing Microchips. *Anal. Chem.* **2006,** *78*, 2565-2570.

19. Liu, J.; Sun, X.; Farnsworth, P. B.; Lee, M. L., Fabrication of Conductive Membrane in a Polymeric Electric Field Gradient Focusing Microdevice. *Anal. Chem.* **2006,** *78*, 4654-4662.

20. Petsev, D. N.; Lopez, G. P.; Ivory, C. F.; Sibbet, S. S., Microchannel Protein Separation by Electric Field Gradient Focusing. *Lab Chip* **2005,** *5*, 587-597.

21. Warnick, K. F.; Francom, S. J.; Humble, P. H.; Kelly, R. T.; Woolley, A. T.; Lee, M. L.; Tolley, H. D., Field Gradient Electrophoresis. *Electrophoresis* **2005,** *26*, 405-414.

22. Cui, H.; Horiuchi, K.; Dutta, P.; Ivory, C. F., Isoelectric Focusing in a Poly(dimethylsiloxane) Microfluidic Chip. *Anal. Chem.* **2005**, *77*, 1303-1309.

23. Dauriac, V.; Descroix, S.; Chen, Y.; Peltre, G.; Sénéchal, H., Isoelectric Focusing in an Ordered Micropillar Array. *Electrophoresis* **2008**, *29*, 2945-2952.

24. Herr, A. E.; Molho, J. I.; Drouvalakis, K. A.; Mikkelsen, J. C.; Utz, P. J.; Santiago, J. G.; Kenny, T. W., On-Chip Coupling of Isoelectric Focusing and Free Solution Electrophoresis for Multidimensional Separations. *Anal. Chem.* **2003**, *75*, 1180-1187.

25. Li, C.; Yang, Y.; Craighead, H. G.; Lee, K. H., Isoelectric Focusing in Cyclic Olefin Copolymer Microfluidic Channels Coated by Polyacrylamide Using a UV Photografting Method. *Electrophoresis* **2005**, *26*, 1800-1806.

26. Yao, B.; Yang, H.; Liang, Q.; Luo, G.; Wang, L.; Ren, K.; Gao, Y.; Wang, Y.; Qiu, Y., High-Speed, Whole-Column Fluorescence Imaging Detection for Isoelectric Focusing on a Microchip Using an Organic Light Emitting Diode as Light Source. *Anal. Chem.* **2006**, *78*, 5845-5850.

27. Cannon, D. M., Jr.; Kuo, T.-C.; Bohn, P. W.; Sweedler, J. V., Nanocapillary Array Interconnects for Gated Analyte

Injections and Electrophoretic Separations in Multilayer Microfluidic Architectures. *Anal. Chem.* **2003,** *75*, 2224-2230.

28. Dhopeshwarkar, R.; Sun, L.; Crooks, R. M., Electrokinetic Concentration Enrichment Within a Microfluidic Device Using a Hydrogel Microplug. *Lab Chip* **2005,** *5*, 1148-1154.

29. Foote, R. S.; Khandurina, J.; Jacobson, S. C.; Ramsey, J. M., Preconcentration of Proteins on Microfluidic Devices Using Porous Silica Membranes. *Anal. Chem.* **2005,** *77*, 57-63.

30. Gatimu, E. N.; King, T. L.; Sweedler, J. V.; Bohn, P. W., Three-Dimensional Integrated Microfluidic Architectures Enabled Through Electrically Switchable Nanocapillary Array Membranes. *Biomicrofluidics* **2007,** *1*, 021502.

31. Han, J.; Fu, J.; Schoch, R. B., Molecular Sieving Using Nanofilters: Past, Present and Future. *Lab Chip* **2008,** *8*, 23-33.

32. Hlushkou, D.; Dhopeshwarkar, R.; Crooks, R. M.; Tallarek, U., The Influence of Membrane Ion-Permselectivity on Electrokinetic Concentration Enrichment in Membrane-Based Preconcentration Units. *Lab Chip* **2008,** *8*, 1153-1162.

33. Jin, X.; Joseph, S.; Gatimu, E. N.; Bohn, P. W.; Aluru, N. R., Induced Electrokinetic Transport in Micro-

Nanofluidic Interconnect Devices. *Langmuir* **2007,** *23*, 13209-13222.

34. Khandurina, J.; Jacobson, S. C.; Waters, L. C.; Foote, R. S.; Ramsey, J. M., Microfabricated Porous Membrane Structure for Sample Concentration and Electrophoretic Analysis. *Anal. Chem.* **1999,** *71*, 1815-1819.

35. Kim, S. M.; Burns, M. A.; Hasselbrink, E. F., Electrokinetic Protein Preconcentration Using a Simple Glass/Poly(dimethylsiloxane) Microfluidic Chip. *Anal. Chem.* **2006,** *78*, 4779-4785.

36. Kim, T.; Meyhöfer, E., Nanofluidic Concentration of Selectively Extracted Biomolecule Analytes by Microtubules. *Anal. Chem.* **2008,** *80*, 5383-5390.

37. Piruska, A.; Branagan, S.; Cropek, D. M.; Sweedler, J. V.; Bohn, P. W., Electrokinetically Driven Fluidic Transport in Integrated Three-Dimensional Microfluidic Devices Incorporating Gold-Coated Nanocapillary Array Membranes. *Lab Chip* **2008,** *8*, 1625-1631.

38. Song, S.; Singh, A. K.; Kirby, B. J., Electrophoretic Concentration of Proteins at Laser-Patterned Nanoporous Membranes in Microchips. *Anal. Chem.* **2004,** *76*, 4589-4592.

39. Wang, Y.-C.; Stevens, A. L.; Han, J., Million-fold Preconcentration of Proteins and Peptides by Nanofluidic Filter. *Anal. Chem.* **2005,** *77*, 4293-4299.

40. Zhang, Y.; Timperman, A. T., Integration of Nanocapillary Arrays into Microfluidic Devices for Use as Analyte Concentrators. *Analyst* **2003,** *128*, 537-542.

41. Zhou, K.; Kovarik, M. L.; Jacobson, S. C., Surface-Charge Induced Ion Depletion and Sample Stacking near Single Nanopores in Microfluidic Devices. *J. Am. Chem. Soc.* **2008,** *130*, 8614-8616.

42. Balss, K. M.; Vreeland, W. N.; Phinney, K. W.; Ross, D., Simultaneous Concentration and Separation of Enantiomers with Chiral Temperature Gradient Focusing. *Anal. Chem.* **2004,** *76*, 7243-7249.

43. Hoebel, S. J.; Balss, K. M.; Jones, B. J.; Malliaris, C. D.; Munson, M. S.; Vreeland, W. N.; Ross, D., Scanning Temperature Gradient Focusing. *Anal. Chem.* **2006,** *78*, 7186-7190.

44. Kim, S. M.; Sommer, G. J.; Burns, M. A.; Hasselbrink, E. F., Low-Power Concentration and Separation Using Temperature Gradient Focusing via Joule Heating. *Anal. Chem.* **2006,** *78*, 8028-8035.

45. Ross, D.; Locascio, L. E., Microfluidic Temperature Gradient Focusing. *Anal. Chem.* **2002**, *74*, 2556-2564.

46. Song, S.; Singh, A., On-Chip Sample Preconcentration for Integrated Microfluidic Analysis. *Anal. Bioanal. Chem.* **2006**, *384*, 41-43.

47. Huang, Z.; Ivory, C. F., Digitally Controlled Electrophoretic Focusing. *Anal. Chem.* **1999**, *71*, 1628-1632.

48. Duval, J.; Kleijn, J. M.; van Leeuwen, H. P., Bipolar Electrode Behaviour of the Aluminium Surface in a Lateral Electric Field. *J. Electroanal. Chem.* **2001**, *505*, 1-11.

49. Bard, A. J.; Faulkner, L. R., *Electrochemical Methods: Fundamentals and Applications*. 2 ed.; John Wiley & Sons: 2001; p 833.

50. Perdue, R. K.; Laws, D. R.; Hlushkou, D.; Tallarek, U.; Crooks, R. M., Bipolar Electrode Focusing: The Effect of Current and Electric Field on Concentration Enrichment. *Anal. Chem.* **2009**, *81*, 10149-10155.

51. Hofmann, O.; Che, D.; Cruickshank, K. A.; Müller, U. R., Adaptation of Capillary Isoelectric Focusing to Microchannels on a Glass Chip. *Anal. Chem.* **1998**, *71*, 678-686.

52. Yang, H.; Chien, R.-L., Sample Stacking in Laboratory-on-a-Chip Devices. *J. Chromatogr., A* **2001**, *924*, 155-163.

53. Gebauer, P.; Bocek, P., Recent Progress in Capillary Isotachophoresis. *Electrophoresis* **2002**, *23*, 3858-3864.

54. Shackman, J. G.; Ross, D., Counter-Flow Gradient Electrofocusing. *Electrophoresis* **2007**, *28*, 556-571.

55. Humble, P. H.; Kelly, R. T.; Woolley, A. T.; Tolley, H. D.; Lee, M. L., Electric Field Gradient Focusing of Proteins Based on Shaped Ionically Conductive Acrylic Polymer. *Anal. Chem.* **2004**, *76*, 5641-5648.

56. Koegler, W. S.; Ivory, C. F., Focusing Proteins in an Electric Field Gradient. *J. Chromatogr., A* **1996**, *726*, 229-236.

57. Lin, S.-L.; Li, Y.; Tolley, H. D.; Humble, P. H.; Lee, M. L., Tandem Electric Field Gradient Focusing System for Isolation and Concentration of Target Proteins. *J. Chromatogr., A* **2006**, *1125*, 254-262.

58. Lin, S.-L.; Li, Y.; Woolley, A. T.; Lee, M. L.; Tolley, H. D.; Warnick, K. F., Programed Elution and Peak Profiles in Electric Field Gradient Focusing. *Electrophoresis* **2008**, *29*, 1058-1066.

59. Meighan, M. M.; Staton, S. J. R.; Hayes, M. A., Bioanalytical Separations Using Electric Field Gradient Techniques. *Electrophoresis* **2009,** *30*, 852-865.

60. Sun, X.; Farnsworth, P. B.; Tolley, H. D.; Warnick, K. F.; Woolley, A. T.; Lee, M. L., Performance Optimization in Electric Field Gradient Focusing. *J. Chromatogr., A* **2009,** *1216*, 159-164.

61. Burke, J. M.; Huang, Z.; Ivory, C. F., Simultaneous Separation of Negatively and Positively Charged Species in Dynamic Field Gradient Focusing Using a Dual Polarity Electric Field. *Anal. Chem.* **2009,** *81*, 8236-8243.

62. Burke, J. M.; Smith, C. D.; Ivory, C. F., Development of a Membrane-less Dynamic Field Gradient Focusing Device for the Separation of Low-Molecular-Weight Molecules. *Electrophoresis* **2010,** *31*, 902-909.

63. Höltzel, A.; Tallarek, U., Ionic Conductance of Nanopores in Microscale Analysis Systems: Where Microfluidics Meets Nanofluidics. *J. Sep. Sci.* **2007,** *30*, 1398-1419.

64. Kim, S. J.; Li, L. D.; Han, J., Amplified Electrokinetic Response by Concentration Polarization near Nanofluidic Channel. *Langmuir* **2009,** *25*, 7759-7765.

65. Hellmich, W.; Regtmeier, J.; Duong, T. T.; Ros, R.; Anselmetti, D.; Ros, A., Poly(oxyethylene) Based Surface Coatings for Poly(dimethylsiloxane) Microchannels. *Langmuir* **2005**, *21*, 7551-7557.

66. Huang, K.-D.; Yang, R.-J., A Nanochannel-Based Concentrator Utilizing the Concentration Polarization Effect. *Electrophoresis* **2008**, *29*, 4862-4870.

67. Kim, S. J.; Song, Y.-A.; Han, J., Nanofluidic Concentration Devices for Biomolecules Utilizing Ion Concentration Polarization: Theory, Fabrication, and Applications. *Chem. Soc. Rev.* **2010**, *39*, 912-922.

68. Maynes, D.; Tenny, J.; Webb, B. W.; Lee, M. L., Influence of Varying Electroosmotic Flow on the Effective Diffusion in Electric Field Gradient Separations. *Electrophoresis* **2008**, *29*, 549-560.

69. Anand, R. K.; Sheridan, E.; Hlushkou, D.; Tallarek, U.; Crooks, R. M., Bipolar Electrode Focusing: Tuning the Electric Field Gradient. *Lab Chip*, In press (DOI:10.1039/C0LC00351D).

70. Chiu, D. T., Interfacing Droplet Microfluidics with Chemical Separation for Cellular Analysis. *Anal. Bioanal. Chem.* **2010**, *397*, 3179-3183.

71. Tia, S.; Herr, A. E., On-Chip Technologies for Multidimensional Separations. *Lab Chip* **2009**, *9*, 2524-2536.

72. Borland, L. M.; Kottegoda, S.; Phillips, K. S.; Allbritton, N. L., Chemical Analysis of Single Cells. *Annu. Rev. Anal. Chem.* **2008**, *1*, 191-227.

73. Bocquet, L.; Charlaix, E., Nanofluidics, from Bulk to Interfaces. *Chem. Soc. Rev.* **2010**, *39*, 1073-1095.

74. Kovarik, M. L.; Jacobson, S. C., Nanofluidics in Lab-on-a-Chip Devices. *Anal. Chem.* **2009**, *81*, 7133-7140.

75. Lorenz, R. M.; Chiu, D. T., Chemistry and Biology in Femtoliter and Picoliter Volume Droplets. *Acc. Chem. Res.* **2009**, *42*, 649-658.

76. Theberge, A. B.; Courtois, F.; Schaerli, Y.; Fischlechner, M.; Abell, C.; Hollfelder, F.; Huck, W. T. S., Microdroplets in Microfluidics: An Evolving Platform for Discoveries in Chemistry and Biology. *Angew. Chem. Int. Ed.* **2010**, *49*, 5846-5868.

77. Ohno, K.-i.; Tachikawa, K.; Manz, A., Microfluidics: Applications for Analytical Purposes in Chemistry and Biochemistry. *Electrophoresis* **2008**, *29*, 4443-4453.

78. Zangle, T. A.; Mani, A.; Santiago, J. G., Theory and Experiments of Concentration Polarization and Ion Focusing

at Microchannel and Nanochannel Interfaces. *Chem. Soc. Rev.* **2010**, *39*, 1014-1035.

79. Zangle, T. A.; Mani, A.; Santiago, J. G., On the Propagation of Concentration Polarization from Microchannel-Nanochannel Interfaces: Numerical and Experimental Study. *Langmuir* **2009**, *25*, 3909-3916.

Vita

Robbyn K. Perdue received her Bachelor of Arts degree from Anderson University, IN in 2004. She is expected to receive her doctoral degree in Chemistry under the guidance of Professor Richard M. Crooks from The University of Texas at Austin in December 2010.

Permanent address: 16610 NE 36th Ct, Apt. FF204, Redmond, WA 98052

This dissertation was typed by the author.